Magnetic Island Dynamics Induced by Rotating Magnetic Perturbations in Tokamak plasma

David Alan Maurer

Submitted in partial fulfillment of the
requirements for the degree
of Doctor of Philosophy
in the Graduate School of Arts and Sciences

COLUMBIA UNIVERSITY

2000

ABSTRACT

Magnetic Island Dynamics Induced by Rotating Magnetic Perturbations in Tokamak plasma

David Alan Maurer

This thesis reports the results of active rotation control experiments of magnetic islands on the HBT-EP tokamak. A compact modular saddle coil set generates magnetic perturbations used to apply local torque to pre-existing m/n=2/1 magnetic islands. Here m and n are the poloidal and toroidal mode numbers of the island structure. Factor of approximately 2 change in island frequency is observed during these *magnetic stirring* experiments with an applied radial saddle coil field of the order of the poloidal field fluctuation of the island measured at the edge of the plasma. To better quantify the coil-island interaction a simple cylindrical model of the electromagnetic, inertial, and viscous torque balance near a large amplitude magnetic island is developed and compared to experimental island frequency locking torque requirements. The measured order of magnitude of the electromagnetic torque required to frequency lock HBT-EP islands is consistent with toroidally driven island motion by these rotating resonant magnetic perturbations. This observation supports the inclusion of poloidal flow damping physics in describing HBT-EP magnetic island dynamics. To ascertain the effect of viscous coupling to the core plasma region and aid in estimates of magnetic island size, island induced emissivity fluctuations are studied and an average current profile constructed. Using these emissivity fluctuations the rotation of the core m/n=1/1 island is observed to be strongly

coupled to that of the edge m/n=2/1 island for both natural propagation and during active rotation of the 2/1 surface. This thesis concludes with observations of magnetic island amplitude dynamics during these rotation control experiments. Island amplitude behavior is complex and reveals the existence of a frequency dependent amplitude effect when the rotation rate of the magnetic island is changed from its natural pre-existing speed. HBT-EP magnetic islands are observed to grow when accelerated and are suppressed or damped when the magnetic island is decelerated during rotation control experiments. This response is consistent with order of magnitude estimates of the inertial current driven by changes in island rotation including the effect of poloidal flow damping on ion inertia. Damping of poloidal plasma rotation leads to an effective increase in perpendicular plasma inertia due to coupling of transverse and longitudinal flow across and along the magnetic field. The observed asymmetry in growth and damping with acceleration and deceleration of these magnetic islands is consistent with a *destabilizing* inertial contribution to the island width evolution equation of motion. Inspired by the possibility of a frequency modulated asynchronous control perturbation having an influence on island size, these perturbations, when applied to disruptive target plasma, were observed to mitigate core thermal and particle loss. This discovery offers the possibility of a simple control technique to ameliorate the consequences of sudden discharge termination from plasma disruption.

TABLE OF CONTENTS

To my love, Renée

ACKNOWLEDGEMENTS

I would like to start by thanking my advisor Professor Jerry Navratil for sticking it out with me through all these years of hard work. I have been more than challenged by working for him on HBT-EP than I thought possible. I hope some of his great intuition and insight into plasma physics has rubbed-off after working together these years. I also owe a large debt of thanks to Professor Mike Mauel for his enthusiasm and perspective during the course of this thesis work. Mike is always willing to discuss and debate questions about HBT-EP magnetic island physics and this is a better thesis as a result of his help. I would also like to thank Professor Allen Boozer for his open door policy and readiness to answer or work through perhaps not quite well formulated questions.

Marlene Arbo and Lydia Argote deserve special mention. I am grateful to you both for helping me navigate the myriad intricacies of Columbia and its wonderful bureaucracy with good cheer and humor. You both make the Applied Physics and Applied Mathematics department a special one to attend.

There is no possible way this thesis would have been finished were it not for the efforts of Nick Rivera, Estuardo Rodas, and Maurice Cea. Their finger prints might not be directly visible in the pages that follow, but there hard work, insight, and ability to make the Columbia Plasma Physics Laboratory a place that *works* form the backbone or foundation upon which this thesis was built. I thank them all and look forward to keeping in close contact in the future.

I have been lucky to be part of the original HBT-EP gang. I would like to thank all of this old crew as well as the new generation of graduate students and

scientists. Thanks go to Tom Ivers, Raed Kombargi, Andrea Garofalo, Xiao Qingjun, Ned Eisner, and David Nadle. Without their help and humor the lab would have been a very dull place indeed. To the new generation, I would like to thank Cory Cates, Mikhail Shilov, Suparna Mukherjee, and Hossein Dahi for all their understanding and help during the last years of this work.

Lastly and most importantly, I would like to thank my family for all their support over these many years of graduate school. Thank you Mom and Dad for all the help and support during these years in New York, and of course all those that went before it. Renée and I both owe you more than words can say. Finally, I would like to thank Renée, who stood by me and supported me throughout. I would have drowned without you my love. I dedicate this thesis to you.

Every time you look up at the sky, every one of those points of light is a reminder that fusion power is extractable from hydrogen and other light elements, and it is an everyday reality throughout the Milky Way Galaxy.

- Carl Sagan, Spitzer Lecture, Princeton University, October 1991

1.0 Introduction

Fusion energy, the source of power for our sun and other stars in the sky above, is at present the preferred method of power production throughout our universe. All the bright points of light in the night time sky attest to this fact. Unfortunately the same situation is not an everyday reality here on planet earth. To date, the quest of developing an analogous terrestrial-based fusion power source capable of generating billion Watt thermal power levels has occupied the concentrated efforts of research scientists and engineers for a span of some fifty years during the last half of the twentieth century. Pursuit of this grand challenge goal to bring the power source of the sun and stars down to earth, while much nearer to being reality than it was during its inception, is still on the horizon of our scientific and technical experience.

Steady progress has been made in advancing necessary plasma parameter values into the range required for significant fusion energy generation over this period of time. Earth-based laboratory plasmas can now be generated with temperatures higher than the center of our own sun confined by magnetic fields for long periods of time. Up to 10 million Watts of fusion power production and

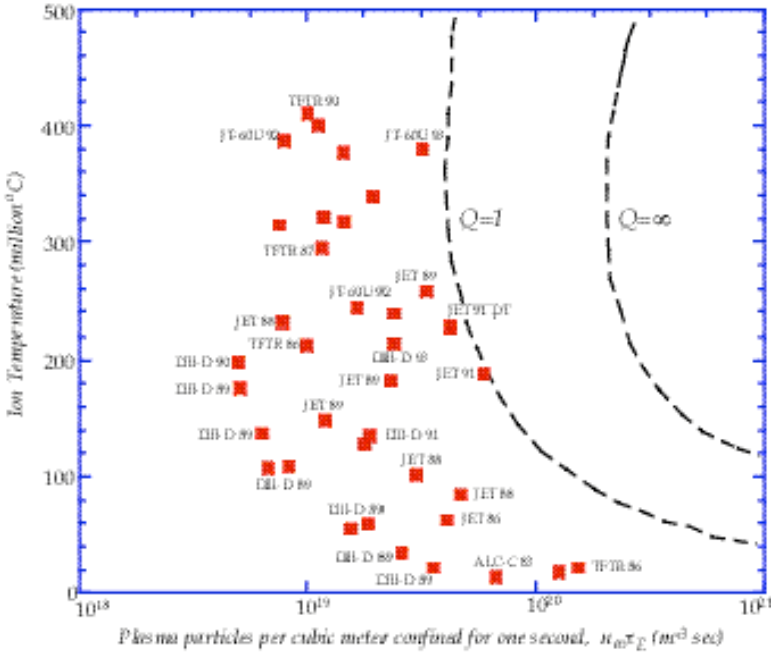

Figure 1.0 Fusion plasma performance for a variety of tokamak devices showing approach to breakeven Q=1 conditions. Here Q denotes the ratio of fusion generated power to input power used to heat the plasma (after Schissel and Leuer 1996).

20 million Joules of fusion energy have recently been generated in tokamak devices employing deuterium and tritium isotopes of hydrogen as the fusing fuel (Hawryluk 1998).

Long-term confinement of fusion-grade plasma requires balancing of the plasma pressure gradient with some other available, appropriately directed force density. In normal room temperature condensed matter this is easily accomplished using solid material walls. Unfortunately, the high temperatures required for fusion energy generation, approximately 100 million degrees, preclude such simple means of isolating the hot plasma from its material surroundings. A simple container would quickly ablate or vaporize when put in

contact with fusion grade plasma. Therefore some other means of holding on to and isolating the high temperature plasma is necessary.

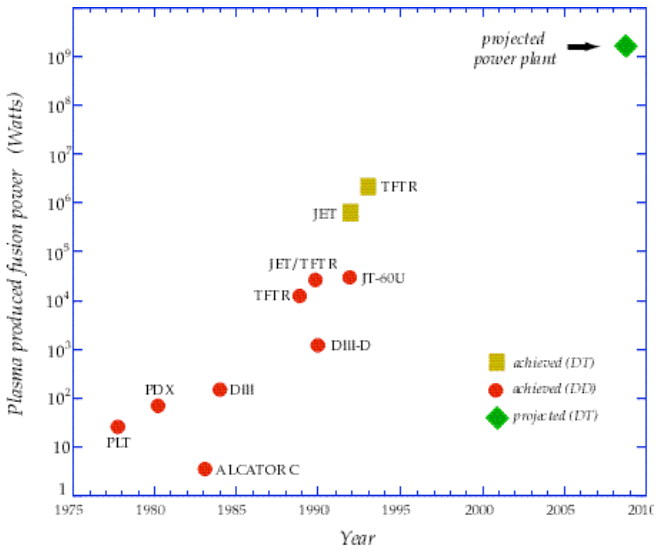

Figure 1.1 Progress in fusion power production over the last three decades of the twentieth century including projected reactor fusion power production (after Schissel and Leuer 1996).

Presently, the two dominant approaches to maintaining such hot plasma in equilibrium to generate the required plasma parameters for significant fusion reactions to occur employ either inertial or magnetic forces to counteract the self-expansion generated by the confined plasma pressure (Fowler 1999). This thesis deals with magnetically confined plasma in a tokamak configuration. Externally generated magnetic perturbations are used to probe tokamak plasma behavior and the resultant magnetic field and plasma dynamics are then studied. These external perturbations are generated using a compact saddle coil set designed to apply a magnetic perturbation that is in resonance with the confining magnetic field embedded in the HBT-EP tokamak plasma. The response of the plasma-

magnetic field system is studied and a rich, complex set of interactions is observed depending upon the amplitude, phase, and frequency of both any pre-existing perturbed fields in the plasma as well as that of the externally applied saddle coil magnetic field. The connection and importance of these topics to fusion plasma physics is introduced in the following sections. To understand these issues this introduction briefly overviews the basic physics of magnetic confinement in toroidal devices with special emphasis on the tokamak configuration. Magnetic flux surfaces and their properties as they relate to plasma equilibrium and magnetic island formation are presented. The response of vacuum magnetic fields to resonant perturbation and the importance of magnetic island formation as a result of such perturbation fields is discussed. The effect of static plasma on the response of a magnetic field near a rational surface are outlined. The consequences of plasma rotation are introduced in the context of so-called error field mode locking of magnetic islands. These examples point out the dramatic effect that the plasma can have on the resultant island structure. A historical survey of resonant magnetic perturbation studies is presented next that allows the results of the present work to be put in proper perspective. Finally, this section concludes with a discussion of the principal results and outline of this thesis.

1.1 Fusion plasma

The impetus for much of laboratory plasma physics research has been driven by the quest for generating man-made fusion energy regime plasma conditions. The requirements of the fusing fuel dictate the required plasma parameters that must be achieved in the laboratory. Out of the possible range of most reactive fusion reactions shown below

$$\begin{aligned} &{}_1D^2 + {}_1T^3 \rightarrow {}_2He^4 + {}_0n^1 \quad (17.6MeV) \\ &{}_1D^2 + {}_1D^2 \rightarrow {}_1T^3 + {}_1H^1 \quad (4.03MeV) \\ &{}_1D^2 + {}_2He^3 \rightarrow {}_2He^4 + {}_1H^1 \quad (18.3MeV) \end{aligned} \tag{1.0}$$

the combination of deuterium and tritium yields the easiest target plasma parameters. For this reason they are expected to be used in first generation fusion power sources rather than the other reactions which require higher temperatures. The conditions for generating fusion power are traditionally written using the so-called fusion triple product $nT\tau_E$. Here n is the plasma density, T the kinetic temperature, and τ_E is the energy confinement time, defined as the stored plasma thermal energy divided by the input heating power $\tau_E = W_{Stored}/P_{Input}$. Using the triple product, the condition for substantial fusion energy generation from a plasma made up of deuterium and tritium as fuel can be written as $nT\tau_E \geq 10^{21}$ m^{-3} keV sec (see for example, Wesson 1997). This condition can be satisfied by a plasma containing $n \sim 10^{20}$ particles per m^3 at a temperature of $T \sim 10$keV with a confinement time of $\tau_E \sim 1$sec. For perspective recall that 1eV is equivalent to 11,600 degrees Kelvin. Thus, most molecular and atomic bonds have been broken in a gas heated to 1eV temperature. For fusion conditions of 100 million degrees the electrons and nuclei that make up the

atoms of the fuel have been stripped apart and have been converted into a fully ionized gas or plasma. Hence the study of plasma physics and its importance to the fusion enterprise, fusion conditions can only take place in the state of matter that we call plasma. The basic ideas for confining hot plasma using magnetic fields or magnetic insulation are discussed next. This sets the stage for a discussion of magnetic islands and their importance to the nested flux surface structure used to confine hot plasma.

1.2 Magnetic confinement

The magnetic confinement and insulation of plasma is based upon the magnetic field property that charged particles are channeled along the direction of the field, limiting their perpendicular excursion. This follows simply from the resultant charged particle motion given by the Lorentz force $\vec{F}_{EM} = q(\vec{E} + \vec{v} \times \vec{B})$. Charged particles are constrained to gyrate perpendicular to the field direction. Pictorially this is shown in figure 1.2, where gas particles are seen to simply free stream until they collide with each other or the enclosing container walls. The tube of magnetic flux isolates the particle from wall contact as shown. Flux tube structures that can be arranged parallel to any vacuum container walls appear to offer a simple method to insulate the plasma from wall contact. What flux tube or surface structure confines field lines in a finite volume of space without intercepting bounding material structures?

To confine plasma in a finite volume of space insulating it against contact with any surrounding material structure using a magnetic field implies that magnetic

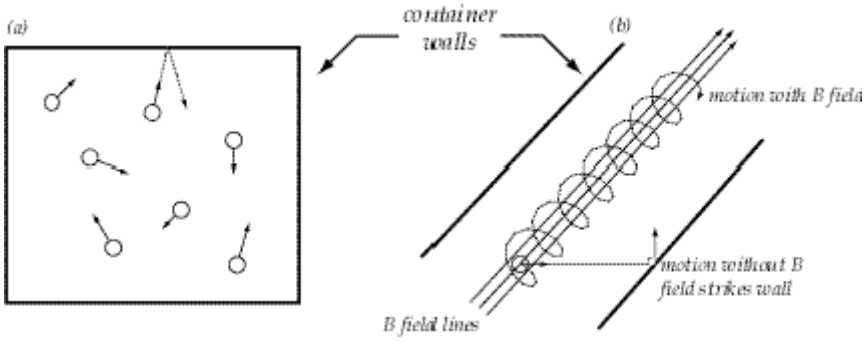

Figure 1.2*(a)*. Low temperature gases such as air can be confined using a material container. *(b)* Energetic plasma particles must be insulated against wall contact. One way to achieve this is to arrange a magnetic field *B* parallel to any container walls as shown.

field lines should lie on topologically toroidal surfaces. This follows from the divergence free nature of the magnetic field (Kruskal and Kulsrud 1958) and is illustrated in figure 1.3. The magnetic field vectors can be smoothly *"combed"*

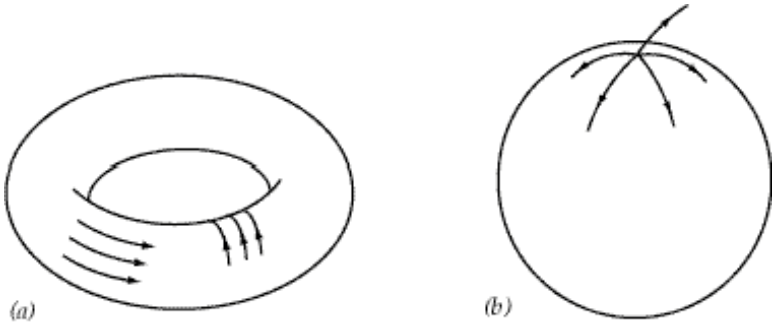

Figure 1.3 Divergence free vector fields, such as the magnetic field, can be smoothly *"combed"* on a torus without field lines leaving a finite region of space as in figure *(a).* This is not possible for other topological shapes without singularity or field lines leaving the volume of interest as in *(b).*

without singularity or field line trajectories leaving the volume of interest on a topological torus. Since the plasma particles are guided along the magnetic field to lowest order in gyro-radius confinement of magnetic field lines is therefore necessary for long time confinement of the plasma.

Specializing to the case of a tokamak, which has net current flowing in the plasma, the magnetic field must also satisfy Ampere's law, $\nabla \times \vec{B} = \mu_o \vec{J}$, and force balance within the plasma volume, $\vec{J} \times \vec{B} = \nabla p$. This implies that the toroidal magnetic surfaces within which the magnetic field vector lies are also constant pressure or isobaric surfaces, $\vec{B} \cdot \nabla p = 0$. In addition, the current density flowing in the plasma is also constant on these same magnetic flux surfaces since

$\vec{J} \cdot \nabla p = 0$. Figure 1.4 shows the typical resultant flux surface structure for such torodial equilibria as found in tokamak plasma.

An important question given the above discussion is whether such equilibria are robust to the addition of small magnetic perturbations to the equilibrium magnetic flux surfaces. Would a small magnetic perturbation destroy the nested structure of the magnetic surfaces and compromise the insulating character of the magnetic field? At first sight, the addition of a small external field of magnitude one part in a thousand, $b/B_o \sim 10^{-3}$, of the confining equilibrium magnetic field would appear to have little effect on the background magnetic field structure and hence plasma.

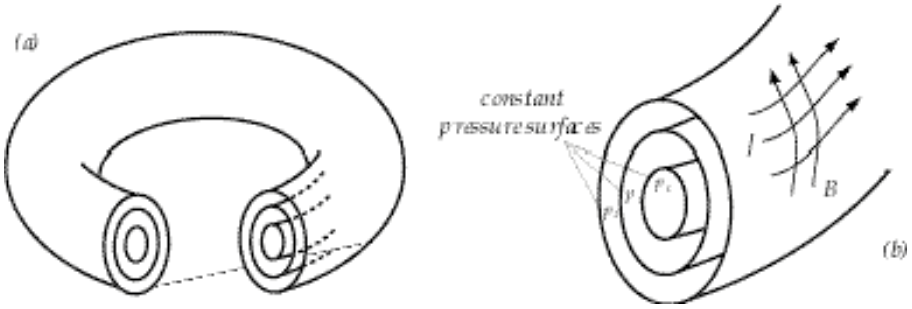

Figure 1.4*(a)* Equilibrium flux surfaces where current density and magnetic field vectors lie are also, *(b)* isobaric or constant pressure surfaces.

The direction of the new equilibrium field $\vec{B}$ is only slightly changed by one part in a thousand, $\vec{B} = \vec{B}_o + \vec{b} = B_o[\hat{B}_o + (b/B_o)\hat{b}] \approx \vec{B}_o$, with $\hat{B}_o$ and $\hat{b}$ unit vectors in the direction of the equilibrium and perturbed fields respectively. The magnitude of the resultant field, $B = B_o\sqrt{1 + b^2/B_o^2} \approx B_o$, is affected to an even less degree by the perturbation. It changes by one part in a million. Thus, the effect of small

perturbations to the equilibrium field appears to be essentially negligible. However, contrary to magnetic perturbation effect on the magnitude and direction of the combined field at a given point in space such small perturbations can have a substantial impact on the plasma by changing equilibrium flux surface structure through a resonance effect. Here the term resonance means that the helical pitch of the perturbation field match that of the equilibrium rational surface.

1.3 Magnetic field structure and magnetic islands

Although the direction and magnitude of the equilibrium field are at most only slightly effected by these small magnetic perturbations, the structure of the nested flux surfaces containing the plasma can be significantly altered for the worse (Morozov and Solov′ev 1966). Rather than consider the combined magnetic field-plasma system response to a magnetic perturbation for this introduction, the simplified case of vacuum field response is treated first for clarity. The possible effect of plasma on this vacuum response is then introduced by considering tearing mode growth in static and rotating plasma in section 1.4. Consider the effect of a perturbing magnetic field on the flux surface structure described above. The combined total field is written as $\vec{B} = \vec{B}_o + \vec{b}$, with $\vec{b}$ the perturbation and $\vec{B}_o$ the equilibrium field. We would like to find new magnetic surfaces of this total field, that is a function $f(\vec{x})$ such that,

$$\vec{B} \cdot \nabla f = 0 . \tag{1.1}$$

These new magnetic surfaces are then surfaces of constant f. To solve equation 1.1 and ascertain the effect of a small perturbation on flux surface structure expand f to first order as $f=f_o+f_1$, then equation 1.1 yields,

$$\vec{B}_o \cdot \nabla f_o = 0, \tag{1.2}$$

$$\vec{B}_o \cdot \nabla f_1 + \vec{b} \cdot \nabla f_o = 0. \tag{1.3}$$

The solution of equation 1.2 is just $f_o(\psi)$ as an arbitrary function of ψ. Using this result and the magnetic differential equation for f_1, equation 1.3, allows us to solve for the perturbed surfaces, $f=f_o+f_1$. Together they imply that (Boozer 1992),

$$f_1 \sim \frac{df_o}{d\psi} \sum_{n,m} \frac{b_{nm}(\psi)}{nq(\psi) - m} \exp\big(i(nq - m)\big). \tag{1.4}$$

The use of the term resonance should now be clear given the denominator $nq(\psi)-m$ of equation 1.4 for the perturbed part of the flux function f_1. When the perturbation helix matches that of the equilibrium rational magnetic surface $q(\psi)=m/n$ at that ψ surface the denominator in 1.4 vanishes leading to $f_1 \to \infty$. This is the resonance alluded to previously. The resolution of this singularity in the vacuum magnetic field response to resonant magnetic perturbations is elegantly understood by noting that the magnetic field constitutes a Hamiltonian system because of its divergence free character, $\nabla \cdot \vec{B} = 0$.

The Hamiltonian nature of two-dimensional divergence free vector fields is well known from fluid dynamics, $\nabla \cdot \vec{v} = 0$. To see the Hamiltonian nature of this incompressible two-dimensional vector field introduce a velocity potential such that $\vec{v} = \hat{z} \times \nabla\phi$. Then the streamlines or integral curves of the velocity field of the system are given by $dx/dt = \partial\phi/\partial y$ and $dy/dt = -\partial\phi/\partial x$, which are

Hamilton's equations with the velocity potential ϕ acting as the Hamiltonian of the system and the Cartesian coordinates acting as the canonical coordinate and conjugate momentum (Tabor 1996). The fact that fully three-dimensional divergence free vector fields are also Hamiltonian is not obvious and requires more subtle treatment (Boozer 1982, Cary and Littlejohn 1983).

In the three dimensional magnetic field case the introduction of a vector potential of the form $\vec{A} = \varphi\nabla\theta + \chi\nabla\phi + \nabla f$ guarantees the Hamiltonian nature of the problem (Boozer 1992) albeit at the cost of introducing four potential functions $\psi, \theta, \phi,$ and χ. Calculating the magnetic field from $\vec{A}$ in the usual way yields, $\vec{B} = \nabla \times \vec{A} = \nabla\psi \times \nabla\theta + \nabla\phi \times \nabla\chi$. Physically, the potentials are interpreted as the toroidal magnetic flux ψ, the poloidal magnetic flux χ, and toroidal and poloidal angles ϕ and θ. The Hamiltonian equations for what are now magnetic field lines can be written as,

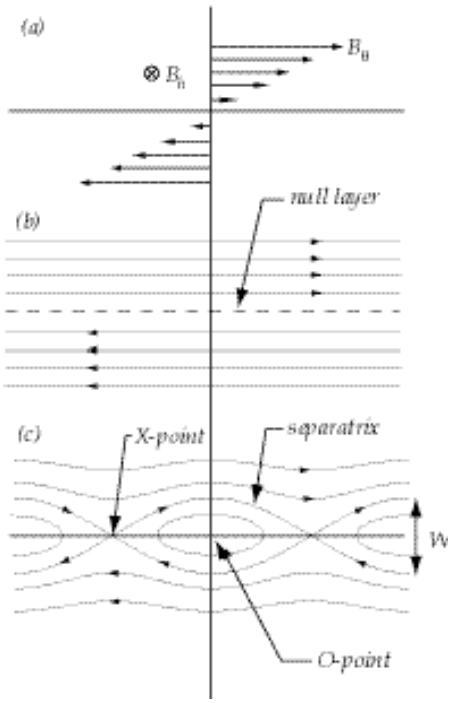

Figure 1.5*(a)* Magnetic field near a rational surface in a tokamak is composed of helical and sheared components, with a *(b)* null layer located at the position of the rational surface. *(c)* A magnetic island forms when a resonant perturbation is present

$$d\psi/d\varphi = \partial\chi/\partial\theta, \qquad (1.2)$$

$$d\theta/d\varphi = -\partial\chi/\partial\psi, \qquad (1.3)$$

with the poloidal flux function the magnetic field line Hamiltonian. Recognizing this fact then allows us to invoke the generic Hamiltonian response that rational surfaces under resonant

perturbation break up into phase space island chains (Lichtenberg and Lieberman 1992). In the magnetic field case these phase space islands are *magnetic islands* in three-dimensional physical space.

Consider the magnetic field depicted in figure 1.5*(a)* with equilibrium flux surfaces in *(b)*. What would the radial width of an island be if it does form? The width of the resulting vacuum magnetic island given a resonant perturbation b_r is (Batemen 1978),

$$\frac{W_{vac}}{r_s} = 4\sqrt{\frac{L_s}{mr_s}\frac{b_r}{B_\phi}}. \qquad (1.4)$$

Here L_s is the shear scale length of the magnetic field, r_s is the radius of the resonant surface, m the poloidal mode number of the perturbation, and B_ϕ the toroidal magnetic field strength. For typical tokamak parameters relatively small perturbation $b_r/B_\phi \sim 1\%$ can give a large normalized island width, $W_{vac}/r_s \sim 10\%$. Further inspection of figure 1.5*(c)* indicates why magnetic island formation is an important issue for magnetic confinement. The nested flux surface structure of the equilibrium field in 1.5*(b)* that insulates the plasma pressure has been *"short-circuited"* at the separatrix *x*-points shown in *(c)* thus allowing plasma to leak out of the confining field more easily. In the case of many large separate magnetic islands at distinct rational surfaces the nested flux surface topology can be destroyed altogether causing the collapse or disruption of the discharge.

Thus the generic response of a magnetic field to resonant perturbation is the formation of magnetic islands at resonant rational surfaces. These islands are important because they compromise the integrity of the confining magnetic field.

An interesting question to now consider is what happens when the magnetic field is embedded in conducting plasma? This complicates the dynamic response of the magnetic surface to resonant perturbations considerably. The presence of plasma near the resonant surface can inhibit or amplify the natural response of the magnetic field. The plasma conductivity allows local currents to flow near the rational surface that can lead to healing of the magnetic island or amplification of island size relative to the vacuum field response given by equation 1.4.

1.4 Plasma response and magnetic island formation

The natural response of vacuum magnetic fields to resonant perturbation is the opening of a magnetic island at the resonant rational surface. Near a rational surface embedded in plasma how is this vacuum response modified? This is the problem of magnetic reconnection and is germane to many areas of physics from solar flare to magneto-tail activity as well as magnetic island formation and disruptive processes in laboratory plasma.

In an ideal plasma with zero electrical resistivity magnetic field evolution is driven only by plasma flow, since $\partial\vec{B}/\partial t = \nabla\times(\vec{v}\times\vec{B})$. This fact is typically stated saying the magnetic field is frozen to the plasma (Friedberg 1987). This frozen flux relation implies that magnetic flux through an arbitrary surface that moves with the plasma fluid is constant, that is, the topology of the magnetic surfaces does not change and island formation is inhibited. Plasma response to an elliptical deformation is shown in figure 1.6. For a ideal plasma the magnetic

surfaces merely displace from the circular equilibrium as depicted in figure 1.6*(b)*. How does this response change in weakly non-ideal plasma with finite resistivity?

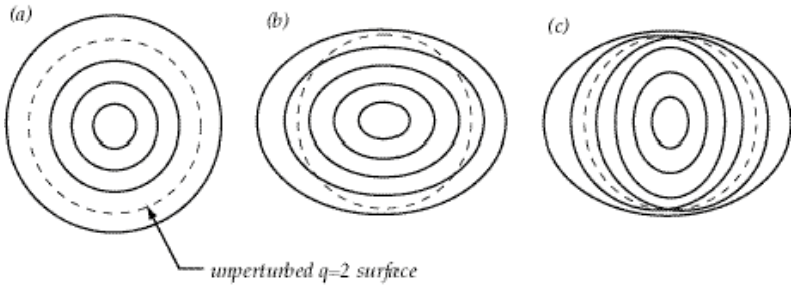

Figure 1.6*(a)*. Cross-sectional view of equilibrium flux surfaces. *(b)*. Ideal plasma response without island. *(c)*. Resistive plasma response with island formation.

Consider the classic sheared tearing layer geometry shown in figure 1.5 again. This field structure is locally equivalent to the rational surface fields in a tokamak if the helical pitch of B_h matches that of the resonance $q(r_s)=m/n$, with q the so-called safety factor or winding number of the field $q(r)=rB_\phi/R_oB_\theta$. To better understand the concept of magnetic island formation in the presence of plasma consider driving a radial flow v_r of plasma across the field B_ϑ with finite resisitivity. In resistive plasma $\vec{v}_r \times \vec{B}_\vartheta$ will drive a helical current of magnitude $j_h = v_r B_\vartheta / \eta_{//}$. The resulting Lorentz force $|\vec{j}_h \times \vec{B}_\vartheta| \sim v_r B_\vartheta^2 / \eta_{//}$ tends to oppose the original fluid motion across the magnetic field and is infinite in the limit that the plasma resistivity vanishes $\eta_{//} \to 0$. This can be thought of as the mechanism for plasma-field coupling or *freezing* of the magnetic field lines and plasma embodied in the ideal Ohm's law, $\vec{E} + \vec{v} \times \vec{B} = 0$ (White 1983). How does this inform our discussion of island formation in the presence of plasma? Slipping of

the plasma through the field and hence reconnection of the field can take place at the null layer centered on the resonant surface. Since B_ϑ vanishes at the resonance even in the presence of small resistivity the restoring Lorentz force also vanishes and hence rapid diffusion, reconnection, and magnetic island formation are still possible in a narrow resistive boundary layer about the rational surface (Furth *et al* 1962).

The preceding discussion assumed that plasma away from the rational surface was at rest. If the plasma is in motion or other driving forces are present the reconnection rate will be affected as well as the resultant island width. As an example of the effects of rotation and other external driving forces and how they might change the vacuum island width consider the case of a magnetic island driven by a static external source in a tearing stable rotating plasma.

This is the problem of error field driven reconnection of magnetic islands (Hender *et al* 1993, La Haye 1994). How does the island width change from its vacuum value in resistive rotating plasma? In this case the resultant normalized island width can be written as (for an overview see La Haye 1996),

$$\frac{W}{r_s} = \frac{W_{vac}}{r_s}\left(\frac{2m}{-\Delta' r_s}\right)^{1/2}\left(\frac{1}{1+\left(\omega\tau_{rec}\right)^2}\right)^{1/4}. \qquad (1.5)$$

The first term on the right hand side is the normalized vacuum island width W_{vac}/r_s of equation 1.4. The next two factors describe effects of the plasma as a current carrying medium rotating with respect to the static magnetic perturbation. The second factor in equation 1.5 gives the effect of the plasma

helical current response at the rational surface. Here Δ' is a measure of the magnetic free energy associated with the stable tearing mode, $\Delta' < 0$. As marginal stability is approached, $\Delta' \to 0$, the plasma amplifies island size over its vacuum value, $W/W_{vac}>>1$. The third and final term parameterizes the effect of differential rotation of magnitude ω between the rational surface where the island will form and the exterior stationary perturbation driving the island. Here τ_{rec} is the boundary layer reconnection time scale at the rational surface. Thus, plasma rotation relative to the perturbation can also have a substantial impact on island width. If the rational surface rotates quickly compared to the characteristic time scale for flux reconnection, $\omega\tau_{rec}>>1$, the driven island is highly attenuated with $W/W_{vac}<<1$. If the island is frequency locked to the stationary perturbation $\omega \to 0$ then the vacuum island can again be amplified due to the Δ' helical current response as described above.

The effect of plasma on the resulting island structure, given the simple examples above, can be quite profound. Magnetic islands can be either amplified, shielded from the equilibrium, or take on an intermediate width depending upon the exact parameters describing the plasma near and far away from the resonance. In general, the algebraic formula of equations 1.4 and 1.5 that were used to introduce and motivate magnetic island formation and the possible effects of plasma resistivity, rotation, and external free energy drive are to simplistic to capture magnetic island dynamical behavior. Instead we deal with evolution equations for the island width W and island rotation frequency ω. Island rotation frequency is described by a torque balance equation reflecting the

effects of plasma inertia, viscosity, and applied saddle coil electromagnetic torque of the form,

$$\alpha \frac{\partial \omega}{\partial t} = \beta\left(\omega - \omega_0\right) + \gamma \sin\left(\Delta\phi\right). \tag{1.6}$$

The acceleration term on the left-hand side of 1.6 represents the inertia that co-rotates with the island while the terms on the right represent the effects of plasma viscous and saddle coil torque. This island torque balance equation is studied in section 4.2.1 and compared with HBT-EP island frequency dynamics during rotation control experiments. Magnetic island width evolution is governed by a similar equation that reflects any driving sources of free energy that affect island size,

$$\frac{\partial W}{\partial t} \sim \left(\text{free energy sources or sinks}\right) \sim \Delta'(W, \omega, \Delta\phi, ...). \tag{1.7}$$

Traditionally, these are referred to as "delta prime" contributions, Δ', and can be a function of island amplitude, frequency, phase difference with other external perturbations or islands within the plasma among others, as indicated in equation 1.7. For HBT-EP islands the important terms are,

$$\frac{\mu_o}{1.2\eta}\frac{\partial W}{\partial t} = \Delta'_o\left(1 - \frac{W}{W_{sat}}\right) + \delta\cos\left(\Delta\phi\right) + \lambda\frac{\left(\omega - \omega_o\right)^2}{W^3} \tag{1.8}$$

Here changes in island width are driven by the three terms on the right–side of equation 1.8. The first represents the natural instability drive of the current profile, while the second and third represent the effects of the saddle coil and plasma inertia on island size. Magnetic island amplitude dynamics during active rotation control experiments are studied in section 4.3 of this thesis.

1.5 Resonant magnetic perturbation research

Magnetic perturbations have been applied to toroidal plasmas for several decades. This experimental program has predominantly been carried out on tokamak devices in the past, although recent experimental work has been also done on reverse field pinch (Den Hartog *et al* 1994) and stellarator (Knowlton *et al* 1997) plasmas as well. These perturbing magnetic fields have been employed for varying purposes in order to control and study magnetic island behavior. Active feedback control of magnetic island width has been studied (Bol *et al* 1974, Arsenin *et al* 1975, Navratil *et al* 1998) and discharge enhancement has been observed (Morris *et al* 1990). Magnetic island suppression and asynchronous disruption avoidance employing static perturbations (Karger *et al* 1974, Yoshida *et al* 1983, Zhao *et al* 1985) have stabilized small amplitude islands and extended discharge lifetime under certain plasma conditions. Externally generated perturbations have also been used to stimulate or induce disruptions and study the resulting disruption evolution (Bagdasarov *et al* 1893, Roberts *et al* 1991, Ivers *et al* 1995). Generation of an ergodic magnetic limiter or divertor at the plasma boundary using static magnetic perturbations as a means of edge particle and power exhaust control have been examined (Vallet *et al* 1991, McCool *et al* 1989), and are being currently being revisited employing rotating control fields (Finken 1999). Penetration of resonant error fields have been studied extensively using static perturbations during the last decade (Scoville *et al* 1991, Hender *et al* 1992) in order to understand the operational limits imposed by these locked non-rotating magnetic islands. To put the research of this thesis in proper perspective, given the broad application of magnetic perturbations outlined

above, a survey of resonant magnetic perturbation research is presented focussing on the specific application of asynchronous rotating control fields and their interaction with long wavelength magnetohydrodynamic modes.

Broadly speaking, magnetic perturbation experiments can be divided into those that actively detect the magnetohydrodynamic mode of interest in real time and use this signal to derive an appropriate response perturbation and those that apply a given control field independent of the plasma magnetic island behavior. These two categories are termed synchronous (*closed loop*) and asynchronous (*open loop*) island or mode control respectively. The work of this thesis deals only with open loop applied control perturbation signals. Details of the HBT-EP control coil geometry and driving electronics are discussed in chapter four.

Rotating resonant perturbations were first applied to toroidal plasmas in experiments on the ATC device at Princeton (Bol *et al* 1975) and the TO-1 tokamak at the Kurchatov Institute (Arsenin *et al* 1978). Measured external magnetic field fluctuations were interpreted as magnetic islands at the m/n=2/1 surface. Frequency locking of these pre-existing fluctuations to applied magnetic perturbations was reported on both devices. Effects of island growth or suppression due to the driven deviation in island frequency from the applied field were not noted. Island frequency locking to the external control perturbation was later treated theoretically (Invanov and Arsenin 1978) by invoking a nonlinear oscillator model of the island-coil interaction. Frequency locking of the pre-existing island was then interpreted as the entrainment of one oscillator (*the island*) to that of the driving oscillator (*magnetic perturbation*).

Rotating magnetic perturbations were applied to magnetic fluctuations in the JFT-2M tokamak (Oasa 1995). Measurement of impurity Carbon rotation using a neutral beam for spatial localization during these experiments showed an essentially rigid shift of the Carbon flow profile across the entire plasma minor radius. Possible reasons for the absence of a more localized interaction near the dominant rational surface (m/n=2/1 in this case) are not advanced. After switching off of the stirring perturbation, relaxation of island rotation back to its equilibrium value observed to be characterized by two time scales. A fast relaxation occurs first, τ_{fast}~ several hundred mircoseconds, and is thought to be due to rearrangement of the island structure itself. The second characteristic time is thought to be due to viscous relaxation, τ_{slow}~ several milliseconds. No effects of island amplitude during these magnetic perturbation experiments were reported.

The experiments on active rotation of magnetic islands on HBT-EP have demonstrated a simple compact coil technique whose coverage is consistent with passive wall stabilization requirements. These experiments have extended the frequency and angular acceleration range and frequency modulation characteristics used in previous island rotation experiments. This has lead to the observation of an asymmetry in the damping and growth of island size due to island frequency changes induced by applied saddle coil torque. This observed asymmetric response is consistent with a destabilizing contribution to the island width evolution equation.

1.6 Principal results and thesis outline

Using the flexible mode control system developed on the HBT-EP tokamak (Navratil *et al* 1998) for magnetic island studies the experiments reported on in this thesis have demonstrated new methods for interacting and studying the behavior of magnetic islands in tokamak plasma.

Rotational control of magnetic islands has been demonstrated over an approximate factor of two change in island frequency using a simple highly modular saddle coil set. A detailed investigation of the toroidal and poloidal torque balance near the m/n=2/1 magnetic island has been conducted to better understand island-perturbation interaction physics. It is found that the order of magnitude of the applied saddle coil torque needed to induce a given frequency change in HBT-EP islands is consistent with toroidally driven island motion. This observation supports the inclusion of poloidal flow damping physics for magnetic islands in the collisional edge plasma of HBT-EP. Experimental observation of induced m/n=1/1 mode frequency change during m/n=2/1 island rotation control indicates that the two islands rotate as a coupled magnetic structure regardless of external magnetic stirring.

Magnetic island amplitude effects are also observed during active rotation control experiments. Observation of a correlation between damping and island deceleration below its natural rotation rate and growth of island amplitude or width with acceleration during fast rotational change driven by the saddle coil electromagnetic torque has been demonstrated. This amplitude response is

consistent with simple estimates of the magnitude of ion polarization currents driven by these fast changes in island rotation, including the effects of poloidal flow damping. The observed asymmetry in growth and damping with acceleration and deceleration of these magnetic islands is consistent with a *destabilizing* inertial contribution to the island width evolution equation of motion. This observation constitutes the first experimental evidence for the destabilizing role of ion inertia in magnetic island dynamics. Finally, using an applied saddle coil perturbation of this type it has been demonstrated for the first time that the severity of disruptions is greatly diminished by applying this frequency modulated control field. When applied to disruptive plasmas core thermal and particle loss is inhibited due to maintenance of outer flux surface integrity.

Preliminary to discussing the frequency and amplitude behavior of HBT-EP magnetic islands a brief machine description of the HBT-EP tokamak, its magnetic island control system, and a brief resume of basic diagnostics is given in chapter two. Chapter three develops the necessary analysis tools used to study magnetic island behavior for this thesis. A more detailed discussion is given of those measurements used to quantify island response of both the m/n=2/1 and 1/1 islands. This includes an equilibrium current profile estimated using soft x-ray measurements to locate positions of rational surfaces within the plasma volume. Chapter four contains the main results of the frequency and amplitude behavior of islands under the action of applied rotating magnetic perturbations. Here the measured torque balance near a large amplitude HBT-EP magnetic island is developed. A description of the torque

balance model is given along with experimentally measured locking torque estimates. Chapter four also summarizes the observed frequency dependent amplitude growth and damping observed of HBT-EP magnetic islands induced by changing island rotation away from its natural rate by the applied saddle coil control fields. Estimates of the effect of inertia for HBT-EP islands is discussed in detail, and the asymmetric response observed is shown to be consistent with a destabilizing delta prime contribution to the island evolution equation. These perturbations are then applied to disruptive target plasma and found to inhibit core thermal and particle loss. Chapter five concludes this thesis with a summary of island control dynamics and thoughts for future work.

2.0 HBT-EP machine description

The High Beta Tokamak-Extended Pulse (HBT-EP) was designed and built to study active and passive control techniques applicable to long wavelength magnetohydrodynamic instabilities (Mauel *et al* 1991, Sankar *et al* 1993). In order to ameliorate the unwanted effect of these plasma performance limiting magnetohydrodynamic modes, the HBT-EP program has concentrated on demonstrating passive wall stabilization of ideal kink-type instabilities and active control of resistive tearing modes employing an external coil set able to generate resonant magnetic perturbations. This chapter briefly describes the HBT-EP tokamak, plasma formation, and basic diagnostic set used to conduct the research of this thesis. A brief summary of past HBT-EP mode control research is given next as an introduction to the machine description.

Initial studies of high β_N driven global kink–type modes and edge current gradient driven kinks demonstrated passive wall stabilization of these modes with reduced mode amplitude and extended discharge lifetime (Gates 1993, Ivers *et al* 1995). Here the normalized plasma β is defined as,

$$\beta_N \equiv \frac{\beta}{I_p / aB_\phi}, \tag{2.0}$$

with the ratio of plasma energy density to confining magnetic field energy density, or traditional plasma β given by,

$$\beta \equiv \frac{(1/V_p)\int p dV}{B^2/2\mu_o}. \tag{2.1}$$

Here p is the kinetic pressure of the plasma, B is the magnetic field strength and V_p is the plasma volume under consideration. For β measured in percent, the plasma current I_p in mega-Amperes, plasma minor radius a in meters, and the toroidal field strength on the machine axis B_ϕ in Tesla, equation 2.0 above gives $\beta_N \sim 1$ to 2 for typical HBT-EP operating parameters. In a fusion context, maximizing β is important since fusion power production scales as the plasma β squared, $P_{fusion} \sim \beta^2$. These early HBT-EP experiments correlated the suppression of kink instability occurrence, lengthened discharge lifetime, and higher operational β_N performance critical to economical fusion energy production when the movable conducting wall segments were inserted near the plasma surface for maximum passive stabilization.

Subsequent wall stabilization work elucidated wall influence on disruption dynamics (Kombargi 1997), compared experimental measurements of equilibrium and stability of wall stabilized discharges with ideal MHD computational modeling (Garofalo 1997, Garofalo *et al* 1998), and measured the effects of segmented wall symmetry and coverage on kink mode suppression (Eisner 1998). With these quickly growing modes wall stabilized attention focussed on residual instabilities that affected plasma behavior. In order to deal with these more slowly growing instabilities not effected by a close conducting boundary, an active means of interacting with these internal instabilities was developed on the HBT-EP tokamak. This active control system uses an external coil set designed to generate an applied field in resonance with the equilibrium magnetic field line pitch of the dominant m/n=2/1 internal instabilities observed

on HBT-EP. These modes manifest themselves as a magnetic island chain in the edge plasma of HBT-EP.

The first resonant magnetic perturbation experiments to influence m/n=2/1 mode behavior on HBT-EP demonstrated magnetic island braking, locking, and induced plasma disruption (Ivers *et al* 1994). A capacitor bank driven perturbation was used in these early experiments, creating a static non-rotating applied magnetic field in the laboratory frame of reference. Single-phase standing wave perturbations were next applied to the coil set and characteristic island frequency modulation was observed (Mauel *et al* 1996). Later work initiated studies of magnetic feedback control of resistive tearing mode amplitude and frequency employing a rotating magnetic perturbation generated by a two-phase saddle coil set (Ivers *et al* 1995, Mauel *et al* 1998, Navratil *et al* 1998). Xiao has performed a mode structure analysis of MHD modes during both passive wall stabilization experiments and active rotation control of magnetic islands (Xiao 1998). These rotating control magnetic fields have been used in an extensive study of active, synchronous feedback (Nadle 2000) and its associated phase instability (Nadle *et al* 2000). Taylor has investigated the effect of magnetic islands on local HBT-EP plasma behavior using Mach-Langmuir probe apparatus (Taylor 2000). These measurements confirmed induced ion flow change during the rotation control or magnetic stirring of HBT-EP islands.

Current HBT-EP experimental work aims at influencing these long wavelength magnetohydrodyanmic modes using a hopefully synergistic combination of passive and active control techniques. The implementation of a so-called *"smart"*

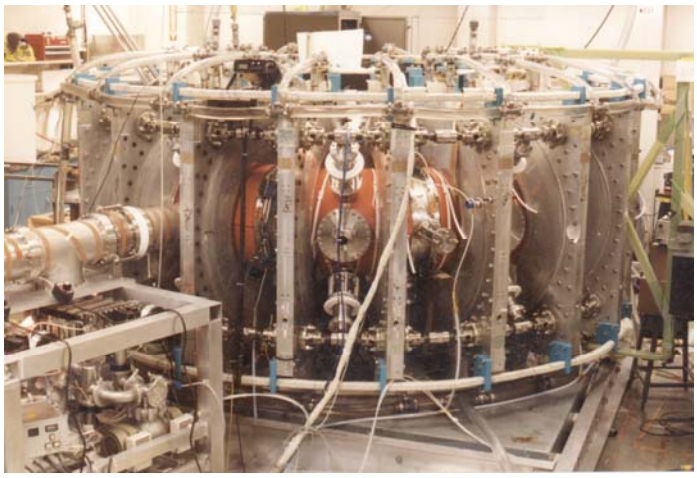

Figure 2.0 North-eastern view of the High Beta Tokamak-Extended Pulse (HBT-EP) at Columbia University Plasma Physics Laboratory.

or *"intelligent"* shell concept has shown promising initial ability to control resistive wall kink modes (Cates *et al* 2000). Next, the HBT-EP tokamak and its basic parameters are discussed as well as the target plasmas developed for the study of magnetic islands under the action of externally applied rotating resonant magnetic perturbations.

The HBT-EP tokamak is a high aspect ratio device with several novel features including a movable conducting segmented wall, quartz insulating vacuum chamber breaks for fast magnetic field penetration and a flexible saddle coil set for magnetic island studies. A brief discussion of the equilibrium magnetic field coil systems, vacuum chamber and pumping system, and basic plasma diagnostics is given. More detailed discussion of specific diagnostics and their analysis used in measurement of specific m/n=2/1 and 1/1 magnetic island characteristics are reserved until chapter three. The details of the saddle coil system and driving electronics are given in chapter four.

The HBT-EP tokamak (see figure 2.0) is an Ohmically heated device capable of sustaining positive loop voltage for a 10msec period. Typical discharge lifetimes range from several milliseconds to ~7 to 12msec depending upon the specific operational regime in question. Table 2.0 lists characteristic operating parameters of the device for the discharges examined in this thesis. The plasmas created here were run in a configuration with produced a sustained large amplitude m/n =2/1 magnetic island. This mode would typically go naturally unstable at approximately 2 to 3msec into the discharge lifetime and saturate at ~3 to 5G amplitude measured at the edge of the plasma. The typical natural rotation rate of the magnetic islands is approximately ~8 to 10kHz. Figure 2.1. shows a side view of HBT-EP tokamak and its torodial, vertical, and Ohmic field coil sets. The torodial field is limited to 3.3kG on axis due to voltage and impulsive force considerations on the coilset. The Ohmic circuits and coil system are the most complex and allow for a variety of plasma formation techniques and plasma current ramp rates (see Gates 1993). This allows flexibility in the generation of different plasma instabilities by effectively varying the resultant current profile in the plasma. This technique has been used extensively in wall stabilization studies in the past (Ivers *et al* 1995). The plasma is kept in major radial force balance by the vertical field coil system. These coils make a magnetic field that pushes back in on the plasma hoop force when crossed into the equilibrium plasma current. Balancing these two forces

Major radius, R_o	0.92-0.97 m
Minor radius, a	0.15-0.19 m
Plasma current, I_p	≤ 25 kA
Torodial field, B_φ	≤ 3.3 kG
Pulse length	5-15 ms
Temperature, $<T_e>$	≤70 eV
Density, n_e	~1x10^{13} cm^{-3}
Alfven time, $\tau_A=a(\mu_o\rho/B_\theta^{2)1/2}$	~0.5 x10^{-6} sec
Resistive diffusion time, $\tau_R=(\mu_o a^2)/\eta$	~10 x10^{-3} sec

Table 2.0 Typical HBT-EP operating parameters for magnetic island studies.

via the magnitude of the vertical and Ohmic fields determines the gross major radial position of the plasma.

A distinguishing feature of the tokamak is its segmented movable wall shown in figure 2.2. Each Aluminum shell or wall segment is 1 cm thick and can be retracted from the plasma surface a radial distance of ~8cm. A typical plasma with a major radius of R_o=92cm and minor radius of a=15cm is shown in figure 2.3 along with the segmented wall in its fully inserted position for maximum wall stabilization. The wall time constant for equilibrium field penetration is ~8ms. For the m/n=2/1 magnetic islands studied in this thesis, the product of island angular frequency and wall time constant is approximately $2\pi f_{2/1}\tau_{wall}$~50. This fact allows the neglect of wall torque contributions to the experimental torque balance examined in chapter 4. The actual plasma boundary is defined by

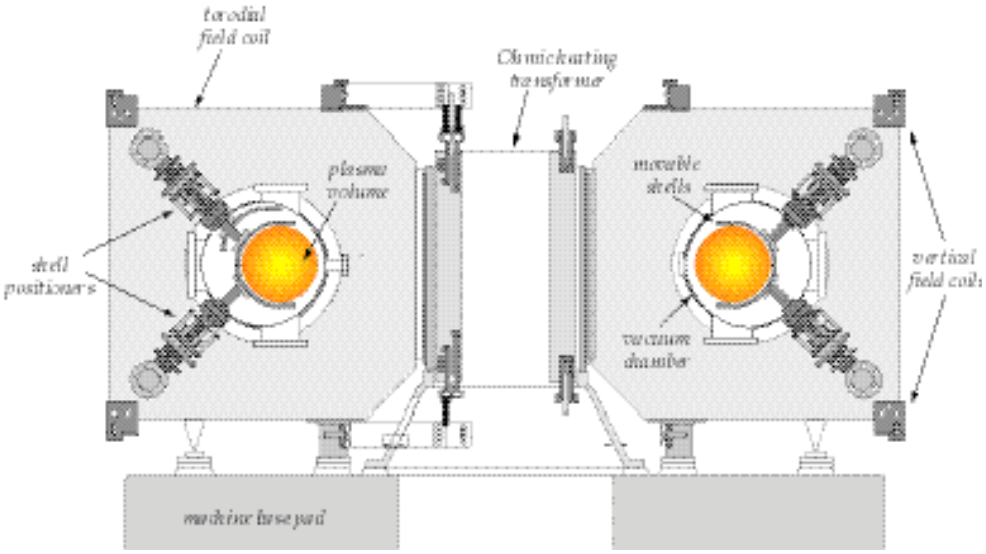

Figure 2.1 Side view of the HBT-EP tokamak showing major machine coil systems, vacuum chamber structure and typical plasma volume cross section.

contact with several material boundaries, termed limiters. The limiters are made of six 3/8″ stainless steel blades mounted on spool vacuum chamber sections separated toroidally by 144° (see Kombargi 1998).

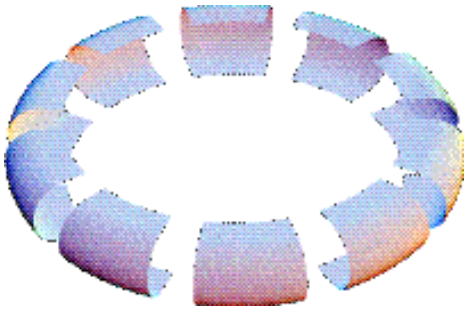

Figure 2.2 Conducting shell segments in their fully inserted configuration.

The target plasmas sought for resonant magnetic perturbation experiments were all generated with the movable conducting shells in their fully inserted position with the wall ~1cm from the surface of the plasma for maximum wall stabilization. Discharge cleaning plasmas were formed to *"scrub"* the limiters and nearby shell segments at the start of each run day. This procedure ensured relatively reproducible target plasmas with a large saturated m/n=2/1 magnetic island in the plasma edge for resonant magnetic perturbation experiments. These target HBT-EP plasmas were typically well centered with a major radius of ~93 to 95cm.

A top view of the HBT-EP tokamak is provided in figure 2.4 showing the position of the major machine diagnostics. Those diagnostics used in detail specifically for magnetic island diagnosis are described along with their analysis techniques in the next chapter on HBT-EP magnetic *"islandography"*

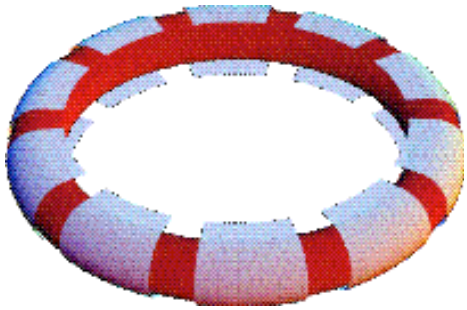

Figure 2.3 Perspective view of plasma with shell segments fully inserted.

or the study of magnetic islands. These diagnostics include an external pickup coil array to measure poloidal field fluctuations and soft x-ray fan and tomography arrays for use in measuring island induced emissivity perturbations.

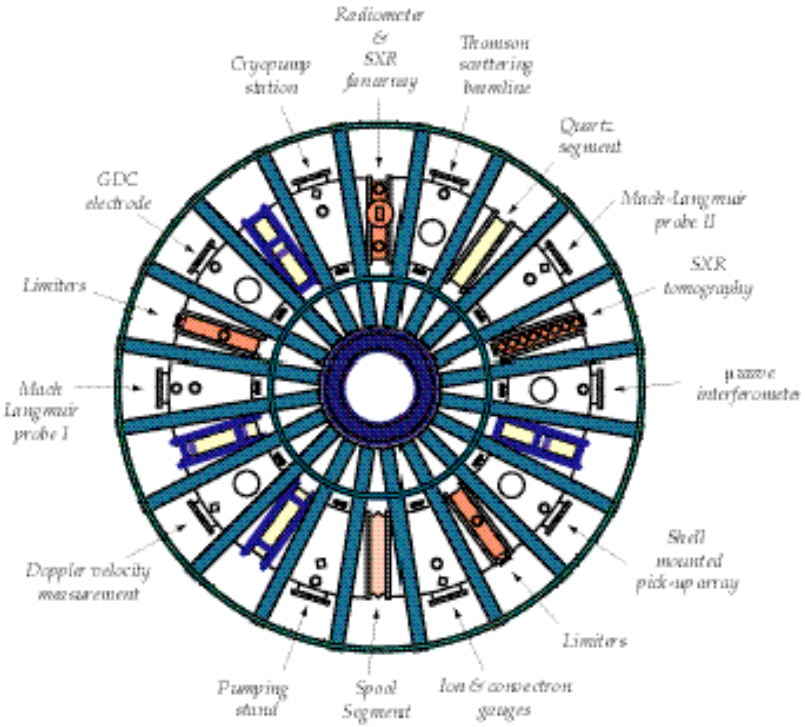

Figure 2.4 The HBT-EP tokamak showing main diagnostic locations. Quartz sections are shown in yellow with saddle coils in blue at same toroidal positions. Stainless steel "spool" segments are shown in orange.

3.0 HBT-EP magnetic islandography

In this chapter we study the properties of long wavelength magnetic fluctuations observed on the HBT-EP tokamak. These external magnetic fluctuations are interpreted as arising from a magnetic island chain located on the resonant q=2 surface inside the plasma. This inference is confirmed by internal soft x-ray emissivity measurements which show a local phase inversion layer at the position of the mode rational surface (Xiao 1998). This emissivity inversion surface is a result of the pre-existing plasma electron density or temperature profile adjusting to the details of the new magnetic topology introduced by the island structure. Phase inversion observations are a primary method for distinguishing between simple flux surface distortion or displacement which does not change magnetic surface topology and the splitting or tearing of a surface which does alter the magnetic topology of the configuration (recall figure 1.6 of the introduction).

First details of the external magnetic analysis used to measure the m=2 component of the fluctuation spectrum is described. The direction of natural m=2 mode propagation poloidally and in the electron drift direction is shown. Next, interpretation of soft x-ray emissivity measurements as they relate to diagnosis of magnetic islands is examined and details of the tomographic and core fan array detectors are given. The analysis of m/n=2/1 island builds on previous work of Xiao (1998). These soft x-ray measurements are then used to give an estimate of the position of the q=2 surface. This is later used to construct an average current density profile in section 3.4. Spectral quantities of the m=2

emissivity fluctuation are constructed using the Hilbert transform technique of Taylor and coworkers (1999) to confirm corotation of the m=2 emissivity perturbation and magnetic perturbation. Next the analysis of m/n=1/1 island emissivity fluctuations is explained. This uses a robust combination of singular value decomposition (SVD) as advocated by Dudok de Wit (1994) and Hilbert transformation (Taylor *et al* 1999) to extract m/n=1/1 mode spectral behavior. The chapter concludes by pulling these three diagnostic sections together in constructing an approximate current density and q-profile to estimate magnetic island widths using the vacuum island width formula discussed in the introduction.

3.1 External magnetic mode analysis

In this section the basic magnetic modal analysis used to diagnosis m/n=2/1 magnetic islands on HBT-EP is described. The natural island propagation direction is observed for target plasmas that will later be used in the rotational control studies presented in chapter four.

An array of inductive pick-up coils located on the inner side of the conducting shells is used to measure the fluctuating and equilibrium values of the poloidal magnetic field. These probes have been used extensively in past experiments to characterize the magnetohydrodynamic behavior of HBT-EP plasmas (Garofalo 1997). For the purposes of this thesis the extraction of the fluctuating m=2 component serves as one of the main indicators of magnetic island behavior, giving a measure of mode amplitude, phase and frequency. The circular geometry and high aspect ratio of HBT-EP plasmas minimizes many of the typical difficulties encountered in external magnetic diagnosis of MHD fluctuations (Hammet and McGuire 1982, Strait 1995). This allows a relatively simple procedure to extract the Fourier component of interest, in this case m=2. The $sin2\theta$ and $cos2\theta$ Fourier components of the fluctuating magnetic field, $h(t) = a(t)\sin[2\theta(t)]$ and $g(t) = a(t)\cos[2\theta(t)]$, are derived from the total signal, after equilibrium subtraction, by a least squares fit to the data using singular value decomposition. The $sin2\theta$ and $cos2\theta$ components are then used to construct the magnitude and phase of the m=2 fluctuation via,

$$\tilde{b}_\theta(t) = \sqrt{h(t)^2 + g(t)^2} = a(t) \qquad (3.0)$$

$$\varphi(t) = \tan^{-1}\left(\frac{h(t)}{g(t)}\right) = 2\theta(t), \tag{3.1}$$

$$f_{2/1}(t) = \frac{1}{2\pi}\frac{d\varphi}{dt}. \tag{3.2}$$

Figure 3.0 shows the magnitude and phase results of the above calculation for a typical target plasma. The phase information obtained form the quadrature analysis is used to derive the m=2 component frequency using a simple least squares fit over a specified time window in the following chapter. The phase information described in the preceding section shows the poloidal direction of mode propagation from the outboard side of the tokamak to the inboard side. This direction has also been confirmed by plotting the total fluctuation measured by the pickup coil array (Nadle 2000). Toroidal propagation is in the direction counter to the equilibrium plasma current (Ivers *et al* 1995). These observations confirm that the magnetic field fluctuation rotates in the electron drift direction.

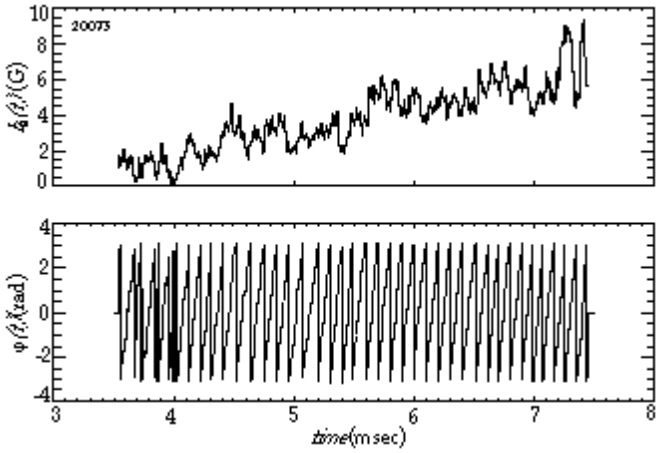

Figure 3.0 Amplitude and phase of the m=2 magnetic field fluctuation measured at the edge of the plasma.

3.2 Emissivity measurements of magnetic islands

3.2.1 An introduction

Here observation of soft *x*-ray radiation is described that gives an internal measurement of the *m*=2 mode structure in the edge region and the *m*=1 mode in the core plasma of HBT-EP. These emissivity observations are made using two complementary arrays of soft *x*-ray detectors. A sixteen channel fan array (Kombargi 1997) that resolves core sawtooth oscillation and *m*=1 mode behavior and a thirty-two channel tomographic array (Xiao 1998) with good edge sensitivity for diagnosis of *m*=2 island induced emissivity fluctuations.

First, the functional form of the emissivity and its relation to plasma parameters such as temperature and density is briefly reviewed. Unfortunately, even in a simple approximate form the emissivity is a convolution of several plasma parameters that can be spatially and temporally varying. In the limit where the impurity content or average ion charge state in the plasma is low and the ionic species are not significantly changing in time the emissivity is predominantly a function of electron temperature and density. Even in the context of this simplification the chord integrated nature of the emissivity measurement precludes a simple interpretation of the emissivity fluctuation in terms of associated local temperature and density fluctuation amplitudes induced by the magnetic island. After discussion of the *m*=2 island induced soft *x*-ray fluctuations, details and diagnosis of the core m/n=1/1 mode and associated core emissivity relaxation oscillations or sawteeth are presented.

The behavior of the m/n=1/1 mode in the core of HBT-EP discharges is diagnosed using the fan-array of soft x-ray detectors. To separate sawtooth activity from 1/1 mode dynamics singular decomposition of the fan-array channel time series into distinct biorthogonal eigenfunctions is used. These singular eigenmodes deconvolve the m/n=1/1 mode from the n=0 and m=0 sawtooth rise, crash, and inversion. This deconvolution then allows calculation of m/n=1/1 mode amplitude, phase, and frequency that is later used in m/n=2/1 magnetic island interaction studies with an external resonant magnetic perturbation.

This m=2 and m=1 emissivity analysis is also used in section 3.4 to construct an average current density and q-profiles that are then used in estimation of m=2 magnetic island width calculations. The functional form of the plasma emissivity and relevant plasma parameter scalings are discussed next.

3.2.2 Emissivity and its relation to plasma parameters

Plasmas emit radiant energy over a broad spectral range from the near infrared up to photon energies of order the plasma electron temperature (Bekefi 1966). The HBT-EP tokamak is equipped with two soft x-ray diagnostics that are used to measure plasma photon emission in the $\hbar\omega$ ~20 to 150eV energy range. A sixteen channel fan-array that measures core sawtooth and m/n=1/1 activity and a thirty-two channel tomography system that is able to resolve emissivity fluctuations at the m/n=2/1 surface near the plasma edge. The dominant physical processes leading to this emission are free-free, free-bound, and bound-

bound electron-ion interactions termed Bremstrahlung, recombination radiation, and line radiation respectively. For simplicity only the continuum (bremstrahlung and recombination) contribution to the emissivity will be discussed in detail here.

Following the discussion given by Hutchinson (1993), the total continuum radiation from electron-ion collisions for the i*th* ionic species can be written as,

$$j_i(\omega) = Z_i^2 n_e n_i \left(\frac{e^2}{4\pi\varepsilon_o}\right)^3 \frac{4}{3\sqrt{3}m_e^2c^3}\sqrt{\frac{2m_e}{\pi T_e}}\exp\left[-\left(\frac{\hbar\omega}{T_e}\right)\right] \times \left\{\bar{g}_{ff} + G_n\frac{\xi}{n^3}\left(\frac{\chi_i}{T_e}\right)\exp\left[\frac{\chi_i}{T_e}\right] + \sum_{\nu=n+1}^{\infty} G_\nu \frac{2}{\nu}\left(\frac{Z_i^2 R_y}{\nu^2 T_e}\right)\exp\left[\frac{Z_i^2 R_y}{\nu^2 T_e}\right]\right\} \quad . \quad (3.3)$$

The first term in curly brackets is the free-free contribution and the second and third terms represent free-bound transitions to the lowest unfilled energy level and to all other available levels respectively of the given ion. This radiation results from the electron accelerating and decelerating in the attractive Coulomb field of the ion in question. If the total energy of the electron-ion system is positive the electron is merely deflected (*free-free transition*) by the ion Coulombic field, while a negative total energy implies the electron is captured (*free-bound transition*) and recombines with the ion. Here,

$$\begin{aligned} Z_i &\equiv \text{charge state of the i}th\text{ ion} \\ n_i &\equiv \text{number density of the i}th\text{ ion} \\ g_{ff} &\equiv \text{free - free Gaunt factor} \\ G_k &\equiv \text{free - bound Gaunt factor for k}th\text{ level} \\ R_y &\equiv \text{Rydberg energy } = 13.6eV \end{aligned} \quad (3.4)$$

$\chi_i \equiv$ ionization potential of unrecombined ion

$\xi \equiv$ available states in lowest level (3.4)

and, the other symbols have their usual meaning. The main temperature dependence comes through the exponential terms, which depend sensitively on electron temperature, $j \sim \exp(-\omega/T)$, and the particular ionic configuration, $j \sim (Z^2 R_y/T)\exp(Z^2 R_y/T)$. The emissivity also scales strongly with density. For the majority deuterons we have $j \sim n^2$. The above equation pertains to a single ionic species in the plasma, say an oxygen impurity or perhaps the majority plasma deuterons. For multiple species the emissivity must be summed over each particular ionic configuration and no general simplification of equation 3.3.1 occurs. If recombination is unimportant the sum simplifies to the emission being proportional to the average or effective ion charge state of the plasma, denoted Z_{eff}. The definition of this effective ion charge state is

$$Z_{eff} \equiv \sum_i n_i Z_i^2 \Big/ \sum_i n_i Z_i \,. \tag{3.5}$$

For HBT-EP conditions, we expect that $Z_{eff} \leq 2$ since high-Z impurity states that might inflate the average ion charge are not accessible due to the relatively modest temperature conditions of the device. Although the impurity composition is unknown, we will take $Z_{eff} \sim 1.5$ as typical of the discharges presented here. Thus we see that the plasma emissivity is a sensitive function of electron temperature, density and ionic constitution of the plasma. For the arrays employed on HBT-EP both the bremstralung and recombination terms discussed here are expected to contribute to the observed emissivity. Bound-bound state transitions or line radiation not explicitly discussed will also contribute to the observed emissivity. The complicated dependence of the

emissivity on electron temperature and density make it difficult to interpret in terms of simple profile change of either parameter. Next details of the tomographic array are given and the analysis and correlation of the observed edge emissivity fluctuations with the external magnetic measurements of the m=2 island are described.

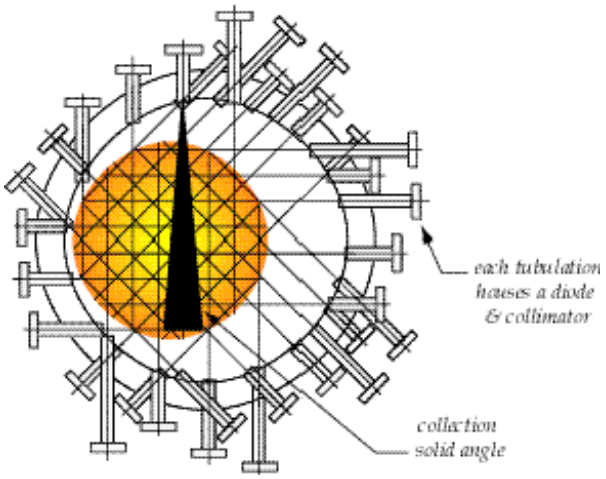

Figure 3.1 Tomographic array channel arrangement and typical solid angle

3.3.2 *Soft x-ray m=2 magnetic island observations*

A thirty-two channel soft x-ray detector system has been developed on the HBT-EP Tokimec with good edge sensitivity for q=2 diagnosis (Xiao 1998). This tomographic array employs specially designed and manufactured photo-detectors with a thin film filter composite of Zr/Ti/C deposited directly onto the diode surface (Xiao and Navratil 1996). The channel spatial distribution is shown in figure 3.1. The array consists of four sets of eight channels with horizontal, vertical, and 45 degree above and below the midplane

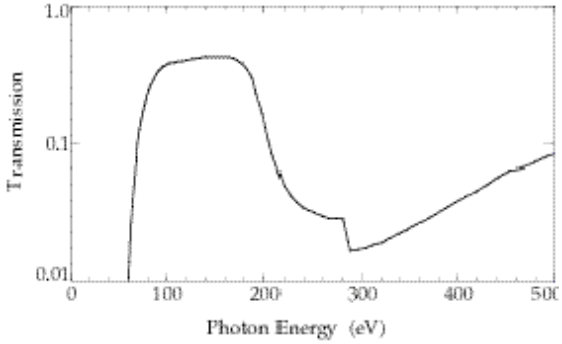

Figure 3.2 Calculated transmission of Zr/Ti/C composite filter as a function of photon energy(after Xiao 1998).

views. Chordal spacing for each of the eight channel sets is 4 cm. The typical channel width mapped to the midplane of the tokamak is approximately ~4cm. The calculated transmission for the composite filter is shown in figure 3.2.

Typical raw signals measured using the top 45^{o} array are shown in figure 3.3. The signals are composed of a slow equilibrium rise with small fluctuations present riding atop the equilibrium signal. Two important signatures are observable in contour plots of the total emissivity signal and of the fluctuating component. The contour plots of figure 3.4. show that the oscillation that is present on several of the channels with varying amplitude is even-*m* in nature since both the inboard and outboard major radial sides of the plasma have the same phasing. Also there is evidence of propagation of the fluctuation since a small phase shift is observable in the total emissivity contour edge oscillations. Fluctuation propagation is more evident in the contour plot of the emissivity perturbation shown in figure 3.4*(a)*. Here the equilibrium emissivity contribution has been subtracted using a moving box car average over a 200 microsecond window. Contour propagation from the outboard to inboard

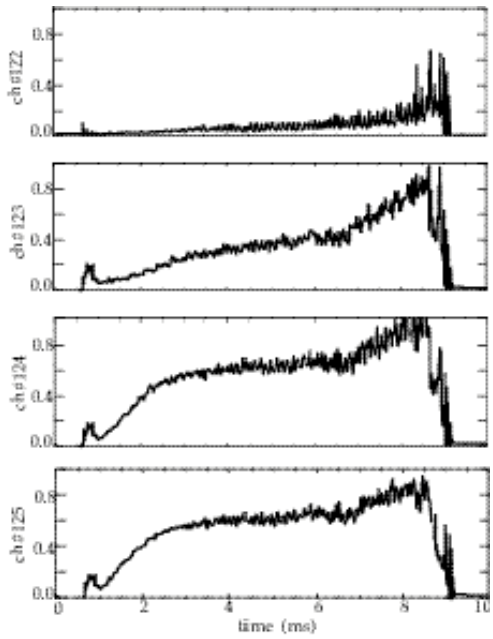

Figure 3.3 Typical unprocessed soft *x*-ray emissivity fluctuations measured by the tomographic array. Note equilibrium rise and fluctuating component are present.

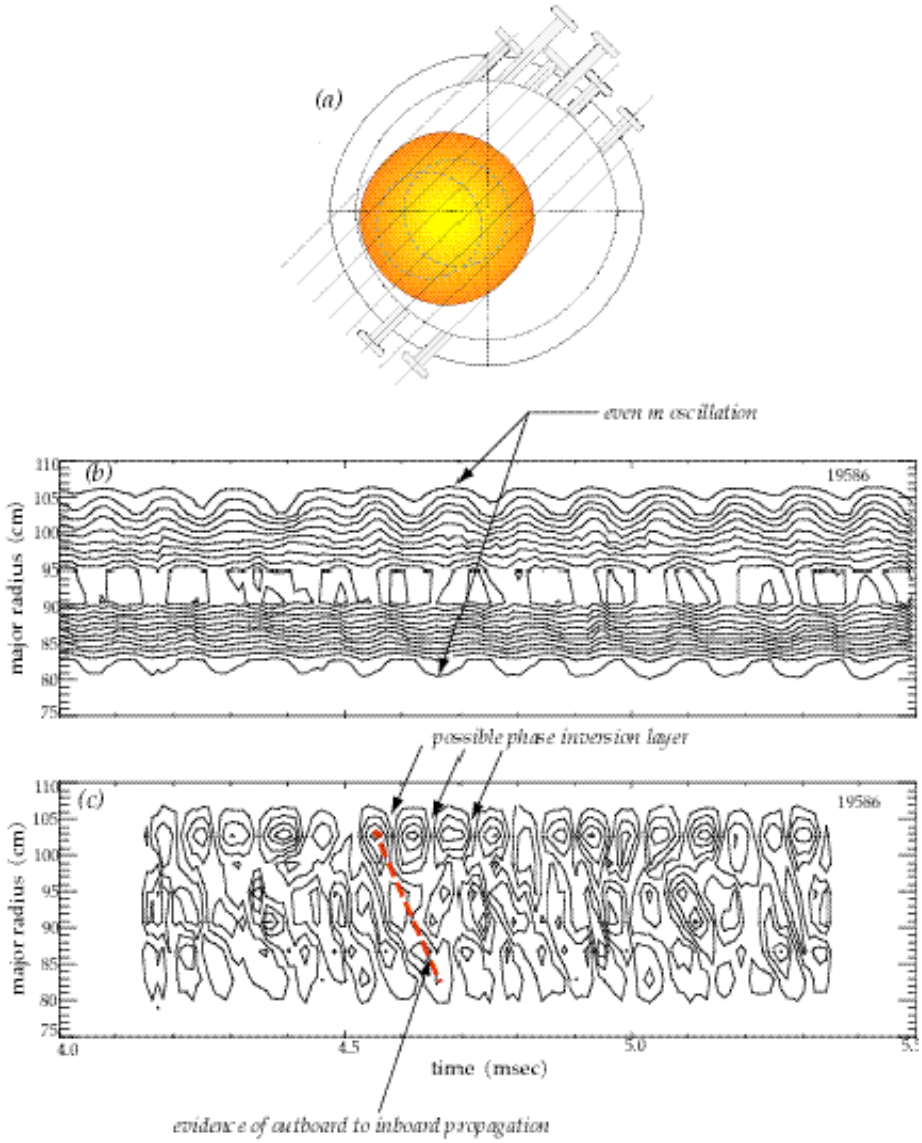

Figure 3.4*(a)* Eight viewing chords of the 45 degree top array *(b.)* Contour plot of the total emissivity ot the top array shown in *(a)* versus tangent radius. *(c.)* Perturbed emissivity showing fluctuation propagation and phase inversion.

major radius is observed along with a possible phase inversion layer most obvious on the outboard profile side. The propagation direction is consistent with the previous magnetic analysis presented in section 3.1.

The fluctuation phasing from channel
degrees is seen most clearly in the raw s
characteristic of a magnetic island indu
noted by Xiao 1998. The soft *x*-ray sign
indicative of a magnetic island structur
why the diagnostic signature of an islar
phase of the soft *x*-rays, consider a map
resonant rational surface, as depicted ir

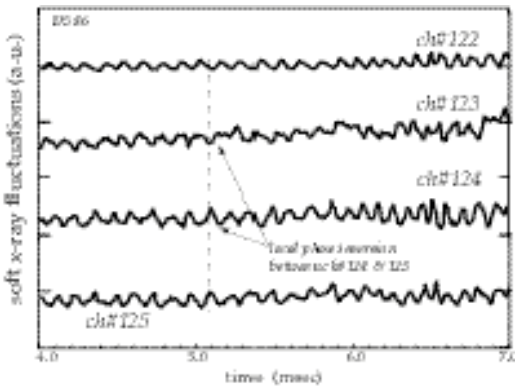

Figure 3.5. Unprocessed soft *x*-ray fluctuations showing local phase inversion signature of a magnetic island

n

flux surfaces are equipotential surfaces of the plasma parameter being measured, say temperature or density for concreteness sake. This implies that the interior of the island is at a constant value of temperature and density in the absence of sources and sinks. Magnetic island flux surfaces are depicted in figure 3.6 along with the positions of several localized point measurements. As the island moves relative to the position of the point measurement the signal fluctuates in a characteristic way dependent upon its location relative to the island separatrix. The expected fluctuation at the indicated points are shown below the island flux plot. The fluctuation amplitude is at a maximum for a measurement made an island half width away from the unperturbed rational surface. Note the inverted diagnostic phasing in moving across the island in minor radius. This inversion is a consequence of profile equilibration on the reconnected island flux surfaces. These are the signal characteristics if the island width, *W*, is greater than the inter-channel spacing, δx. Alternately, if the island width is smaller than the channel spacing, $W < \delta x$, the diagnostic signals will still show a phase inversion although the clipped portion of the waveform will not be evident because the

interior of the island is not sampled. For the soft *x*-ray signals shown in figure 3.5 the chordal spacing is $\delta x \sim 4\text{cm} \sim W$. Any observation of signal clipping will most likely be washed out by integration effects of the large channel spacing and finite solid angle of the diagnostic channels.

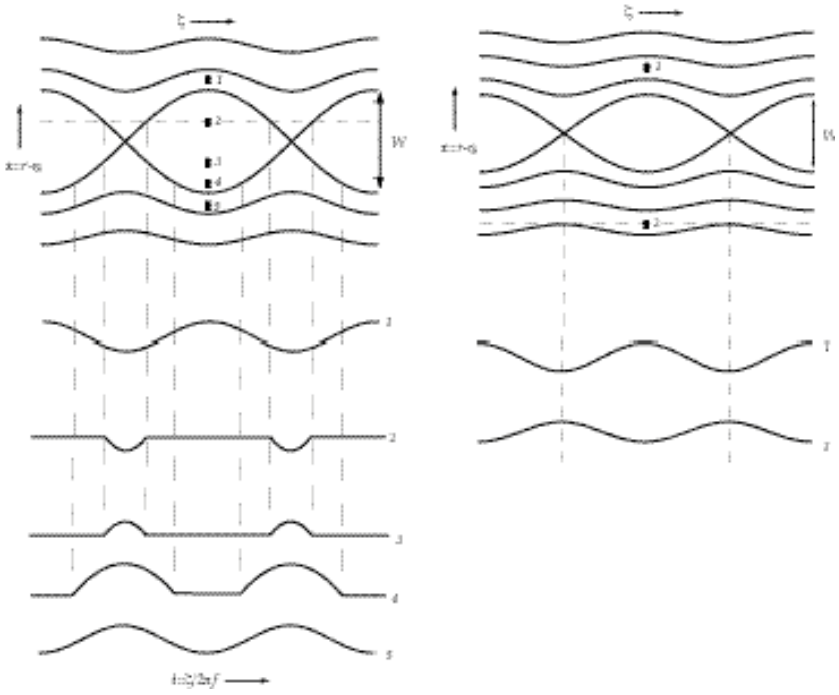

Figure 3.6. Schematic representation of local island induced fluctuations measured at various locations relative to the island structure. Profile flattening inside of the island separatrix has been assumed in constructing the fluctuations. Phase inversion is still observable for islands smaller or of the order of channel spacing.

3.3 Sawtooth oscillations and m/n=1/1 mode diagnosis

In this section an analysis method of core soft *x*-ray emissivity measurements is developed that allows diagnosis of the m/n=1/1 instability in HBT-EP sawtoothing discharges. This analysis allows study of m/n=1/1 mode behavior during resonant magnetic perturbation experiments described in chapter five. There m/n=1/1 mode frequency is used as an indicator of change in core plasma rotation during external resonant magnetic perturbation experiments. This analysis was developed to allow measurement estimates of the extent of core viscous coupling to rotational change induced at the q=2 surface by the applied magnetic perturbations. This attempt to quantify viscous diffusion into the core was foiled due to the observed co-rotation of the m=1 and m=2 islands. Useful information is still obtained, however, and the implications of induced core rotation to the perturbed torque balance of chapter four will be discussed in section 4.2.4.

In addition to core rotation the position of the q=1 surface inferred from the m=1 emissivity perturbation analysis is also used to construct an average current density and *q(r)* profile in conjunction with m=2 emissivity fluctuations observed on the tomographic array and q^* measurements in section 3.4. These average profiles are then used to constrain the slope of the *q(r)* profile at the m/n=2/1 surface, $\left(dq/dr\right)_{q=2}$, in m=2 island width calculations in section 3.4.2.

Extraction of m/n=1/1 mode behavior in the central region of HBT-EP discharges is accomplished using a fan array (Kombargi 1997) of soft x-ray detectors. Singular value decomposition of the fan-array channel time series into distinct biorthogonal spatial and temporal eigenmodes proves useful in separating m/n=1/1 mode behavior from sawtooth activity. Calculation of the amplitude, phase and frequency of the m=1 mode from these biorthogonal eigenmodes is accomplished using Hilbert transformation as described in the m=2 emissivity analysis. Comparison of the inferred m=1 rotation frequency with the external magnetic analysis of the m=2 island previously presented is made. Here it is found that the m=1 mode in the plasma core propagates at the same frequency as the m=2 island in the edge plasma. Finally, this section concludes with a discussion of the implications of the observed equality of the m=1 and m=2 mode frequencies as to whether equilibrium island rotation in HBT-EP is predominantly torodial or poloidal in direction. First, the characteristics of the fan-array camera of soft x-ray detectors are briefly discussed in the context of m=1 mode detection and sawtooth observations.

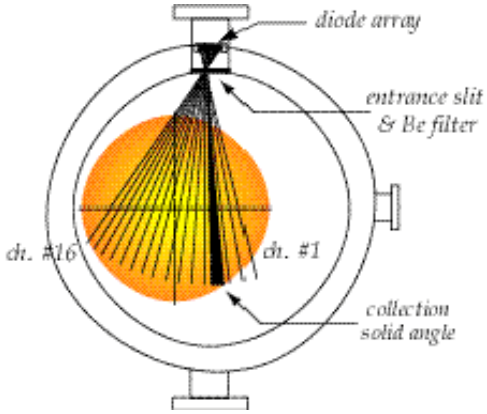

Figure 3.10 Cross-sectional view of the fan-array of soft x-ray detectors along with channel viewing chords.

A fan-array camera of soft x-ray detectors, originally developed and used to characterize emissivity fluctuations during wall stabilization experiments (Ivers

et al. 1996, Kombargi 1997), views the central core plasma region of the HBT-EP device. A spatial map of the sixteen channel array is depicted in figure 3.10. Channel spacing is 2cm on the midplane of the tokamak. The channel width due to finite collection solid angle is also approximately ~2cm on the tokamak midplane. At the diode housing entry window, a 400nm thick Beryllium filter absorbs low energy visible and ultraviolet light. The calculated transmission function of this filter is shown in figure 3.11 The filter assembly thus allows photons in the energy range of E_{ph}~40 to 111eV to pass and excite photo-carriers at the diode surface. The reduction in transmission for E_{ph}>111eV is due to strong K_{edge} absorption of the Beryllium. Details of the design and calibration of this diagnostic are given in Kombargi (1997).

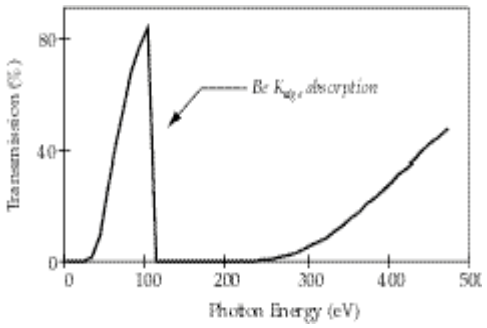

Figure 3.11 Calculated transmission of the 400nm thick fan-array Beryllium filter(after Kombargi 1997).

Typical raw signals are shown from the central ten channels of the sixteen channel fan array in figure 3.12. Note the wide variety of temporal and spatial scales involved. The plasma density measured using microwave interferometry is essentially constant after ~1ms into the discharge. Thus the equilibrium rise of the soft *x*-rays reflects an increasing electron temperature due to Ohmic power deposition with $\varepsilon \sim Z_{eff} n_e^2 \sqrt{T_e}$. This predominantly heats the plasma electron fluid and gives rise to the overall radial profile that can be distinguished in the raw signals. Sawtooth, razor-like, oscillations are

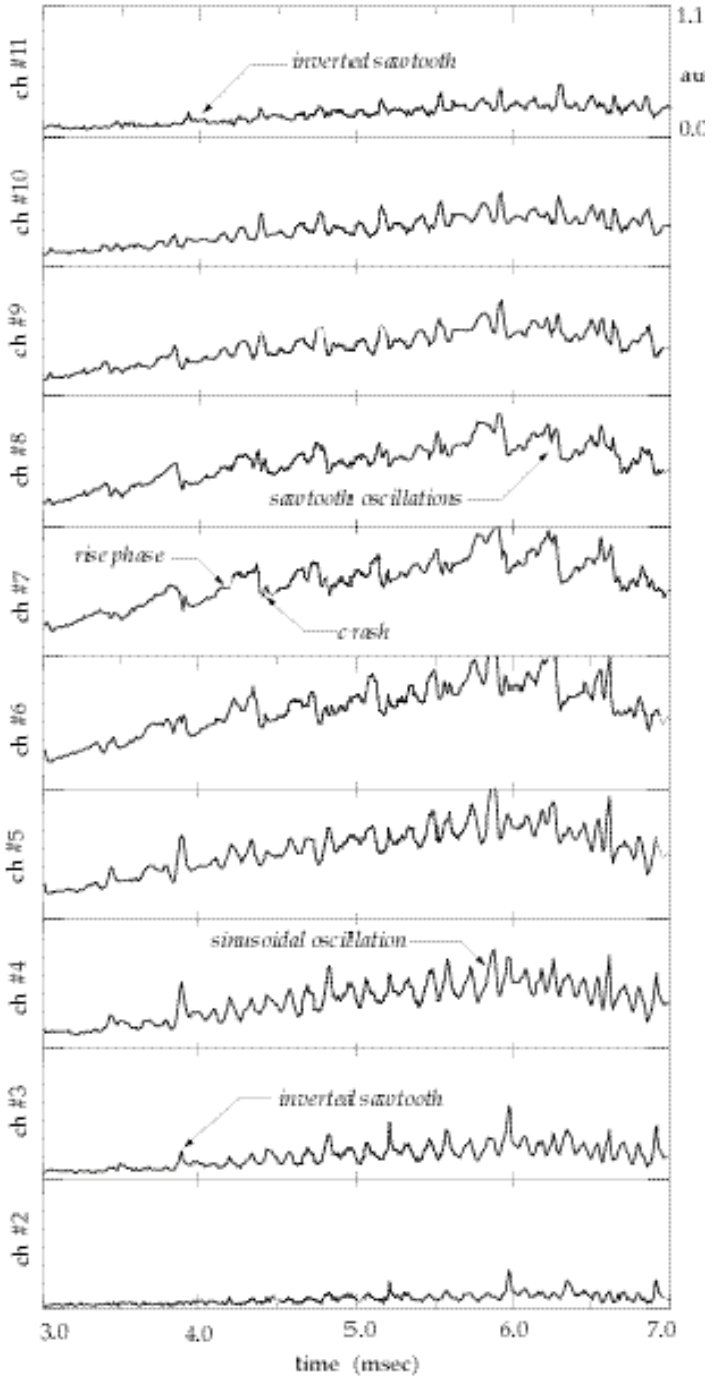

Figure 3.12 Typical fan-array signals showing equilibrium soft *x*-ray rise, sawtooth and *m*=1 oscillations in the plasma core of HBT-EP.

prevalent on the central channels and become smaller and inverted at larger values of minor radius. The sawtooth rise is approximately linear and abruptly crashes on a time scale roughly ~10 times shorter than the rising portion of the sawtooth. Still other channels have more sinusoidal-like oscillations present at intermediate positions between the rising sawteeth in the core region and small inverted sawteeth on the peripheral channels.

Sawtooth relaxation oscillations, sometimes termed *internal disruptions*, were first observed on the ST tokamak at Princeton (von Goeler *et al* 1974) and have been an active area of fusion plasma physics research over the ensuing years. Our purpose here is not to study sawtooth physics, but to use known properties of sawtooth phenomenology in order to interpret HBT-EP sawtooth activity. In particular, the position of the q=1 surface and the frequency of the resonant m/n=1/1 mode will be used in the following study of m/n=2/1 magnetic island frequency locking behavior under the action of externally applied resonant magnetic perturbations. A brief survey of sawtooth physics is given next to motivate the association of a q=1 mode rational surface and its associated m/n=1/1 instability with observed HBT-EP sawtooth behavior.

3.3.1 Sawtooth phenomenology and HBT-EP sawteeth

The relaxation oscillations, or sawteeth, that ride atop the equilibrium emissivity depicted in figure 3.12 are driven by a combination of thermal and magnetohydrodynamic instability. The rising portion of the sawtooth oscillation is the result of Ohmic heating deposition in the core plasma. The Ohmic heat

input raises core electron temperature and hence soft *x*-ray emission. The conductivity of the core plasma also increases and
channels more current in the discharge center. This heightened core current density causes increased heat deposition, temperature rise, and *x*-ray emission. This thermally unstable situation continues to channel more current and hence heating power in the center of the discharge. The rising core current density allows q on axis to reach q_0=1 when the central current density is equal to $j_o \sim 2B_\phi/\mu_o R_o$. The appearance of a q=1 surface in the plasma then allows the m/n=1/1 mode to be driven unstable and grow in amplitude. Growing sinusoidal-like m/n=1/1 emissivity fluctuations are typically observed coincident with the rise phase of the sawtooth (von Goeler *et al* 1974). The m/n=1/1 mode grows to large size, dependent upon available free energy, whereupon it precipitates loss of core thermal confinement or sawtooth crash.

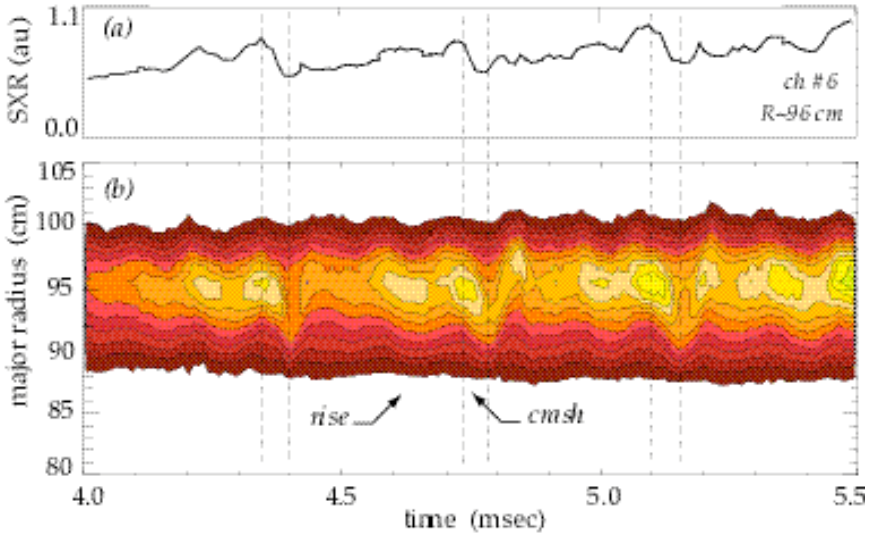

Figure 3.13*(a)*. Central soft *x*-ray fan-array channel. *(b)*. Contour plot of full sixteen channel array showing sawtooth rise and crash phases.

The exact nature of the crash phase is unknown and varies depending upon numerous factors, in particular collisionality (Wesson 1991).

An early theoretical sawtooth model, due to Kadomtsev, based on an m=1 island growing nonlinearly until it envelopes the entire core region (Kadomtsev 1975) has numerical (Sykes and Wesson 1976) and experimental (Jahns *et al* 1978, Goetz *et al* 1990) evidence supporting a complete reconnection model of the sawtooth oscillation. However, doubt was cast on this simple senario in other experimental studies (Dubois *et al* 1980, Snipes and Gentle 1986) where observed m=1 oscillations continue throughout the entire sawtooth cycle. Theoretical models have been developed to explain observed core temperature collapse in the absence of Kadomstsev-style core envelopment and complete reconnection of the m/n=1/1 island. These models invoke other physical mechanisms during the nonlinear development of the m/n=1/1 mode to bring about loss of confinement and hence sawtooth crash, including enhanced turbulence (Dubois *et al* 1983), magnetic stochasticity (Lichtenberg 1984) and recently ballooning effects (Nishimura *et al* 1998) among others.

For the present study, we wish to skirt difficulties in current understanding of tokamak sawteeth, and use the well-known fact that they are associated with a m/n=1/1 mode resonant at the q=1 surface in the plasma core. This information allows the position of the q=1 surface and the amplitude, phase, and frequency of the m=1 mode to be interpreted from the fan array signals. Next we discuss the extraction of the q=1 position and m/n=1/1 mode information from typical fan-

array data. This is accomplished using singular value decomposition and Hilbert transformation of the fan-array channel time series

3.3.2 *Singular value decomposition and m/n=1/1 mode diagnosis*

Consider a function of both space and time such as the poloidal field at the edge of the plasma $B_\theta(\theta,t)$ or the soft x-ray emissivity as a function of channel number and time $\varepsilon(l,t)$. Singular value decomposition is a familiar form of matrix reduction from linear algebra, and has well known applications in solving for pseudo-inverse matrices in systems of linear equations. Rather than using the decomposition to project onto a specified solution space, we investigate the individual eigenmodes of the decomposition and interpret them physically. This approach to using the singular eigenmodes has its origins in nonlinear dynamics (Aubry *et al* 1991) where it has been used to study wave propagation in hydrodynamic systems (Aubry *et al* 1994) and chaotic bifurcation events (Lima 1992). In a plasma context, it is particularly well suited for distinguishing coherent structures and phenomena from background turbulence and random noise. It has been profitably used in x-ray and magnetic measurements of MHD mode structure (Nardone 1992, Kim *et al* 1999), sawtooth behavior (Dudok de Wit 1995), and perturbative transport studies (Dudok de Wit *et al* 1998) in a fusion plasma physics context.

The singular value or biorthogonal decomposition of such a spatio-temporal signal set consists of a representation that attempts to split the time and space dependent information of a bivariate function into an expansion of the form,

$$f(x,t) = \sum_k A_k \phi_k(x) \psi_k(t). \tag{3.12}$$

The spatial basis functions φ_k sometimes referred to as *topos* (Aubry *et al* 1991), and temporal basis ψ_k functions or *chronos* are so constructed that they are orthonormal to the other members of their respective eigen-set as follows:

$$\int \phi_i(x)\phi_k(x)dx = \delta_{ik}, \tag{3.13}$$

$$\int \psi_i(t)\psi_k(t)dt = \delta_{ik}. \tag{3.14}$$

Here δ_{ik} is the Kronecker delta and the integrations in 3.13 and 3.14 are over the relevant spatial and temporal domains of the time series involved. The A_k coefficients in the expansion of equation 3.12 measure the contribution of each (φ_k ,ψ_k) to the total signal and can also be interpreted as eigenvalues of an associated eigenvalue problem (Noble and Gentle 1978). The biorthogonal components of equations 3.12 to 3.14 are determined from the soft *x*-ray measurements using singular value decomposition. Take a matrix of observational channels, $y(x_k, t_i) = (\mathbf{Y})_{ik}$, with $y(x_k,t_i)$ the sampled version of some scalar field, in this case the measured soft *x*-ray flux. The spatial and temporal eigenmodes are constructed using singular value decomposition, $\mathbf{Y} = \mathbf{VAU}^*$. The vectors $\mathbf{V} = [\psi_1, \psi_2, \ldots, \psi_M]$ and $\mathbf{U} = [\varphi_1, \varphi_2, \ldots, \varphi_M]$ contain the spatial and temporal eigenmodes of equation 3.12, and the diagonal matrix **A** contains the expansion coefficients or singular values.

A difficulty in employing an expansion of the type of equation 3.12 is in interpreting the resulting series. Since the basis functions are constructed from the data itself a simple interpretation is often lacking. In the special case of sinusoidal oscillation the decomposition is equivalent to Fourier analysis (Dudok de Wit *et al* 1994). This implies that sinusoidally varying structures will appear in distinct eigenmodes with an invariant spatial structure mode and a temporal eigenmode that reflects frequency and amplitude change of the structure in question. For the soft *x*-ray signals discussed here, since the phenomena under study are in some sense well known, interpretation is relatively straightforward.

For use here in analyzing the fan-array multi-channel data set the biorthogonal decomposition is useful for two distinct reasons. In fan array observations of core sawtooth and m/n=1/1 mode activity the raw soft *x*-ray signals have essentially four characteristic time scales associated with macroscopic, coherent plasma behavior. The background equilibrium emission value typically changes over a few milliseconds time scale due to global profile evolution. The sawtooth oscillation has two characteristic time scales associated with it. The sawtooth rise time is approximately ~300 to 400μsec depending upon discharge conditions, while the crash time is of order ~50μsec. The m/n=1/1 mode rotation period sets an intermediate scale between the sawtooth rise and fall times. Typically, two to three oscillation cycles or periods of the m/n=1/1 mode per sawtooth period are observed. Here the sawtooth period is defined as the sum of the rise and crash time scales, τ_{ST}~400 to 500μsec . Thus, the m/n=1/1 mode period is approximately ~100 to 200μsec. It is thus

difficult, for example, to extract m/n=1/1 mode dynamics from the multiple time scale phenomena present in the overall signal via simple temporal or spatial domain frequency filtering since the above phenomena are not contained in distinct temporal or spatial frequency bands. In contrast, biorthogonal or singular value decomposition is well suited to an analysis of this kind and as will be shown separates out the observed macroscopic phenomena just described into distinct biorthogonal components, the (φ_k, ψ_k) pairs of equations 3.12 through 3.14, that can then be separately characterized and interpreted. In addition, the expansion of a signal array into a series of the form of equation 3.12 allows the effective rejection of uncorrelated *"noise"* in the data by simply retaining only the significant biorthogonal components of concern for a particular application. Thus, biorthogonal or singular value decomposition can, in a sense, provide a spatio-temporal filter against unwanted space-time components of a signal set that are uncorrelated with the signal of interest.

The resulting biorthogonal decomposition of the full sixteen-channel array for the discharge in figure 3.12. is given in figure 3.14. The singular weights A_K are shown in figure 3.15. There are essentially three dominant weights for the expansion of the fan-array. The largest weight A_0=11 has a eigenmode

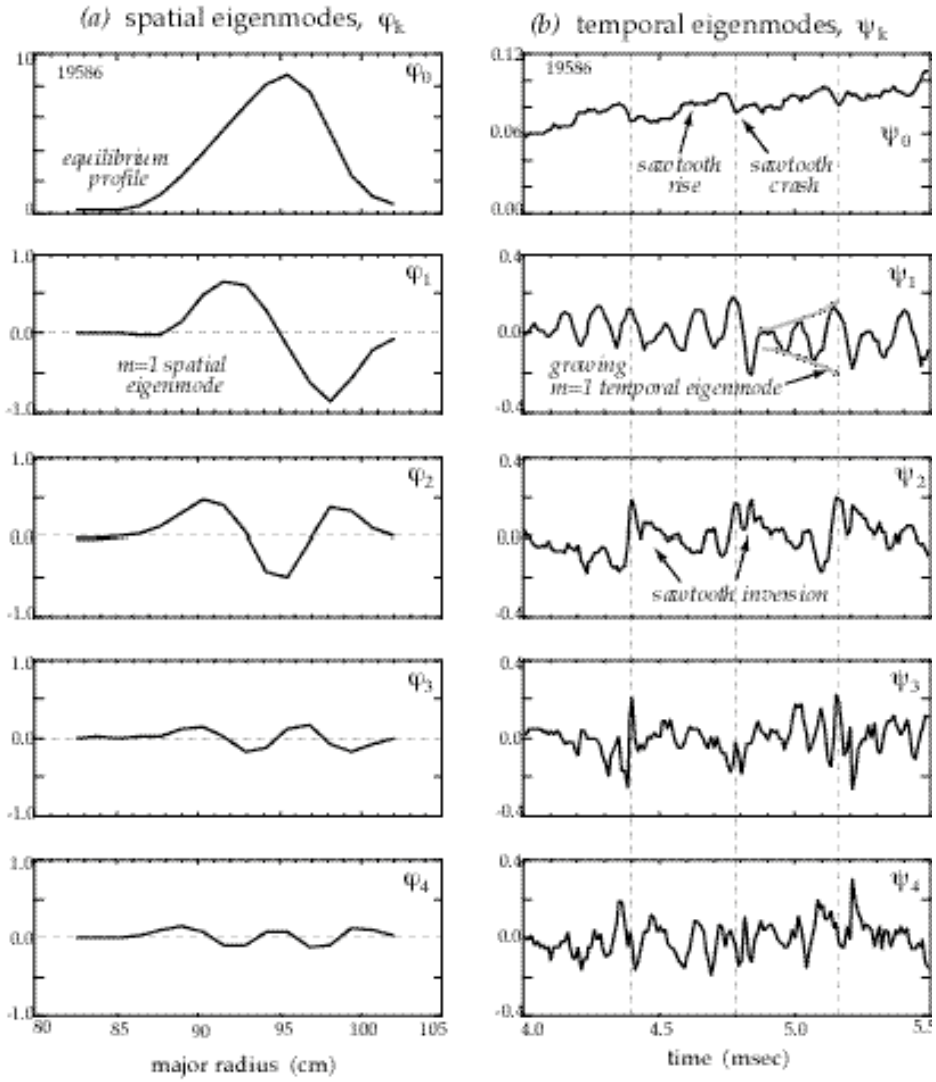

Figure 3.14*(a).* Spatial eigenmodes and *(b)* temporal eigenmodes constructed from the fan-array times series shown in figure 3.12. Note separation of sawtooth rise and crash phases, sawtooth inversion at large radii and an oscillatory odd eigenmode into essentially distinct biorthogonal components.

pair (φ_0,ψ_0) whose spatial component gives the equilibrium radial brightness profile and whose temporal component captures the time evolution of the sawtooth oscillation rise and crash phases along with long-time equilibrium evolution of the overall profile.

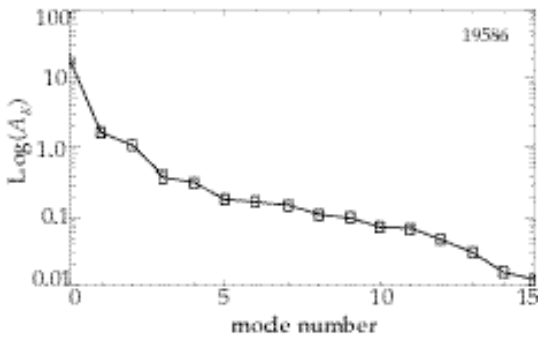

Figure 3.15. Singular value weight spectrum of the fan-array decomposition of figure 3.14.

The next eigenmode pair (φ_1,ψ_1) contains a spatial component we identify as an m=1 radial fluctuation with its characteristic odd structure. The temporal m=1 component is a growing sinusoidal-like oscillation that reaches its maximum amplitude at the onset of the crash phase of the sawtooth and, is then quenched to low amplitude during and just after the crash phase is complete. This is consistent with typical m=1 behavior in sawtoothing tokamaks described above. The position of the q=1 surface is identified as the location of peak amplitude in the m=1 emissivity perturbation. A contour plot of the m=1 oscillation is shown in figure 3.16. The approximate position of q=1 inferred from this analysis is r_{s1}~3cm.

The third pair of biorthogonal components (φ_2,ψ_2) contain additional sawtooth behavior. The temporal eigenmode ψ_2 shows inverted sawteeth from those of the equilibrium ψ_0 component. The spatial component φ_2 is an even function of minor radius that results in additional peaking of the equilibrium during the rise phase and flattens the brightness profile during the sawtooth crash. The (φ_0,ψ_0) and (φ_2,ψ_2) eigen-pairs capture what is

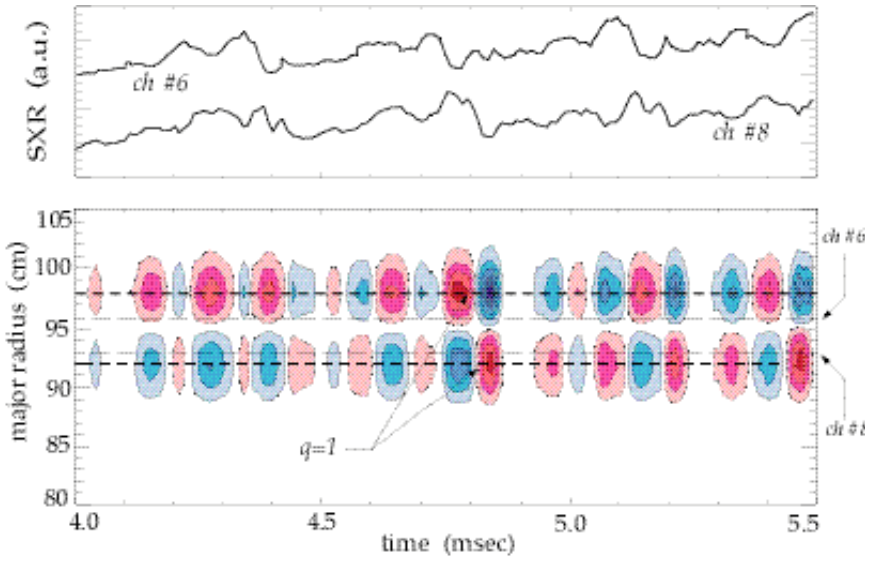

Figure 3.16*(a)* Contour plot of m=1 emissivity perturbation showing approximate location of the q=1 surface. *(b).* core soft x-ray channels for comparison.

traditionally called the n=0 and m=0 axisymmetric component of the sawtooth rise and crash.

The remaining higher order eigenfunctions typically have small oscillatory-like spatial modes and temporal modes that become increasingly *"noise-like"* and lacking in any coherent behavior. To demonstrate the ability of the decomposition to concentrate signal information into a few important biorthogonal components compare the contour plot of the dominant three weights $\varepsilon_{012}=A_0\varphi_0\psi_0+A_1\varphi_1\psi_1+A_2\varphi_2\psi_2$ in figure 3.17 and the total emissivity contour plot of figure 3.13*(b).* All large-scale, coherent behavior of the total fan-array data set is reproduced by the largest three decomposition components. The ability of the decomposition to concentrate information into a few eigenmode pairs can be made quantitative by defining a signal energy in terms of the individual A_K weights as follows,

$$E = \sum_{K=1}^{K} A_K^2, \tag{3.15}$$

and a dimensionless energy for each component, $p_K = A_K^2/E$. The p_K measure the relative contribution or stored energy in each eigenmode pair to the total signal. For the fan-array signals of figure 3.12 and decomposition of 3.14 the dominant three weights represent ~98% of the signal energy.

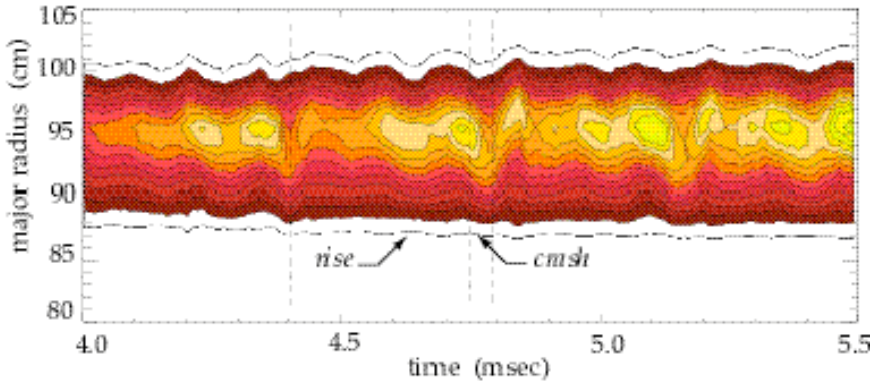

Figure 3.17 A contour plot of fan-array data using only the dominant three biorthogonal components shown in figure 3.1.5. captures essentially all macroscopic, coherent behavior shown in the total emissivity contour plot of figure 3.1.4.

The amplitude and phase of the m=1 mode identified above is given in figure 3.18, along with a central soft x-ray channel for comparison. The amplitude and phase are constructed from the temporal eigenmode of the m=1 fluctuation using the Hilbert transform technique discussed in 3.2.4. Notice that the m=1 mode amplitude reaches its maximum value during the crash time, after which, it is reduced in amplitude and starts to grow anew in synchrony with the sawtooth oscillation. The rotational frequency of the mode is calculated using a least squares fit of a straight line to the m=1 phase data as in the magnetic analysis of the m=2 island. The frequencies of the m=1 mode measured with the fan array

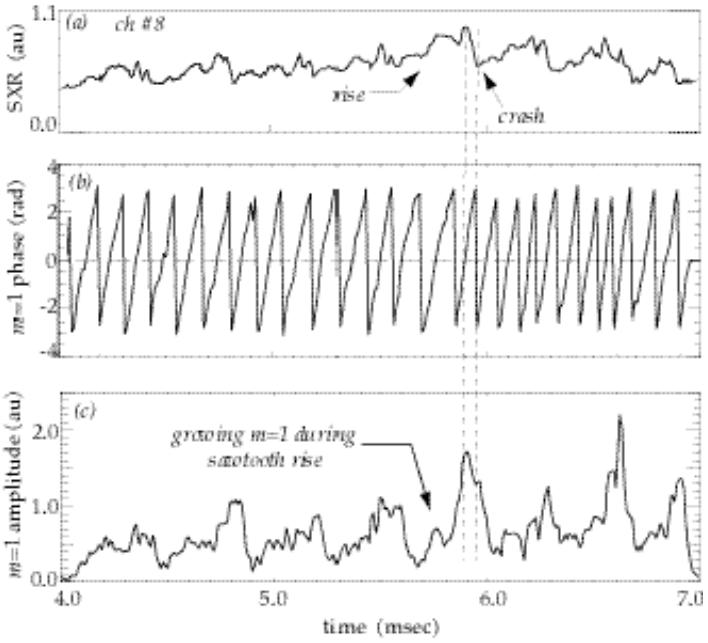

Figure 3.18*(a).* Core soft x-ray channel *(b).* Phase of m=1 mode emissivity perturbation. *(c).* Amplitude of m=1 mode showing classic m=1 and sawtooth behavior.

and the m=2 island from the external magnetic pickup coil set are plotted in figure 3.19. The two fluctuations co-rotate at the same frequency. This fact allows us to quantify the intrinsic mode rotation direction on HBT-EP by defining a phase velocity for each MHD perturbation as $v_{ph}=\omega/k$.

The observation that $\omega_1=\omega_2$(see figure 3.19) implies the following equality between the projections of the electron fluid velocities at the q=1 and q=2 surfaces,

$$\vec{v}_1 \cdot \vec{k}_1 = \vec{v}_2 \cdot \vec{k}_2 . \tag{3.16}$$

In component form, for the m/n=1/1 and 2/1 modes this becomes, taking the wave number vectors of the two rational surfaces to be given by $\vec{k} = (m/r_s)\hat{\theta} + (n/R_o)\hat{\varphi}$ yields the following relationship between the

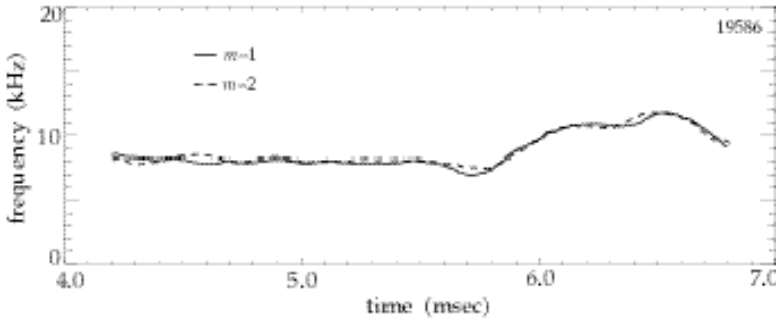

Figure 3.19 Comparison of frequency evolution of m=2 magnetic perturbation and m=1 emissivity perturbation showing frequency locking of the two fluctuations.

components of the two velocities,

$$v_{1\theta}\frac{1}{r_{s1}} + v_{1\varphi}\frac{1}{R_o} = v_{2\theta}\frac{2}{r_{s2}} + v_{2\varphi}\frac{1}{R_o}. \qquad (3.17)$$

In the solid body poloidal rotation limit, $v_{1\varphi}$=$v_{2\varphi}$=0, and the ratio of the mode frequencies is proportional to the ratio of their poloidal mode numbers f_1/f_2=1/2. Hence, pure poloidal rotation is incompatible with the observed ratio f_1/f_2=1. The opposite limit of pure torodial rotation with, $v_{1\theta}$=$v_{2\,\theta}$=0, gives the ratio of the modal frequencies as the ratio of their torodial mode numbers f_1/f_2=1/1. This is consistent with the observed m/n =1/1 and 2/1 frequencies. To make further progress, we invoke observations of m/n=3/2 MHD activity in HBT-EP plasmas prior to high beta disruption. In these plasmas a m/n=3/2 mode was observed to propagate at approximately twice the frequency of the 2/1 mode (Ivers *et al* 1996). This observation is also consistent with essentially rigid body torodial rotation of HBT-EP magnetohydrodynamic activity.

These observations therefore suggest that the mode rotation on HBT-EP is predominantly torodial in direction although direct proof is lacking. This result

will be quantified further in chapter four, where an analysis of the perturbed torque balance near the m/n=2/1 surface is presented and the limiting cases of only poloidal or torodial motion are considered again in the context of mode locking to applied resonant magnetic perturbations.

4.0 Resonant magnetic perturbation experiments

Resonant magnetic perturbations are used to study and control island rotation dynamics in this chapter. A simple compact saddle coil system is demonstrated to have significant impact on inducing magnetic island frequency and amplitude change. Details of the island control system developed on HBT-EP are described first in section 4.1, before magnetic island frequency and amplitude effects are presented in section 4.2 and 4.3.

Basic frequency locking characteristics of HBT-EP magnetic islands are described using the diagnostic analysis tools developed in chapter three in section 4.2. A model of the perturbed electromagnetic, viscous, and inertial torque balance near a large amplitude magnetic island is developed following traditional mode-locking theory and compared with experimental order of magnitude estimates of the various torque contributions. Implications of the experimental torque balance in relation to poloidal and toroidal equilibrium island rotation and possible poloidal flow damping mechanisms is discussed next. The experimental torque required to lock an island is shown to be consistent with toroidally driven magnetic island motion by the rotating control fields. This implies the effect of substantial poloidal flow damping of any possible poloidally driven motion by the magnetic perturbation. The observed locking torque magnitude and the effects of flow damping are also important for the evolution of magnetic island size due to the effective renormalization of ion inertia in a poloidally flow damped system (Smolyakov *et al* 1995). The observation of core induced motion as indicated by the m/n=1/1 emissivity

fluctuation analysis during the rotation control experiments of the 2/1 island are presented next and the implications for driving sheared rotation employing two distinct rational surfaces in the plasma is discussed in section 4.2.1.

Observed island amplitude dynamics are discussed next. Using frequency modulated perturbations to drive island rotational change, the amplitude of these islands is observed to be affected by this magnetic stirring. Study of an ensemble of similarly prepared plasmas indicates a correlation between magnetic island frequency modulation and the growth and damping of magnetic island size. More specifically, accelerated magnetic islands are observed to grow in amplitude and those that are decelerated are damped in size. Simple estimates of the possible effect of inertia as agent of the observed island suppression are presented. The observed asymmetric response is then shown to be consistent with a destabilizing inertial term in Rutherford's island width evolution equation (Waelbroeck and Fitzpatrick 1997). Finally, this chapter concludes with the demonstration of disruption mitigation using this simple asynchronous saddle coil control technique.

4.1 HBT-EP magnetic island control system

Active control of magnetic islands on the HBT-EP tokamak is accomplished with a saddle coil system consisting of four coils connected to approximate a quadrature m/n=2/1 dominant magnetic field structure. The coils are wound out of nine turns of #1 copper cable and are situated on the quartz insulating breaks (see figure 4.0) between vacuum chamber sections. Each coil spans a toroidal angle of ~6° separately. In the quadrature configuration used to generate a rotating magnetic field the toroidal coverage per phase is ~3.5°. Placement of the coils on the quartz insulating segments of the vacuum chamber allows high frequency f_{SC}~20kHz perturbation fields to easily couple to the plasma magnetic island by injecting the perturbing field through the Aluminum passive stabilizing wall gaps shown in figure 4.1. This introduces minimal attenuation and phase shift to the applied control field. The saddle coil current feed and return are in a twisted pair configuration and are run to the center cylinder enclosing the Ohmic transformer. Each coil pair can be easily disconnected and the configuration changed to a single-phase coil set with appropriate poloidal reorientation of the toroidal current elements. The saddle

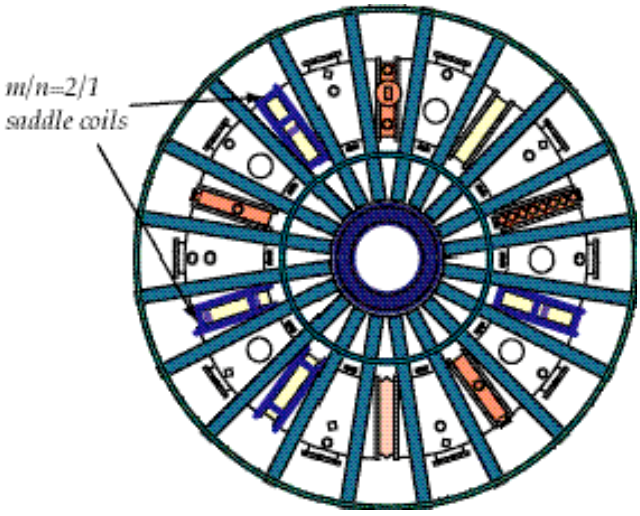

Figure 4.0 Top view of the HBT-EP tokamak showing the toroidal location of the m/n=2/1 saddle coil set. Quartz sections are denoted by yellow.

coil spectrum, calculated using a Biot-Savart code including a flange eddy current model (Nadle 1999), is predominantly m/n=2/1 as shown in figure 4.2*(a)*. The calculated applied field at the position of the m/n=2/1 surface (r_s~9 to 10cm) in the plasma is approximately ~5x10^{-3}G per ampere-turn of coil current. The calculated m/n=1/1 component is a factor of eight smaller than the m/n=2/1 component. The saddle coil set is driven by two 10MW amplifier provided in collaboration with Los Alamos National Laboratory (Reass *et al* 1995). The driving function generator and associated electronics were developed by Nadle (1999) for feedback studies on m/n=2/1 magnetic islands. It consists of a Bittware digital signal processor capable of 14-bit 100kHz output conversion and coupling amplifiers to the saddle coil amplifier inputs (Nadle 1999). For the open-loop experiments conducted for this thesis the schematic layout of the control electronics and coil set is depicted in figure 4.2*(b)*.

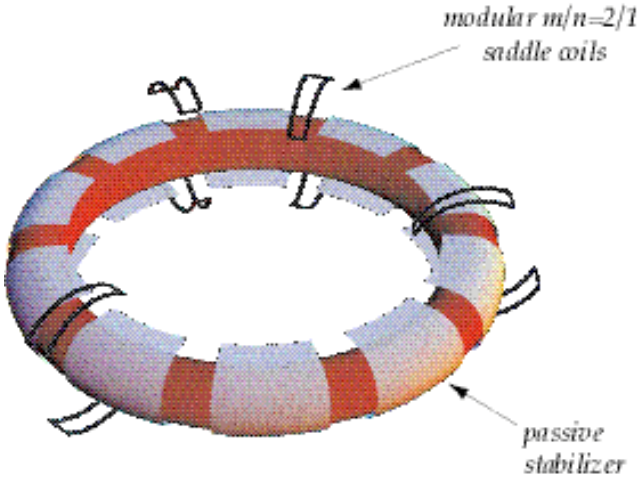

Figure 4.1 Perspective view of the HBT-EP plasma and passive stabilizing wall structure. The m/n=2/1 saddle coils are positioned to inject perturbed field between the shell gaps as shown.

4.2 *Magnetic island frequency locking*

The controlled acceleration and deceleration of magnetic islands has been demonstrated on the HBT-EP tokamak (Navratil *et al* 1998) using the modular compact saddle coil set described in the preceding section. Shown in figure 4.3 is an example of the application of a frequency ramped magnetic perturbation to a pre-existing m/n=2/1 magnetic island. The applied control field is ramped linearly from 2 to 16kHz over a 2msec window. The island natural rotation frequency is $f_{2/1}$~10kHz. After a transient jump upward in frequency when the saddle coil field is first energized the pre-existing island ramps down in frequency, locks onto the applied field and is accelerated up to approximately

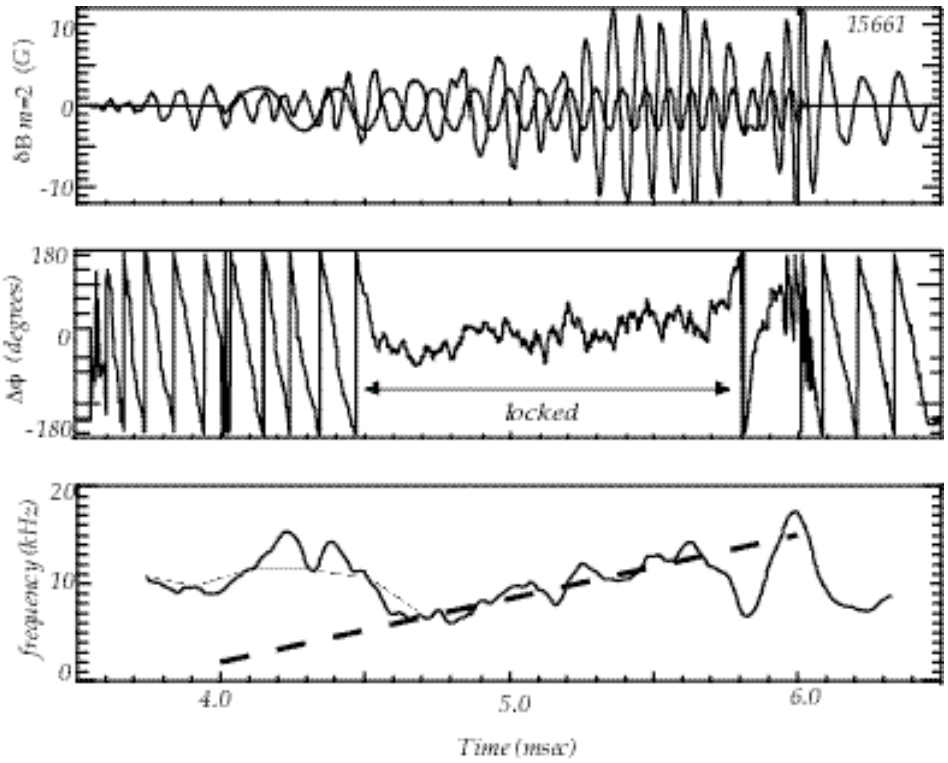

Figure 4.3(a) Island poloidal field fluctuation and saddle coil radial field at the edge of the plasma. *(b)* Phase difference between the island and applied field. *(c)* Frequency evolution of the island and applied field.

14kHz before unlocking from the applied field. The island then relaxes back to its natural rotation rate when the saddle coil field is turned off at 6msec. The measured phase difference between the island and applied saddle coil field slowly slips from negative to positive values as the torque requirements change from deceleration to acceleration of the island structure. Typical applied saddle coil radial fields of the order of the poloidal field fluctuation measured at the edge of the plasma are sufficient to ensure locking of the pre-existing island.

Application of a frequency ramped perturbation starting from a rotation frequency above the natural island frequency is depicted in figure 4.4. Here the applied field ramps linearly from 14 down to 6kHz again over a 3msec window. The island locks to the saddle coil field between 12 and 13kHz, and then is

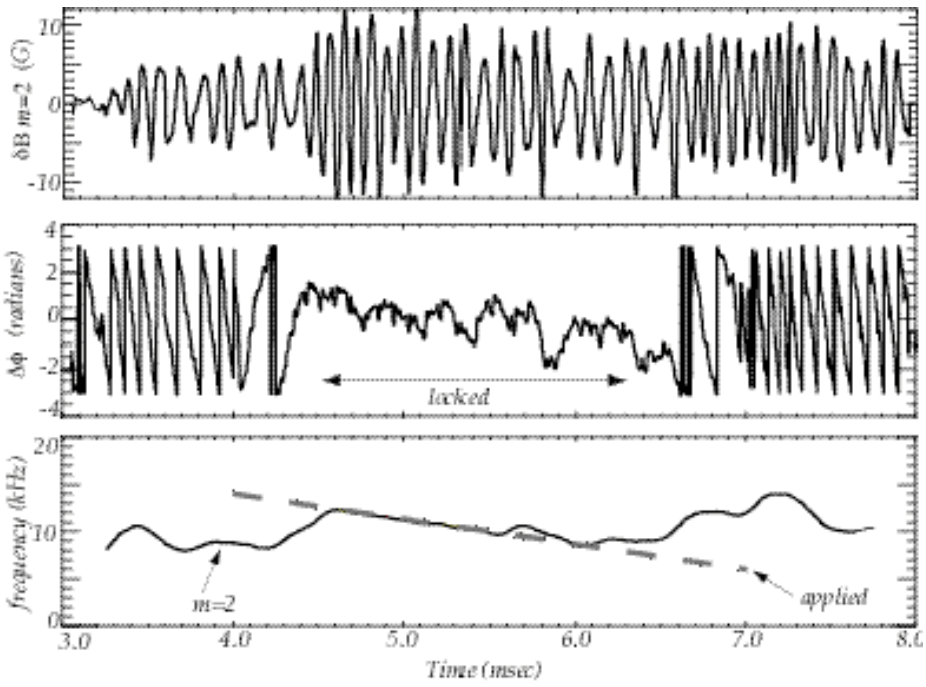

Figure 4.4*(a)* Island poloidal field fluctuation and saddle coil radial field at the edge of the plasma. *(b)* Phase difference between the island and applied field. *(c)* Frequency evolution of the island and applied field.

dragged down in frequency by the control field. Island rotation is slowed down to approximately 7kHz before unlocking, ramping up slightly, and then returning to its natural rate of $f_{2/1}$~10kHz. Note that the relative phase in this case slowly slips from positive to negative values as the torque requirements change from acceleration to deceleration of the island. This can be contrasted with the "ramp-up" applied control field in figure 4.3 which has the opposite phase difference evolution. Induced ion flow during these magnetic stirring experiments has been confirmed with several km per second change in ion fluid toroidal rotation (Navratil *et al* 1998, Talyor 2000).

These HBT-EP experiments on rotation control of an island embedded in plasma form the basis for future work directed at generating sheared flows using two distinct rational surfaces to apply electromagnetic torque and hence drive differential rotation (Jensen *et al* 1994). They have demonstrated a simple compact coil technique compatible with passive stabilization requirements necessary for future high beta advanced tokamak operation scenarios while offering a relatively *"low-tech"* approach to inducing or controlling plasma flow. To further understand the magnetic island-saddle coil interaction the perturbed torque balance near an HBT-EP magnetic island is estimated next.

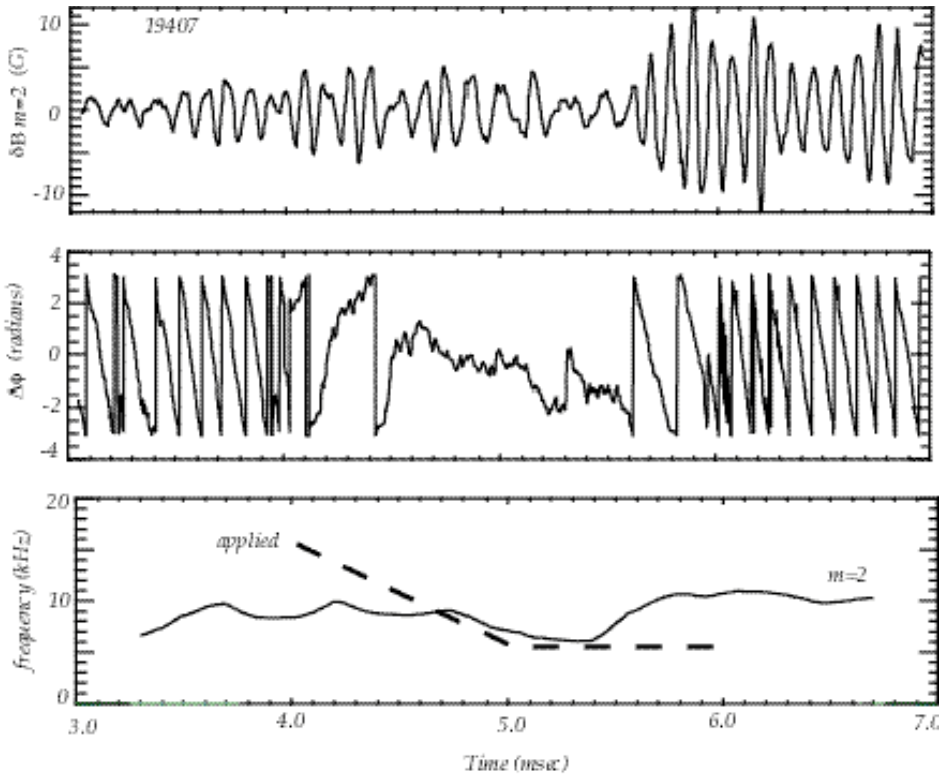

Figure 4.5 Another example of frequency locking showing *(a)* island poloidal field fluctuation and saddle coil radial field at the edge of the plasma. *(b)* Phase difference between the island and applied field. *(c)* Frequency evolution of the island and applied field. Note the large increase in amplitude when the island unlocks and spins back up to its natural rotation speed.

4.2.1 *Torque balance near a magnetic island*

In this section we estimate the perturbed torque balance near an HBT-EP magnetic island. The standard mode locking island theory developed over the past several years (Fitzpartick and Hender 1992, Jensen e*t al* 1993, Fitzpatrick 1994, Boozer 1996, Hegna *et al* 1998) is employed to understand the magnetic island-saddle coil interaction. The perturbed torque balance is separated into poloidal and toroidal directed torque components for convenience. A simple model for poloidal flow damping due to magnetic pumping of the ion fluid is developed in section 4.2.3. Finally, the effect of core induced rotation during these magnetic stirring experiments as measured by the emissivity analysis of section 3.3 is discussed in the context of this torque balance analysis. Implications for driving sheared flow in HBT-EP plasmas using different helicities of applied magnetic perturbations is also reviewed given the co-rotation of the m/n=1/1 island with the 2/1 island. Next, the traditional perturbed island torque balance is described and experimental order of magnitude estimates of the various torque terms are calculated.

4.2.1.1 *Saddle coil electromagnetic torque*

The electromagnetic torque acting upon the island region is given simply by integrating the perturbed Lorentz force density over the volume of the island (Fitzpatrick 1994, Hegna *et al* 1998). Thus we have,

$$\Gamma_{EMz} = \int_W R\hat{z} \cdot \vec{j} \times \vec{b}\, d^3x \qquad (4.1)$$

$$\Gamma_{EM\theta} = \int_W r\hat{\theta} \cdot \vec{j} \times \vec{b}\, d^3x \tag{4.2}$$

with the applied resonant magnetic perturbation $\vec{b}$ crossed into the perturbed island current density $\vec{j}$ at the rational surface. In the outer region, away from the singular layer centered at the rational surface, ideal MHD is valid and no net electromagnetic torque acts due to the applied perturbation. The plasma away from the resonance therefore simply displaces in response to the applied field. The electromagnetic torque acts only in the inner region. The perturbed current is approximately given by $j \cong \Delta' \delta(r - r_s)\Psi$. The torodial electromagnetic torque acting at the rational surface is therefore given by,

$$\Gamma_{EMz} = \int_{r_s - W/2}^{r_s + W/2} dr\, rR \int_0^{2\pi} d\theta \int_0^{2\pi} R\hat{z} \cdot \vec{j} \times \vec{b}\, d\phi \tag{4.3}$$

which can be expressed in terms of the magnetic potential and delta prime as (Fitzpatrick 1994, Hegna *et al* 1998),

$$\Gamma_{EMz} = 8\pi^2 Rn\ \mathrm{Im}\left(r_s \Delta' \left|\psi_s\right|^2\right). \tag{4.4}$$

The imaginary part of equation 4.4 leads to a torque that modulates as $\Gamma_{EM} \sim \sin(\Delta\phi)$, with $\Delta\phi = \phi_W - \phi_{SC}$ the phase difference between the island and applied perturbation. The torodial and poloidal electromagnetic torques are related by,

$$\Gamma_{EM\theta} = -\frac{m}{n}\Gamma_{EMz}. \tag{4.5}$$

Thus, for a tokamak resonance the electromagnetic torque is slightly more poloidal than toroidal since $m \geq n$, whereas for example, in a reversed field

pinch plasma the torque would be essentially toroidal because resonant modes have $n>>m$.

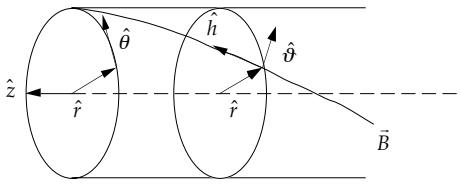

Figure 3.8. Helical and cylindrical basis vectors near the rational surface $r=r_s$ where $q_s=m/n$.

The magnitude relationship between the poloidal and toroidal torque can be seen by considering the perturbed Lorentz force density near the helical rational field line. Consider the following helical basis vectors near a $m/n=2/1$ magnetic surface constructed from the usual cylindrical basis vectors. The helical basis is composed of helical, azmuthal, and radial directions depicted in figure 3.8. Explicitly, they are given in terms of the cylindrical basis they by,

$$\hat{b} = \hat{z} + \frac{nr_s}{mR_o}\hat{\theta}, \qquad \hat{\vartheta} = \hat{\theta} - \frac{nr_s}{mR_o}\hat{z}, \qquad \hat{r} = \hat{r}. \tag{4.6}$$

The perturbed island current is essentially parallel to the equilibrium magnetic field hence, $\vec{j} \cong j_{//}\hat{b}$, while the applied saddle coil magnetic field is predominantly radial, $\vec{b}_{SC} \cong b_{SC}\hat{r}$. Thus the resulting perturbed Lorentz force goes like,

$$F_{EM} \sim \int_W j_{//} b_{SC} \hat{b} \times \hat{r}\, d^3x\,. \tag{4.7}$$

Using the helical basis given in equation 4.6 the torque can be calculated to scale as $T_{EM\theta} \sim -r_s j_{//} b_{SC}$ and $T_{EMz} \sim R_o j_{//} b_{SC}(nr_s/mR_o) \sim -(n/m)T_{EMz}$. Thus, the ratio of the toroidal and poloidal electromagnetic torque merely reflects the geometry of the resonant field line in question. The order of magnitude of these torques for a typical HBT-EP magnetic island are estimated next.

The poloidal field fluctuation mapped backed to the approximate location of the m/n=2/1 magnetic island is of order 10 to 20G for an island width of a few centimeters as described in section 3.4.2. Therefore, the perturbed island current density is approximately $j_{//}(r_s) \sim \tilde{b}_\theta(r_s)/\mu_o W \sim 4\,\mathrm{A/cm^2}$. The radial saddle coil magnetic field at the plasma surface to ensure locking is typically of order the poloidal field fluctuation at the edge of the plasma. Mapping this field strength to the approximate position of the magnetic gives $b_{SC}(r_s)$~2G. The perturbed Lorentz force density F_{EM} is of order F_{EM}~$j_{//}b_{SC}$~20μN/cm^3 and the resultant torque has a magnitude of approximately T_{EM}~$r_s F_{EM} V_W$~70x10^{-3} Nm, with r_s the radius of the rational surface and V_W the effective annular volume of the magnetic island. Next, the balancing viscous restoring torque and the inertial torque due to island acceleration will be calculated.

4.2.1.2 Plasma viscous torque response

The effect of momentum dissipation is modeled as an effective viscosity with diffusivity ν_{eff} that attempts to damp any change in the equilibrium rotation of the island structure (Fitzpatrick 1994, Hegna *et al* 1998). This effective restoring force is operative whenever the island rotation rate changes from its natural or equilibrium value. The change in velocity or velocity shift of the plasma interior to the island is,

$$\Delta\vec{v} = \vec{v} - \vec{v}_o, \tag{4.8}$$

with, $\vec{v}$ the instantaneous rotational velocity of the flow within the island and $\vec{v}_o$ is the equilibrium or natural value of the flow velocity in the absence of any perturbing electromagnetic torque. The island region is modeled as an

essentially annular region of radial width equal to the island width, *W*, centered at the unperturbed rational surface position of $r=r_s$. The natural rotation frequency of the island structure is taken as an input parameter to the model, which only calculates the time evolution of the deviation in island frequency through a perturbed torque balance.

A viscous diffusion equation is then used to couple the regions outside of the island to the background flow profile. Here the notion of an effective viscosity is used for HBT-EP since the traditional perpendicular viscous term modeled in traditional mode locking theories along with ion-neutral damping due to charge exchange reactions (Taylor 1999) is important for HBT-EP momentum damping. The toroidal or axial projection of this perturbed effective viscous force is written as,

$$\rho\frac{\partial\Delta v_z}{\partial t}=\frac{1}{r}\frac{\partial}{\partial r}\rho r\nu_{eff}\frac{\partial\Delta v_z}{\partial r}\equiv f_{VSz}, \tag{4.9}$$

with ν_{eff} a phenomenological viscous diffusivity coefficient and ρ the mass density. This effective diffusivity can be related to the neutral drag and perpendicular viscosity coefficients by inspection of both momentum damping terms in the perturbed force balance. The damping is then given by,

$$\rho\frac{\partial\Delta v_z}{\partial t}=\frac{1}{r}\frac{\partial}{\partial r}\rho r\nu_{\perp}\frac{\partial\Delta v_z}{\partial r}+\frac{\rho\Delta v_z}{\tau_{CX}}. \tag{4.10}$$

Thus, the effective diffusivity is given by,

$$\nu_{eff}=\nu_{\perp}\left(1+\frac{L^2/\tau_{CX}}{\nu_{\perp}}\right), \tag{4.11}$$

with $\nu_\perp$ the perpendicular viscous diffusivity, L the gradient scale length of the velocity perturbation near the magnetic island, and τ_{CX} the charge exchange damping time. This effective diffusivity sets the magnitude of the viscous restoring force that will oppose the action of the magnetic stirring perturbation by relaxing any induced flow profile change. To make connection with standard theory we write the dissipative forces as if they were entirely due to viscosity.

The toroidal and poloidal viscous torques are therefore given by (Fitzpatrick 1994, Hegna *et al* 1998),

$$\Gamma_{VSz} = R_o \int_W f_{VSz}\, d^3x \cong R_o \int_W \rho_s \nu_{eff} \frac{\partial^2 \Delta v_z}{\partial r^2}\, d^3x, \tag{4.12}$$

$$\Gamma_{VS\theta} = r_s \int_W f_{VS\theta}\, d^3x \cong r_s \int_W \rho_s \nu_{eff} \frac{\partial^2 \Delta v_\theta}{\partial r^2}\, d^3x. \tag{4.13}$$

In general, the gradient driving the viscous restoring force can have a jump discontinuity across the island (Fitzpatrick 1994). The magnitude of the torodial viscous torque obtained by integrating the viscous force density over the island can therefore be written as,

$$\Gamma_{VSz} = 4\pi^2 R^2 \left(\rho r \nu_{eff} \frac{\partial \Delta v_z}{\partial r} \right) \Bigg|_{r_{s-}}^{r_{s+}}. \tag{4.14}$$

If we assume that the perturbed velocity has a gradient scale of order the island width $\partial / \partial r \sim 1/W$ allows us to write the toroidal viscous torque as

$$\Gamma_{VS\phi} \cong \frac{4\pi^2 R_o^2 (\rho_s \nu_{eff} r_s R_o \Delta\omega_\phi)}{W}. \tag{4.15}$$

This is evidently a somewhat crude approximation to equation 4.14. This scaling of the viscous gradient implies relatively weak viscous damping since small spatial scales of order the island width survive diffusion. For stronger viscous action these small scale gradients would have diffused away and the profile would relax to the scale of the minor radius or some other intermediate value.

Similarly it can be shown, again taking $\partial / \partial r \sim 1/W$, that the poloidal viscous torque is given by,

$$\Gamma_{VS\theta} \cong \frac{4\pi^2 R_o r_s (\rho_s \nu_{eff} r_s^2 \Delta\omega_\theta)}{W}. \qquad (4.16)$$

Using equations 4.15 and 4.16, the ratio of the poloidal to toroidal viscous damping torques is seen to scale with the square of the inverse aspect ratio of the rational surface and is proportional to the ratio of the respective frequency shifts. For typical HBT-EP islands taking equal measured frequency shifts $\Delta\omega_\theta / \Delta\omega_\phi$=1, favors poloidally driven motion,

$$\frac{\Gamma_{VS\theta}}{\Gamma_{VS\phi}} \cong \left(\frac{r_s}{R_o}\right)^2 \frac{\Delta\omega_\theta}{\Delta\omega_\phi} \sim 10^{-2} \frac{\Delta\omega_\theta}{\Delta\omega_\phi}, \qquad (4.17)$$

since the viscous restoring force will be some two orders of magnitude smaller for poloidally induced rotation. In what way can we characterize the strength of this viscous restoring force on HBT-EP magnetic islands?

Experimentally, we are able to measure a relaxation time τ_{relax}~300μs (Navratil *et al* 1998) for the island to return to its equilibrium rotation frequency. Although useful in characterizing the strength of the restoring

dissipative forces acting on the island it does not specify the scale length L to which the rotation profile is diffusing toward. This would be tantamount to knowledge of the momentum diffusivity in the edge plasma region $\nu_{eff} \sim L^2/\tau_{relax}$. Diagnosing change in the rotational behavior of the m/n=1/1 emissivity fluctuation while stirring the edge plasma with the m/n=2/1 island offers a possible source of information on the strength of viscous coupling to the plasma core region. However, as pointed out in section 3.3.2, the coupled rotation of the m/n=1/1 and m/n=2/1 island structures precludes such diagnosis. This island coupling does offer important information and will be further discussed in section 4.2.4 where an attempt is made to include core rotation effects into the m/n=2/1 torque balance.

Inspection of equations 4.15 and 4.16 highlights the important terms that set the magnitude of the viscous torque. The effective diffusivity ν_{eff} and the gradient scale length of the flow profile set the strength of viscous action. Together they imply a scale length and relaxation time dependence that goes linearly with the gradient scale length, $\nu_{eff}(\partial \Delta v/\partial r) \sim L/\tau_{relax}$. This makes the torque somewhat insensitive to the size of L. For large islands $L \sim W$ will be 3 to 5cm, whereas if L scales with minor radius then $L \sim r_s$ or a can be as large as 10 to 14cm. Thus the viscous torque would vary by a factor of 2 or 3 given the approximate form in 4.15 and 4.16 if L is significantly different from scaling with island width. The magnitude of the resultant diffusivities are $\nu_{eff} \sim W^2/\tau_{relax} \sim 5\text{m}^2/\text{sec}$ and $\nu_{eff} \sim (a/2)^2/\tau_{relax} \sim 20\text{m}^2/\text{sec}$. In section 4.3 these diffusivities are used to estimate an effective Reynolds number to describe

viscosity and inertial effects for the magnetic island flow problem. The magnitude of the poloidal viscous torque is therefore $\Gamma_{VS\theta}$~0.5x10^{-3}Nm for a 2kHz island frequency shift. The toroidal viscous torque is $\Gamma_{VS\phi}$~50x10^{-3}Nm.

4.2.3 *Rotation control implications of m/n=1/1 island motion*

Using the analysis tools developed for the soft *x*-ray fan array discussed in chapter 3 an attempt to quantify viscous effects in the plasma core found that the m/n=1/1 emissivity fluctuation co-propagated with the m/n=2/1 island in the plasma edge. Figure 4.6 shows the evolution the m/n=1/1 and 2/1 island during application of a frequency "ramp-up" magnetic perturbation. The stirring action of the control field described above also changes the resonant m/n=1/1 island rotation in the core plasma region. Hence, the two magnetic islands are strongly coupled even in the presence of a predominantly m/n=2/1 helicity perturbation. Recall that the m/n=1/1 amplitude of the saddle coil set is approximately a

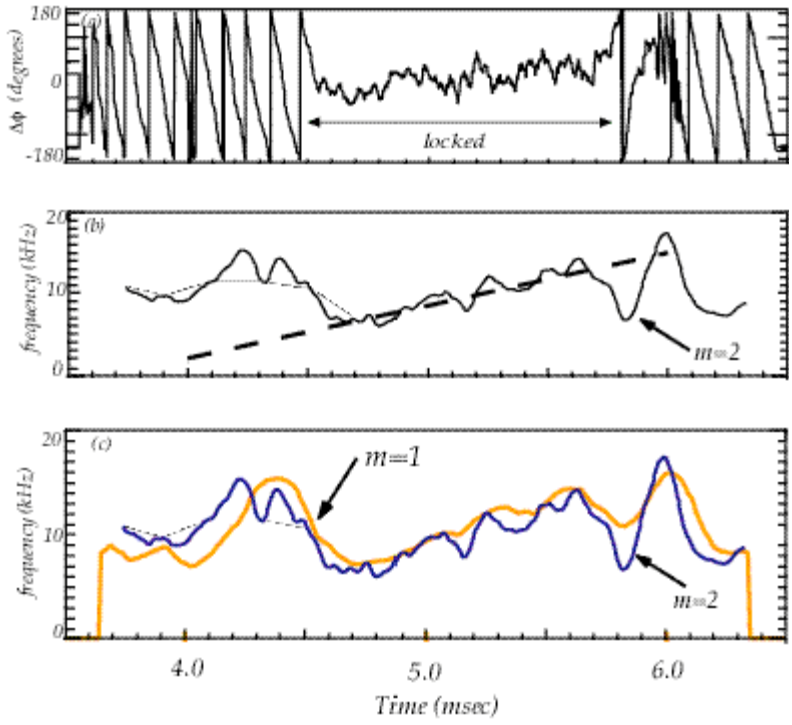

Figure 4.6 Induced m=1 rotation is observed during magnetic stirring experiments on the m=2 island in the plasma edge.

factor of eight smaller than the m/n=2/1 term (see Nadle 1999) for the quadrature two-phase saddle perturbation. Therefore, the direct torque applied to the 1/1 island is reduced by this same factor and hence coupling to the 2/1 island is clearly dominant. Next, we discuss the possible implication of induced core motion in driving differential rotation in the plasma using two distinct rational surfaces (that is, magnetic islands at two different rational surfaces).

The induced core island rotation at first sight would appear to make diving sheared flow difficult in HBT-EP plasmas given the large apparent size and location of the q=2 and q=1 surfaces. Current plans anticipate using a m/n=3/2 island at the q=1.5 surface situated between the m=2 and m=1 islands to induce shear in the velocity profile. A schematic picture of the two islands is given in figure 4.7. The stirring of these two surfaces together must effect the intervening plasma between them. This suggests that it could be difficult to drive significant rotation to lock the 3/2 island. However, it should also be possible to use the coupling of these two islands to either slow down the plasma at the q=1.5 surface

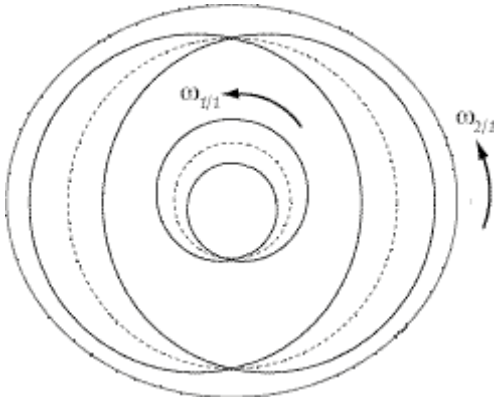

Figure 4.7 Schematic picture of m=1 and m=2 island co-rotation: $\omega_{1/1}=\omega_{2/1}$. Rational surface position and island width drawn approximately to scale.

if a static perturbation is to be applied. Also, the surface could be sped up so that a rotating field would couple significant torque to the 3/2 magnetic island. Note that when naturally occurring 3/2 modes exist in typical HBT-EP plasmas they do propagate at twice the typical n=1 mode rotation rate (Ivers *et al* 1995). This implies a typical frequency of ~20kHz. Once a 3/2 mode has been created the 2/1 surface could then be driven in an appropriate way to possibly drive shear between the two magnetic islands. These issues can obviously only be clarified with further resonant magnetic perturbation experiments on HBT-EP.

4.2.2 *Torque balance summary: poloidal flow damping*

Here we collect the estimates of the previous sections. The main observation to be made is that the preceding torque balance is consistent when poloidal flow damping is taken into account.

The evolution equation for deviation in island velocity for the torodial direction is found by considering the projection of the momentum equation in that direction. Thus for the toroidal torque,

$$\rho \frac{d\Delta v_z}{dt} = \hat{z} \cdot \vec{j} \times \vec{b} - \frac{\partial p}{\partial z} + \nabla \cdot \left(\rho \nu \nabla \Delta v_z \right). \tag{4.24}$$

Integrating this equation, with $\partial p / \partial z \approx 0$, over the island region yields the total torque balance equation for the evolution of the deviation in island velocity whose individual terms have been discussed in the preceding sections (Fitzpatrick 1994, Hegna *et al* 1998),

$$\frac{d}{dt}\left(I_\phi \Delta \omega_\phi \right) \cong I_\phi \frac{d\Delta\omega_\phi}{dt} = T_{VS\phi} + T_{EM\phi} \tag{4.25}$$

for the toroidal frequency evolution, and

$$\frac{d}{dt}\left(I_\theta \Delta \omega_\theta \right) \cong I_\theta \frac{d\Delta\omega_\theta}{dt} = T_{VS\theta} + T_{EM\theta} \tag{4.26}$$

for the poloidal frequency evolution. Using the above estimated torque magnitudes for the poloidal and toroidal terms, the perpendicular torque at the mode rational surface is calculated from,

$$\Gamma_{\perp}^{2} = \Gamma_{\theta}^{2} + (\frac{nr_{s}}{mR_{o}}\Gamma_{\phi})^{2}. \qquad (4.27)$$

The various torque contributions described above are collected in table 4.0. The applied perpendicular electromagnetic torque for a given measured frequency shift and angular acceleration is approximately two orders of magnitude higher than the estimated balancing inertial and viscous torques in the simple cylindrical-slab model developed in the previous sections. This is exactly the factor required to account for the effects of poloidal flow damping of HBT-EP islands. The effective torque is reduced by a factor $\sim(\varepsilon/q)^2 \sim 1/100$ (Smolyakov *et al* 1995). This reduction in effective torque results from the predominantly toroidal motion that flows in tokamak plasma. It also has important consequences for island amplitude dynamics as will be discussed next. Physically, the effective plasma inertia is increased for motion perpendicular to

Torque	Toroidal	Poloidal	Perpendicular
EM	35	70	70
Viscous	50	0.5	3
Inertial	2	0.02	0.1
Inertial (w/ion flow correction)	0.5	0.005 (all units are 10^{-3}Nm)	0.03

Table 4.0 Magnitude of the cylindrical HBT-EP torque balance terms showing the necessity of poloidal damping of island motion.

the magnetic lines of force due to damping of poloidal rotation and coupling of perpendicular and parallel flows in toroidal plasma. This results from the strong damping effect of parallel viscosity due to magnetic pumping. This process converts any directed flow energy in an inhomogeneous magnetic field into heat, that is, field non-uniformities act as a *"magnetic brake"* on the flowing plasma.

This means that the any attempt to drive poloial flow actually results in a driven parallel flow that exactly cancels any poloidal motion and results in a net toroidal flow. The fact that the required electromagnetic torque is consistent with predominantly toroidal island motion supports the inclusion of this important physics for HBT-EP magnetic islands.

4.3 Magnetic island amplitude dynamics

In this section we study the effect of the rotation control experiments on magnetic island width or amplitude. From the perspective of the introductory discussion of chapter one, the possibility of other contributions dependent upon island rotation to the evolution equation for the island width is studied.

Experimentally, a correlation between the island frequency modulation due to this perturbation and the damping and growth of island size is observed. A frequency dependent amplitude term was found essential in modeling of active control experiments on HBT-EP (Navratil *et al* 1998, Nadle 2000). The new observation presented here is that it is experimentally found that acceleration away from the island natural rotation rate leads to island amplitude growth whereas deceleration below the natural island speed gives rise to damping of island size.

A brief discussion of the basic physics of the inertial or ion polarization contribution to the modified Rutherford island width evolution equation and its characteristic magnitude for HBT-EP plasmas is discussed. Next, the island growth and damping asymmetry observed in acceleration and deceleration of HBT-EP islands in response to these rotating control fields is discussed as to whether the sign of the polarization current contribution to Rutherford's equation is stabilizing or destabilizing. The observed correlation of acceleration with island growth and deceleration with island suppression is found o be consistent with a *destabilizing ion polarization current* contribution to magnetic

island width evolution. This observation constitutes the first experimental evidence obtained as to the destabilizing nature of ion inertia to magnetic island growth. The issue as to whether these currents contribute in a stabilizing or destabilizing manner to magnetic island dynamics is a crucial current question in the physics of magnetic island formation in toroidal plasmas. The stabilizing or destabilizing effect of the polarization term has important implications for neoclassical tearing mode threshold levels (La Haye *et al* 2000) and long pulse β-limits observed in some advanced tokamak scenarios (Wilson *et al* 1998). Finally, it was found that application of perturbations of this type to disruptive target plasma inhibited the loss of plasma density and core thermal energy. This simple technique offers a possible method of reducing the impact of sudden discharge termination due to loss of equilibrium in disruptive plasmas.

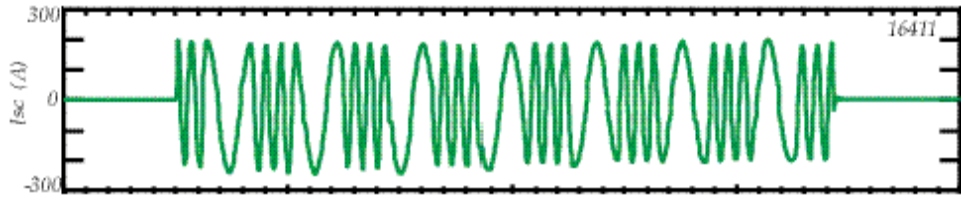

Figure 4.7 Example of a frequency modulated saddle coil current that alternates between frequencies above and below the natural island rotation frequency.

4.3.1 Asymmetric island amplitude growth and suppression

Application of a frequency modulated magnetic perturbation that alternates between a frequency above and below the natural rotation rate of the magnetic island was first suggested by Kurita and coworkers (1994) as a possible candidate for island suppression. Kurita, in simulations of rotating viscous plasma, found

that a frequency modulated magnetic island was suppressed due to viscous forces induced on the island by frequency modulation relative to the equilibrium island flow speed (Kurita 1994). A single phase of such a saddle coil current is shown in figure 4.7. Here the saddle current alternates between 5 and 15kHz, since the natural rotation frequency of the island is $f_{2/1}$~10kHz.

The switching time between frequencies shown in figure 4.7 was chosen to be 200μsec. This allows sufficient time to apply torque to the island structure without allowing the island enough time to frequency lock to the applied control field.

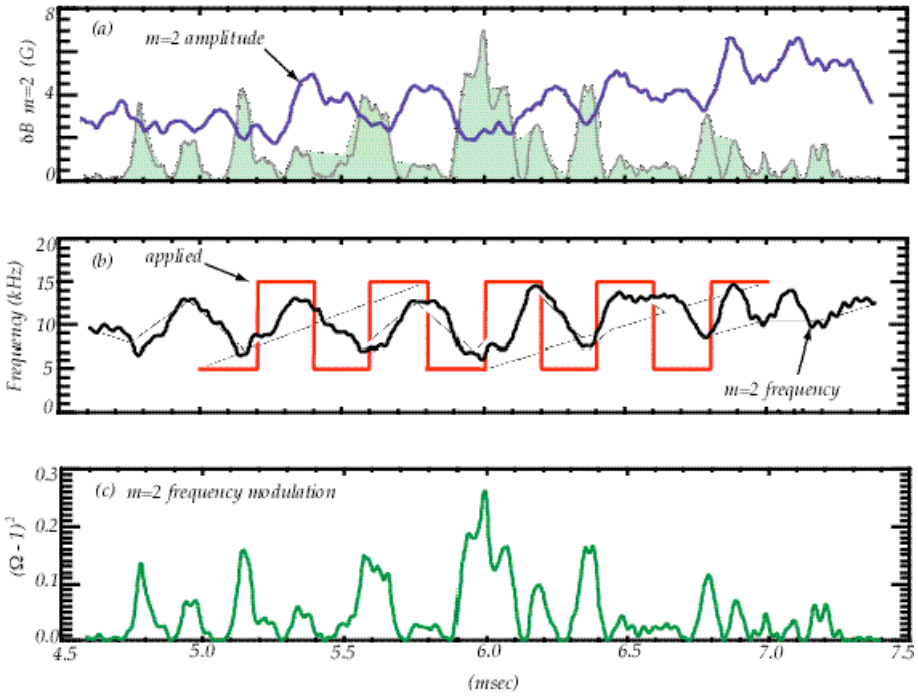

Figure 4.8*(a)* Island amplitude with overlay of frequency changes introduced by the saddle coil current. *(b)* Applied saddle and m=2 island frequencies. *(c)* Modulation in m=2 island frequency.

The response of the magnetic island to a saddle current modulated as in figure 4.7 reconstructed from the external magnetic analysis is shown in figure 4.8. Large bursts of modulation are seen in magnetic island amplitude as shown in 4.8*(a)*. The *m*=2 frequency modulation in 4.8*(c)* was constructed by taking a long-time moving average frequency and then subtracting the instantaneous frequency shown 4.8*(b)*. The measured frequency of the island modulates up to

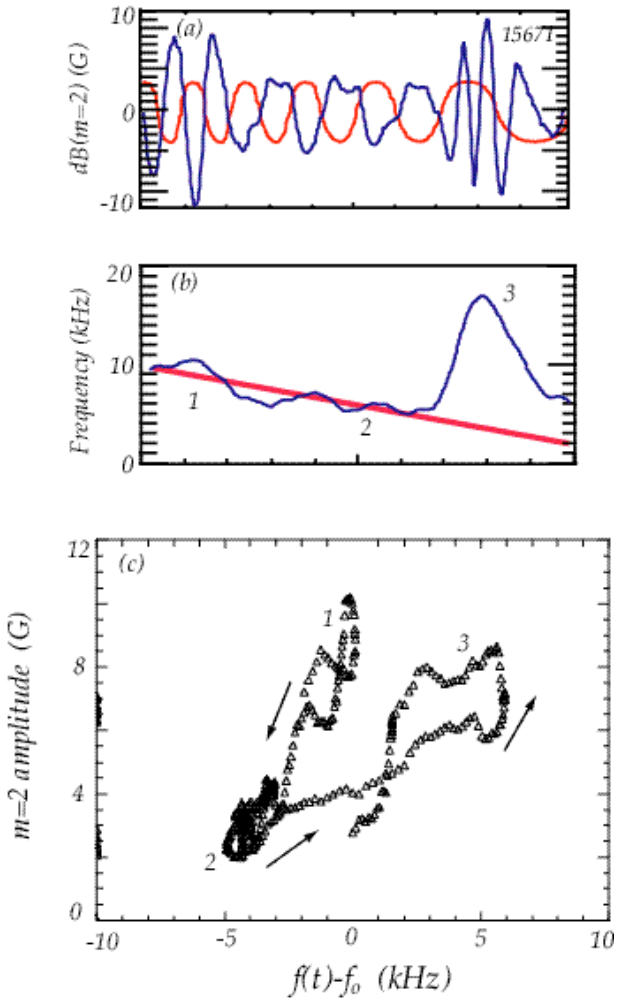

Figure 4.8*(a)* Island and saddle coil amplitudes. *(b)* Frequency evolution of island and ramping saddle coil current. *(c)* Island amplitude-frequency modulation space trajectory showing damping with deceleration and growth with island acceleration.

approximately 15kHz and down to 5kHz with observed mode amplitude changes of several Gauss measured at the edge of the plasma. To further illustrate frequency modulation and its relation to amplitude behavior of HBT-EP magnetic islands, consider the locked phase a frequency ramp-down experiment shown in figure 4.8. Here, the island is locked to the applied field and rather than growing in amplitude undergoes damping when decelerated by the applied field. At the time when the island unlocks from the applied field and rapidly accelerates and then relaxes later to its natural rotation speed a large increase of island amplitude is observed during the acceleration phase of the unlocking. This effect can be more conveniently seen by plotting the island amplitude versus the deviation in instantaneous island frequency from its natural rate of rotation. This trajectory in amplitude-frequency modulation space is shown in figure 4.9*(c)*. The correlation of growth with acceleration and suppression with deceleration of the magnetic island are clearly seen. This asymmetry in island amplitude response has important implications for the sign of the inertial term responsible for this frequency dependent island behavior and will be discussed in section 4.3.1.2. Next, an ensemble of twenty single phase and rotating perturbations as in figure 4.7 applied to HBT-EP plasmas is investigated for similar behavior. The resulting amplitude-frequency modulation scatter plot is shown in figure 4.10. Similar behavior is seen in this set of plasmas as was seen in the ramp-down case presented in figure 4.8.

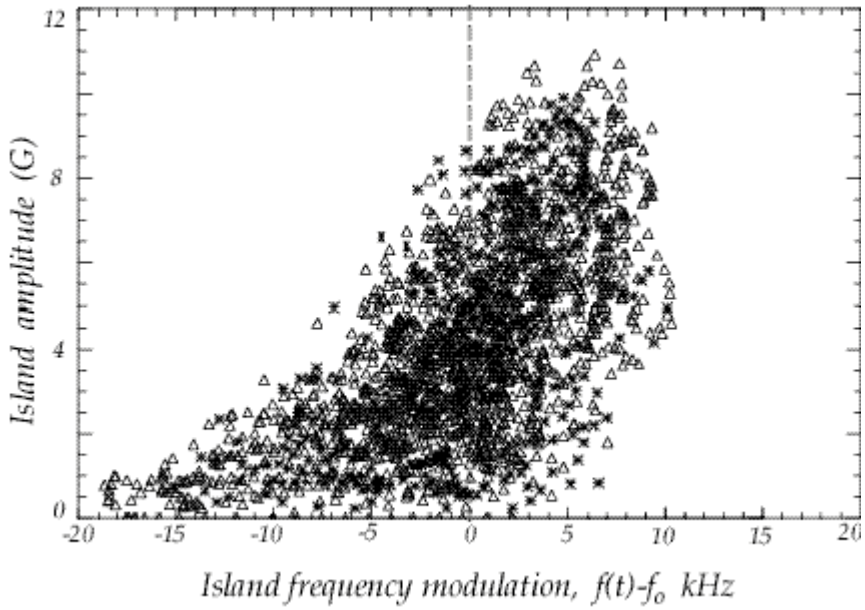

Figure 4.10 Magnetic island amplitude as a function of the deviation in island frequency from its natural rotation speed or modulation observed during active rotation control experiments for an ensemble of twenty plasmas on the HBT-EP tokamak.

4.3.1.1 Ion polarization physics and island rotation

Here a simple heuristic derivation of the ion polarization damping contribution to the Rutherford equation and estimates of its magnitude for typical HBT-EP conditions is given. This driven current depends upon the frame of reference of the ion fluid with respect to the rotating magnetohydrodynamic mode or magnetic island. For simplicity take the ions to be at rest in the lab frame, this is a reasonable approximation since measured torodial ion flows are typically ~1 km/sec in HBT-EP (Taylor 2000), and are small compared to typical mode rotation frequencies. Later, finite ion rotation will be briefly considered.

Take a tearing mode propagating at a frequency, $f_{2/1}$, in the lab (*~ion*) frame of reference. Island rotation induces an electric field through Faraday's Law in the ion frame of reference,

$$\nabla \times \vec{\tilde{E}} = -\frac{\partial \vec{\tilde{b}}}{\partial t}. \tag{4.20}$$

The important component for our purpose is in the theta direction and relates the poloidal field fluctuation of the mode to the induced radial electric field experienced by the ions. This implies the following relation between mode angular frequency, mode wave number and amplitude, and the induced fluctuating radial electric field seen by the ions,

$$\tilde{E}_r = \frac{\omega}{k_\varphi}\tilde{b}_\theta, \tag{4.21}$$

and the wave vector of the magnetohydrodynamic mode satisfying $\vec{k} \cdot \vec{B}_o = 0$.

This formula allows us to estimate the inductive radial electric field. For a typical HBT-EP tearing mode take the following as typical: $b_\theta(r_s)$=10G, $\omega=2\pi f_{2/1}=2\pi$ (10kHz), and $k_\varphi=n/R_o=1/(95\text{cm})$. This gives a fluctuating electric field of ~0.6 V/cm. For comparison the equilibrium radial electric field setup on a particle confinement time scale due to ambipolar diffusion should be of order the electron temperature in the plasma divided by the minor radius: $E_{ro}\sim T_{eo}/a$. Using T_{eo}=100V and a=13cm, gives an equilibrium field of approximately 7 to 8 V/cm. Thus the fluctuating field induced in the ion frame due to island rotation is roughly of order ~10% of the equilibrium radial electric field given the simple estimates here. Next, we estimate the effective force on the ion fluid due to this fluctuating perturbed electric field.

The dominate polarization drift term comes from crossing the perpendicular force felt by the ions with the equilibrium magnetic field. To calculate this force,

$$\vec{F}_\perp = m_i \frac{d\vec{V}_\perp}{dt}, \tag{4.22}$$

where the perpendicular velocity is,

$$\vec{V}_\perp = \vec{V} - V_{//}\hat{b}. \tag{4.23}$$

Using this expression in the perpendicular force and noting that $\vec{V}$ is simply the $\vec{E}\times\vec{B}$ velocity driven by the rotating island, therefore

$$\vec{F}_\perp = m_i \frac{d}{dt}\left(\vec{V}_{\vec{E}\times\vec{B}} - V_{//}\hat{b}\right). \tag{4.24}$$

Writing out the terms in parenthesis for the $\vec{E}\times\vec{B}$ and parallel velocities yields,

$$\vec{F}_{\perp} = m_i \frac{d}{dt}\left\{\left(\frac{\tilde{E}_r B_{o\varphi}}{B_o^2} - V_{//\theta}\right)\hat{\theta} + \left(\frac{\tilde{E}_r B_{o\theta}}{B_o^2} - V_{//\varphi}\right)\hat{\varphi}\right\}. \tag{4.25}$$

Where the only time dependence considered for simplicity is contained in the fluctuating radial electric field. Since parallel flow is, by definition, along the magnetic field direction we can write,

$$\vec{V}_{//} = \frac{V_{//}}{B_o}\left(B_{o\theta}\hat{\theta} + B_{o\varphi}\hat{\varphi}\right), \tag{4.26}$$

and,

$$\vec{V}_{//} = V_{//\theta}\hat{\theta} + V_{//\varphi}\hat{\varphi}. \tag{4.27}$$

Equating components of the two forms above we note that the poloidal and torodial components of the parallel flow must of course satisfy,

$$V_{//\varphi} = V_{//\theta}\frac{B_{o\varphi}}{B_{o\theta}}. \tag{4.28}$$

If parallel viscosity is the dominate dissipation mechanism, one expects the poloidal flow in the plasma to be damped to zero on an ion-ion collision time scale due to magnetic pumping. This is the usual assumption in derivations of the ion polarization term in the literature. If the total poloidal flow is set to zero in the expression for the perpendicular force, this allows us to solve for the poloidal component of the parallel flow,

$$V_{//\theta} = \frac{\tilde{E}_r B_{o\varphi}}{B_o^2} \approx \frac{\tilde{E}_r}{B_{o\varphi}}. \tag{4.29}$$

The poloidal component of the parallel flow then fixes the torodial component of the parallel flow as well,

$$V_{//\varphi} = V_{//\theta}\frac{B_{o\varphi}}{B_{o\theta}} \approx \frac{\tilde{E}_r}{B_{o\theta}}. \tag{4.30}$$

Therefore the perpendicular force becomes,

$$\vec{F}_{\perp} = m_i \frac{d}{dt}\left(\frac{\tilde{E}_r B_{o\theta}}{B_o^2} - \frac{\tilde{E}_r}{B_{o\theta}}\right)\hat{\varphi}, \tag{4.31}$$

if there is strong poloidal flow damping. This can be further simplified by noting that the first term in parenthesis is of order $\sim(\varepsilon/q)^2$ smaller than the second term. Hence,

$$\vec{F}_{\perp} \approx -m_i \frac{d}{dt}\left(\frac{\tilde{E}_r}{B_{o\theta}}\right)\hat{\varphi}, \tag{4.32}$$

or,

$$F_{\perp} \sim -m_i \omega \frac{\tilde{E}_r}{B_{o\theta}}. \tag{4.33}$$

How large is this force for HBT-EP conditions? Taking the electric field value of ~0.6V/cm derived above and estimating $B_{o\theta}=\varepsilon(B_{o\varphi}/q)$=208G, with ε=12/95, q=2, $B_{o\varphi}$=3.3kG, for a $f_{2/1}$=10kHz mode gives a force of $6.28\text{x}10^{-19}$ N on an individual deuteron. This would give rise to a force density ~1μN/cm^3 for typical 10^{13} cm^{-3} plasma densities. This force can now be inserted into the $\vec{F}_{\perp} \times \vec{B}$ drift to evaluate the induced polarization current, with $V_{pol} = F_{\perp}/qB$.

This gives rise to the following the following radial ion current,

$$\vec{j}_{pol} = qn\vec{V}_{pol} = \frac{m_i n \omega^2}{k_{\varphi} B_{o\theta}}\hat{r} \tag{4.34}$$

This induced polarization current is approximately ~2mA/cm^2 for a typical HBT-EP tearing mode. The electron contribution to the current is smaller by a factor of the electron to ion mass ratio (~1/1837) and can be neglected. Next, the parallel current induced by this effectively perpendicular polarization current

following into the island is estimated along with the magnitude of the resulting delta prime contribution of this parallel current to Rutherford's equation.

The mode rotation induced polarization current flowing into the island region drives a parallel current to neutralize any charge density build up, $\nabla \cdot \vec{j} = 0$. The gradient operators near the magnetic island are approximated as $\nabla_{\perp} \sim \partial / \partial r \sim 1/W$ and $\nabla_{//} \sim k_{\theta} W / L_s$. Using this we can write for the magnitude of the parallel current,

$$j_{//} = \left(\frac{L_s}{k_{\theta} W^2} \right) j_{pol} = \left(\frac{L_s}{k_{\theta} W^2} \right) \frac{m_i n \omega^2}{k_{\varphi} B_{o\theta}}. \tag{4.35}$$

It is this current which affects the tearing mode amplitude through its contribution to delta prime in the Rutherford evolution equation. Taking typical HBT-EP parameters the parallel current is calculated to be of order $j_{//} \sim 1/3$ to $1 \mathrm{A/cm^2}$, with L_s (see section 3.4.1) ranging from ~100cm to 300cm for the magnetic shear scale length, $k_{\theta} = m/r_s \sim 2/10\mathrm{cm}$, and $W \sim 3\mathrm{cm}$. For comparison, recall that the parallel current flowing in a 3cm island estimated in section 4.2.1.1 estimated from $j_{//}(r_s) \sim \tilde{b}_{\theta}(r_s) / \mu_o W$ is approximately $4 \mathrm{A/cm^2}$. Thus, the induced polarization current is of the correct order of magnitude for the typical HBT-EP magnetic island size.

Substituting the parallel current from equation 4.35 into the definition of delta prime for a given perturbed current, which can be written as

$$\Delta' = \frac{\mu_o L_s}{B_{o\theta}} \frac{j_{//}}{W}, \tag{4.36}$$

gives the polarization contribution to delta prime as,

$$\Delta' = \frac{\mu_o L_s}{B_{o\theta}} \left(\frac{L_s}{k_\theta W^3} \right) \frac{m_i n \omega^2}{k_\varphi B_{o\theta}}. \tag{4.37}$$

Notice that delta prime scales as $\Delta' \sim \omega^2 / W^3$. Collecting terms and rearranging, the above delta prime can be evaluated using the above estimates to be $r_s \Delta' \approx 2$. This order of magnitude will have a substantial effect on magnetic island size for HBT-EP conditions. Thus, the order of magnitude of the inertial term in the island evolution equation is large enough to affect the observed behavior of m=2 islands during magnetic stirring experiments. These effects are large on HBT-EP due to the relatively large island rotation rate, large saddle coil frequency modulations along with the low machine poloidal field strength and small island size in comparison to other tokamaks. For comparison, we estimate the delta prime contribution using the above formula for an equivalent DIII-D 2/1 magnetic island. For DIII-D we take the following parameters: R_o=1.67m, a=0.67m, B_ϕ=1.3T, f_{MHD}=1.6kHz (La Haye *et al* 1992), and use r_s=0.8a with W/r_s=0.3. This gives an induced polarization current of j_{pol}=8.5x10^{-3}A/cm^2, which is a factor of four times larger than the HBT-EP estimate. This polarization current then drives a parallel current of magnitude $j_{//}$=0.15A/cm^2, or about three to ten times smaller then the HBT-EP estimate. Most importantly, this yields a delta prime contribution for DIII-D of $r_s \Delta' \approx 0.1$, which is at least an order of magnitude smaller than the HBT-EP inertial delta prime estimate. These inertial term effects can therefore be studied more easily in the smaller HBT-EP experiment.

4.3.1.2 Asymmetric amplitude response and ion inertia

The simple inertial effect considered in the previous section estimated the magnitude of the polarization term in the Rutherford island width evolution equation for typical HBT-EP magnetic islands. This inertial contribution is of sufficient magnitude for HBT-EP magnetic islands that observed changes typical in toroidal island motion induced during rotation control experiments can cause a large influx of polarization current. The inclusion of poloidal flow damping and its concomitant ion mass renormalization due to coupling of transverse and longitudinal plasma flow across and along the magnetic field can be viewed as a simple rescaling of the Alfven velocity of the plasma to the poloidal Alfven velocity, $V_A^2 \rightarrow V_{A\theta}^2 = V_A^2 r_s^2 / q^2 R^2$ (Smolyakov *et al* 1996). These terms are crucial in setting the appropriate scale of inertial effects on HBT-EP.

The inclusion of poloidal flow damping and resultant large increase of the inertial contribution to Rutherford's equation are supported by the empirical torque balance developed in section 4.2.1 for typical HBT-EP island locking behavior. There the order of magnitude of any induced island frequency change was consistent with predominantly toroidal motion driven by the external control field torque. Any induced poloidal motion appears to be small in comparison. This is also consistent with negligible poloidal flow changes measured using a Mach probe apparatus during these experiments (Taylor 2000).

Next, we consider the sign of the inertial contribution to the island width equation given the experimental observation of section 4.3.1 that strongly accelerated islands grow in amplitude while those that are decelerated are

suppressed in amplitude. What does this observation imply about the sign of the polarization term in Rutherford's equation.

The effects of inertia and viscosity on island growth and damping have become a source of recent theoretical controversy. In a resistive magnetohydrodynamic context, initial work suggested that ion inertia had a stabilizing effect of island size when the rotation of the island or rational surface is perturbed away from its natural rate (Fitzpatrick and Hender 1991). Later inclusion of finite Larmor radius and diamagnetic effects (Smolyakov 1993, Smolyakov *et al* 1995) and long mean free path physics (Wilson *et al* 1996) opened a window of instability. The instability window is dependent upon island, $\vec{E} \times \vec{B}$ and diamagnetic flow velocities at the position of the magnetic island, but did not change the overall sign of the inertial term from stabilizing to destabilizing. Waelbroek and Fitzpatrick (1997) have recently pointed out that inertia can lead to a destabilizing effect on island width due to essentially a Kelvin-Helmholtz type instability. Recently, work by Mikhailovskii and coworkers (Mikhailovskii*(a) et al* 2000, Mikhailovskii*(b) et al* 2000) have confirmed and extended the original result of Waelbroek and Fitzpatrick. Further theoretical and experimental work will hopefully further clarify these important effects on magnetic island width dynamics in toroidal plasma. Importantly, the effect of these *"separatrix-corrections*" to the polarization delta prime term change its sign while leaving the magnitude of the effect essentially the same (Fitzpatrick and Waelbroek 2000) in the resistive magnetohydrodynamic limit. Thus, we have some confidence that the estimated magnitude of Δ'_{pol} given in section 4.3.1.1 is insensitive to the

overall sign of the term. Experimentally, this also allows us to interpret the observed amplitude asymmetry by effectively treating the magnitude and sign of the inertial term separately.

To understand the observed asymmetry in the amplitude response of magnetic islands on HBT-EP and its implications for the sign of inertial effects consider the dependence of the inertial delta prime on frequency. The simple model of section 4.3.1.1 gave $\Delta'_{pol} \sim \omega^2$. The resistive magnetohydrodynamic result is $\Delta'_{pol} \sim (\omega - \omega_o)^2$ with ω_o the natural propagation frequency of the magnetic island at the local $\vec{E} \times \vec{B}$ speed, $\omega_o \sim \omega_E$. This quadratic scaling with frequency is shown in figure 4.11 for both stabilizing and destabilizing potentials. Consider modulations in island frequency $\omega(t)$ induced by the external saddle coil torque between ω_0-$\Delta\omega$ to ω_0+$\Delta\omega$ as shown. Here, the modulation of island frequency introduces growth for both upward and downward frequency excursions if inertia is destabilizing and damping if inertia is stabilizing. This simple limit is not appropriate for HBT-EP islands given the importance of diamagnetic effects.

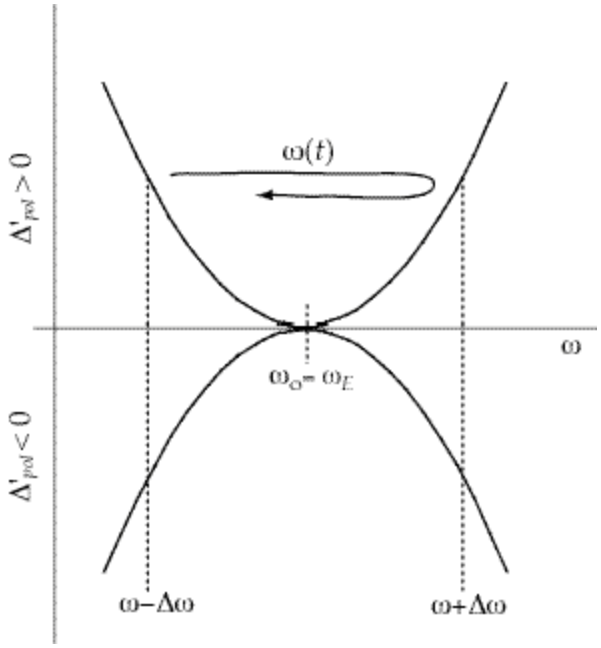

Figure 4.11 Inertial potential well as a function of island frequency in the resistive MHD limit.

For HBT-EP islands the effects of electron diamagnetic propagation can not be ignored and the frequency dependence of the polarization term changes to $\Delta'_{pol} \sim (\omega - \omega_E)(\omega - \omega_E - \omega_{*i})$ (see Smolyakov *et al* 1995). In this case, there are two distinct marginal stability points at $\omega = \omega_E$ and $\omega = \omega_E + \omega_{*i}$. The simple resistive magnetohydrodynamic result of a single marginal point at $\omega = \omega_o = \omega_E$ results from the coalescence of the two distinct zeros in the limiting case of small diamagnetism. The finite ion diamagnetism case is shown in figure 4.12 for both stabilizing and destabilizing potentials for comparison. In addition, the position of typical m/n=2/1 HBT-EP island natural rotation frequency is indicated by $\omega=\omega_E+\omega_{*e}$. The observed amplitude increase with acceleration and amplitude decrease with deceleration away from this frequency are seen to be consistent with a *destabilizing* inertial contribution to the Rutherford equation. If inertia were stabilizing, for the typical ordering of frequencies for HBT-EP, an accelerated island would sample more of the stabilizing branch of the quadratic inertial well and hence would decrease in amplitude. Conversely, a decelerated island would experience less of the

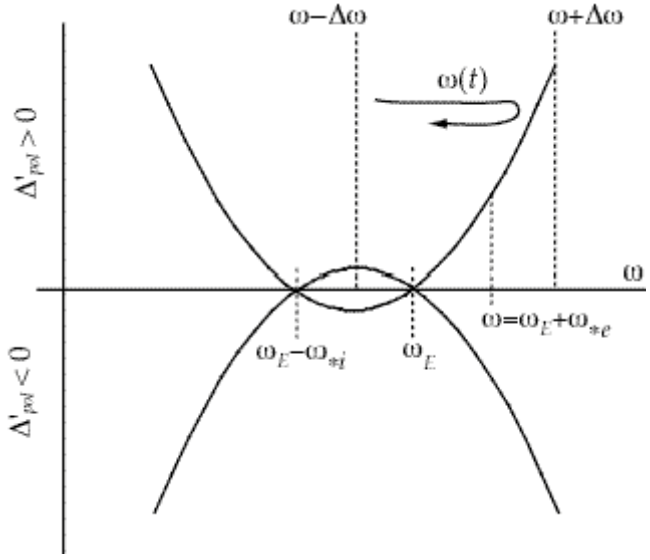

Figure 4.12 Inertial potential well as a function of island frequency including diamagnetic effects. Note the frequency axis is not drawn to scale.

stabilizing influence of inertia and should grow in size. Hence the experimental asymmetry indicates that inertia is again destabilizing since islands grow with acceleration and damp with deceleration. This observation is the first experimental evidence in support of the destabilizing role of ion polarization currents for magnetic island dynamics in toroidal plasma.

4.3.2 *Disruption control using asynchronous control fields*

Motivated by the experimental observation of suppressing island size using a simple asynchronous technique these frequency modulated currents when applied to a disruptive target plasma were found to mitigate the severity of core particle and thermal loss (Navratil *et al* 1998). Application of the modulated Kurita-type saddle currents of figure 4.7 to a disruptive plasma are shown in figure 4.10.

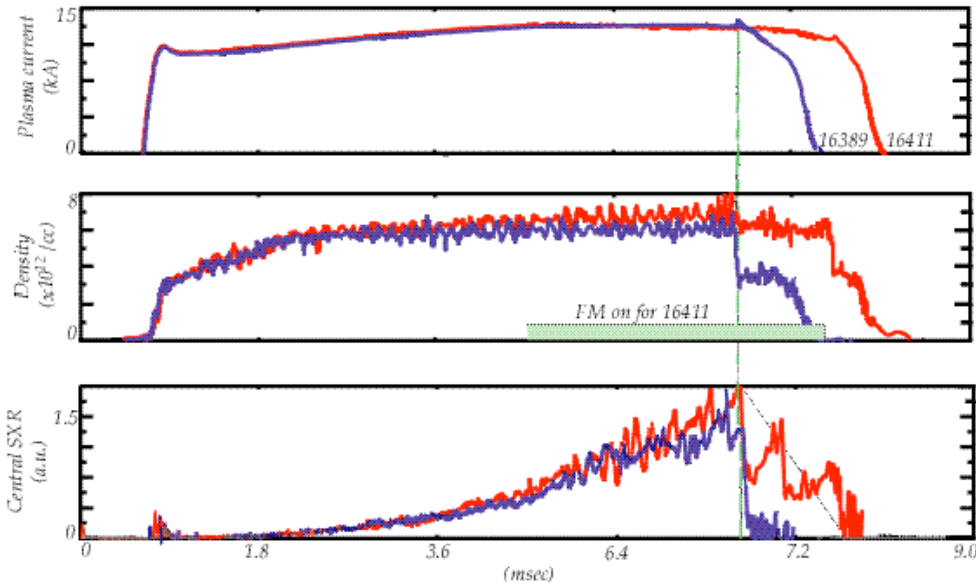

Figure 4.10 Comparison of disruptive plasma with and without the application of frequency modulated saddle coil control field.

In the disruptive target plasma case half of the line integrated plasma density is lost at the time of disruption and core soft x-ray signals completely collapse to zero as shown, indicative of complete core thermal collapse. In the case with an applied control field the plasma density is not lost at the time of disruption and only a partial core thermal collapse is indicated by the soft x-ray signals. The plasma core in the controlled disruption reheats slightly before equilibrium is

lost due to the vertical field force pushing the plasma toward the inner vacuum chamber wall. This simple asynchronous technique offers the possibility of ameliorating the consequences of sudden plasma loss due to disruptive phenomena and its harmful attendant effects on tokamak devices.

5.0 Summary and conclusions

Magnetic island rotation frequency and amplitude dynamics have been studied on the HBT-EP tokamak using a compact saddle coil set able to apply perturbing electromagnetic torque to pre-existing m/n=2/1 islands.

Rotation control and torque balance

Rotation control of these islands was demonstrated over a frequency range of ~5 to 15kHz. The magnetic stirring of the island was studied by constructing a detailed torque balance near the resonant q=2 surface. A simple current density and q-profile was constructed from internal emissivity fluctuation measurements to aid in estimation of m/n=2/1 island width, rational surface location, and magnetic shear. Using these tools, the measured electromagnetic locking torque is found to be consistent with toroidally driven island motion by the external field. The observed electromagnetic locking torque and induced toroidal island rotation point to the importance of poloidal flow damping in describing the physics of HBT-EP magnetic islands. Inclusion of flow damping is also crucial in estimating the magnitude of inertial effects on island size. Observation and analysis of m/n=1/1 island induced motion in the plasma core brought about by the external stirring perturbation was observed and implications of the induced motion for differential rotation studies was explicated. The 1/1 island motion was found to be strongly coupled to the 2/1 island in the edge plasma for both natural propagation and during active control experiments of the 2/1 island.

Magnetic island rotational damping and growth

Magnetic island amplitude dynamics were also examined. Here, using novel frequency modulated control current techniques, a regime of magnetic island suppression and growth has been discovered. Island size is observed to damp when magnetic island frequency is decelerated from its natural rotation rate by the applied magnetic perturbation. It is also observed that acceleration of the island structure induces growth of the pre-existing fluctuation. Simple estimates of the effect of inertia on magnetic island size have been developed and with the inclusion of flow damping yield the correct order of magnitude to account for the observed amplitude changes. The observed asymmetry in acceleration and deceleration with island growth and damping has been shown to be consistent with a d*estabilizing* inertial contribution to the island width evolution equation. This is the first reported experimental evidence to indicate the destabilizing nature of ion polarization currents in the dynamics of magnetic islands, with important consequences, for example, in the role of inertia in error field mode locking penetration levels, threshold characteristics of neoclassical islands, and scaling of the long pulse tokamak β-limit.

Disruption control

Finally, observation of a simple asynchronous control method to alleviate the effects of disruptive plasma loss has been developed and applied to HBT-EP plasmas. The loss of plasma density and core thermal energy was inhibited by application of these control perturbations. It is conjectured that this is due to the maintenance of outer flux surface integrity. The use of such a control technique

4.2.2 *Torque balance summary: poloidal flow damping*

Here we collect the estimates of the previous sections. The main observation to be made is that the preceding torque balance is consistent when poloidal flow damping is taken into account.

The evolution equation for deviation in island velocity for the torodial direction is found by considering the projection of the momentum equation in that direction. Thus for the toroidal torque,

$$\rho \frac{d\Delta v_z}{dt} = \hat{z} \cdot \vec{j} \times \vec{b} - \frac{\partial p}{\partial z} + \nabla \cdot \left(\rho \nu \nabla \Delta v_z \right). \tag{4.24}$$

Integrating this equation, with $\partial p / \partial z \approx 0$, over the island region yields the total torque balance equation for the evolution of the deviation in island velocity whose individual terms have been discussed in the preceding sections (Fitzpatrick 1994, Hegna *et al* 1998),

$$\frac{d}{dt}\left(I_\phi \Delta \omega_\phi \right) \cong I_\phi \frac{d\Delta\omega_\phi}{dt} = T_{VS\phi} + T_{EM\phi} \tag{4.25}$$

for the toroidal frequency evolution, and

$$\frac{d}{dt}\left(I_\theta \Delta \omega_\theta \right) \cong I_\theta \frac{d\Delta\omega_\theta}{dt} = T_{VS\theta} + T_{EM\theta} \tag{4.26}$$

for the poloidal frequency evolution. Using the above estimated torque magnitudes for the poloidal and toroidal terms, the perpendicular torque at the mode rational surface is calculated from,

$$\Gamma_{\perp}^{2} = \Gamma_{\theta}^{2} + (\frac{nr_{s}}{mR_{o}}\Gamma_{\phi})^{2}. \qquad (4.27)$$

The various torque contributions described above are collected in table 4.0. The applied perpendicular electromagnetic torque for a given measured frequency shift and angular acceleration is approximately two orders of magnitude higher than the estimated balancing inertial and viscous torques in the simple cylindrical-slab model developed in the previous sections. This is exactly the factor required to account for the effects of poloidal flow damping of HBT-EP islands. The effective torque is reduced by a factor $\sim(\varepsilon/q)^2 \sim 1/100$ (Smolyakov *et al* 1995). This reduction in effective torque results from the predominantly toroidal motion that flows in tokamak plasma. It also has important consequences for island amplitude dynamics as will be discussed next. Physically, the effective plasma inertia is increased for motion perpendicular to

Torque	Toroidal	Poloidal	Perpendicular
EM	35	70	70
Viscous	50	0.5	3
Inertial	2	0.02	0.1
Inertial (w/ion flow correction)	0.5	0.005 (all units are 10^{-3}Nm)	0.03

Table 4.0 Magnitude of the cylindrical HBT-EP torque balance terms showing the necessity of poloidal damping of island motion.

the magnetic lines of force due to damping of poloidal rotation and coupling of perpendicular and parallel flows in toroidal plasma. This results from the strong damping effect of parallel viscosity due to magnetic pumping. This process converts any directed flow energy in an inhomogeneous magnetic field into heat, that is, field non-uniformities act as a *"magnetic brake"* on the flowing plasma.

This means that the any attempt to drive poloial flow actually results in a driven parallel flow that exactly cancels any poloidal motion and results in a net toroidal flow. The fact that the required electromagnetic torque is consistent with predominantly toroidal island motion supports the inclusion of this important physics for HBT-EP magnetic islands.

to limit device damage during abrupt plasma termination due to disruptive phenomena offers a simple method for mitigating device damage. Knowledge gained during this study of magnetic island and plasma dynamical behavior induced by rotating magnetic perturbations hopefully offers insight and possible solution to some of the many challenges that we encounter in trying bring about the promise of fusion energy here on earth.

References

Arfken, G., (1985), *Mathematical methods for physicists*, Academic Press, 3rd Ed., pg. 890.

Arsenin, V. V., L. I. Artemenkov, N. V. Ivanov, *et al*, (1978) *"Feedback stabilization of kink instability in the TO-1 tokamk,"* in Plasma Physics and Controlled Nuclear Fusion Research, (IAEA 1999), Vol. 2, 197.

Aubry, N., R. Guyonnet, R. Lima, (1991), "*Spatiotemporal analysis of complex signals: theory and applications,"* Jour. Stat. Phys., Vol. 64, Nos. 3/4, 683.

Aubry, N., F. Carbone, R. Lima, and S. Slimani, (1994), "*Wave propagation phenomena from a spatiotemporal viewpoint: resonances and bifurcations,"* Jour. Stat. Phys., Vol. 76, Nos. 3/4, 1005.

Aubry, N. and R. Lima, (1995), *"Spatio-temporal symmetries,"* Jour. Stat. Phys., Vol. 64, Nos. 3/4, 683.

Bagdasarov, A. A., V. F. Denisov, D. P. Ivanov, *et al*, (1982), *"Investigation of transposrt and diruptions in the T-7 tokamak by poloidal field perturbation,"* in Plasma Physics and Controlled Nuclear Fusion Research, (IAEA 1983), Vol. 1, 281.

Bateman, G., (1978), *MHD instabilities*, MIT Press, pg. 197.

Bekefi, G., (1966), *Radiation processes in plasmas*, John Wiley and Sons, Inc., pg. 131.

Bickerton, R. J., (1997), "*Magnetic turbulence and the transport of energy and particles in tokamaks*," Plasma Physics and Cont. Fusion, Vol. 39, 339.

Bol, K., J. L. Cechi, C. C. Daughney, *et al*, (1974), *"Experiments on the Adiabatic Toroidal Compressor,"* in Plasma Physics and Controlled Nuclear Fusion Research, (IAEA 1975), Vol. 1, 83.

Boozer, A. H., (1983), *"Evaluation of the structure of ergodic fields,"* Physics of Fluids B, 26, (5), 1288.

Boozer, A. H., (1985), *"Magnetic field line Hamiltonian,"* PPPL Report 2094R.

Boozer, A. H., (1992), "*Plasma confinement*," Encyclopedia of Physical Science and Technology, Academic Press, Vol. 13.

Boozer, A. H., (1996), "*Shielding of resonant magnetic perturbations by rotation*," Physics of Plasmas, Vol. 3, No. 12, 4620.

Braginskii, S. I., (1965), "*Transport processes in a plasma*," in Reviews of Plasma Physics, Vol. 1, M.A. Leontovich, Ed., 205.

Callen, J. D. and G. L. Jahns, (1977), *"Experimental measurement of electron heat diffusivity in a tokamak,"* Phys. Rev. Lett., Vol. 38, No. 9, 491.

Callen, J. D., (1987), "*Magnetic island charateristics*," in Nuclear Engineering & Engineering Physics 903 Lecture Notes, University of Wisconsin-Madison.

Callen, J. D., (1987), "*Models of plasma confinement and heating in tokamaks,"* University of Wisconsin-Madison, UWPR 89-2.

Cary, J. R. and R. G. Littlejohn, (1983), *"Noncanonical Hamiltonain mechanics and its application to magnetic field line flow,"* Annals of Physics, 151, 1-34, 1.

Cates, C., M. Shilov, M. E. Mauel, *et al*, (2000), *"Suppression of resistive wall instabilities with distributed, independently controlled, active feedback coils,"* Physics of Plasmas, Vol. 7, No. 8, 3133.

Craven, W. A., (1996), "*Resonant External Magnetic Perturbations on the Texas Experimental Tokamak*," Ph.D. Thesis, University of Texas at Austin, FRCR #489.

Den Hartog, D. J., (1996) *"Controlling mode and plasma rotation in MST with a rotating magnetic perturbation,"* Workshop on Feedback Stabilization of MHD Instabilities, Princeton Plasma physics Laboratory, December 11-13, 1996.

deVries, P. C., G. Waidmann, A. Kramer-Fleckner, *et al.*, (1997), "*Temperature profile perturbations due to magnetic islands in TEXTOR*," Plasma Physics and Cont. Fusion, 39, 439.

Dubois, M. A., D. A. Marty, A. Pochelon, (1980), *"Method of cartography of q=1 islands during sawtooth activity in tokamaks,"* Nuclear Fusion, Vol. 20, No. 11.

Dubois, M. A., A. L. Pecquet, C. Reverdin, (1983), *"Internal disruptions in the TFR tokamak: a phenomenological analysis,"* Nuclear Fusion, Vol. 23, No. 2.

Dudok de Wit, T., A. L. Pecquet, J. C. Vallet, and R. Lima, (1994), "*The biorthogonal decompostion as a tool for investigating fluctuations in plasmas,"* Physics of Plasmas, 1, (10) 3288.

Dudok de Wit, T., (1995), "E*nhancement of multichannel data in plasma physics by biorthogonal decomposition,"* Plasma Physics and Cont. Fusion, Vol. 37, 117.

Dudok de Wit, T., M. Erba, M. Mattioli, J. L. Segui, (1998), "*Self-consistent removal of sawtooth oscillations from transient plasma data by generalized singular value decompostion,"* Physics of Plasmas, 5, (5) 1360.

Eisner, E. C., (1998), *"The effects of wall coverage, symmetry, and plasma-wall separation on the stability of tokamak plasmas,"* Ph. D. Thesis, Columbia University Plasma Physics Laboratory Report No. 136.

Finken H. K., (2000), *"Perturbation field penetration into the TEXTOR tokamak and the resulting torque,"* Nuclear Fusion, Vol. 39, No. 6, 707.

Fitzpatrick, R., and T. C. Hender, (1991), "*The interaction of resonant magnetic perturbations with rotating plasmas,"* Physics of Fluids B, 3, (3), 644.

Fitzpatrick, R., (1993), *"Interaction of tearing modes with external structures in cylindrical geometry,"* Nuclear Fusion, Vol. 33 No. 7, 1049.

Fitzpatrick, R., (1995), "*Helical temperature perturbations associated with tearing modes in tokamaks*," Physics of Plasmas, 2, (3) 825.

Friedberg, J. P., (1987), *Ideal magnetohydodynamics*, Plenum Press, pg. 6.

Fowler, T. K., (1999), "*Nulear power – fusion,"* Rev. Mod. Phys., Vol. 71, No. 2, S456.

Furth, H. P., J. Killeen and M. N. Rosenbluth, (1963), *"Finite-resistivity instabilites of a sheet pinch,"* Physics of Fluids, 6, (4), 459.

Garofalo, A. M. V., (1997), "*Measurement and interpretation of eddy currents induced in a segmented conducting wall by MHD instabilites in a tokamak*," Ph. D. Thesis, Columbia University Plasma Physics Laboratory Report No. 130.

Garofalo, A. M., E. Eisner, T. H. Ivers, *et al*, (1999), *"Stabilization of kink instabilites by eddy currents in a segmented wall and comparison with ideal MHD theory,"* Nuclear Fusion, Vol. 38, No. 7, 1029.

Gates, D. A., (1993*), "Passive stabilization of MHD instabilities at high* β_N *in the HBT-EP tokamak,"* Ph. D. Thesis, Columbia University Plasma Physics Laboratory Report No. 127.

Gates, D. A., and T. C. Hender, (1996), *"Resistive wall induced forbidden bands of mode rotation frequency on the Compass-D tokamak,"* Nuclear Fusion, Vol. 36, No. 3, 273.

Gates, D. A., B. Lloyd, A. W. Morris, e*t al*, (1997), *"Neoclassical islands on Compass-D,"* Nuclear Fusion, Vol. 37, No. 11, 1593.

Gilmore, R., (1998), "*Topological analysis of chaotic dynamical systems,"* Rev. Mod. Phys., Vol. 70, No. 4, 1455.

Granetz, R., and P. Smeulders, (1988), *"X-ray tomography on JET,"* Nuclear Fusion, Vol. 28, No. 3, 457.

Hammet, G. and K. McGuire, (1982), "*Analysis of Mirnov oscillations on PDX*," PPPL Report 1854.

Hansen, A. K., A. F. Almagri, D. J. Den Hartog, *et al*, (1998), *"Locking of multiple resonant mode structures in the reversed-field pinch,"* Physics of Plasmas, Vol. 5, No. 8, 2942.

Hassam, A. B. and R. M. Kulsrud, (1978), "*Time evolution of mass flows in a collsional tokamak,"* Physics of Fluids B, Vol. 21, No. 12, 2271.

Hawryluk, R. J., (1998), *"Results from deuterium-tritium tokamak confinement experiments,"* Rev. Mod. Phys., Vol. 70, No. 2, 537.

Hegna, C. C. and J. D. Callen, (1992), "*Pressure profiles, resonant Pfirsch-Schluter currents, thermal instabilities, and magnetic island formation,"* Physics of Fluids B, Vol. 4, No. 12, 4072.

Hegna, C. C. and J. D. Callen, (1992), "*Interaction of bootstrap-current-driven magnetic islands*," Physics of Fluids B, Vol. 4, No. 7, 1855.

Hegna, C. C., (1996), "*Nonlinear tearing mode interactions and mode locking in reversed-field pinches,"* Physics of Plasmas, Vol. 3, No. 12, 46.

Hegna, C. C., (1997), "*The physics of neoclassical magnetohydrodynamic tearing modes,"* Physics of Plasmas, Vol. 5 , No. 5, 1767.

Hender T. C., R. Fitzpatrick, A. W. Morris, *et al*, (1992), *"Effect of resonant magnetic perturbations on Compass-C tokamak discharges,"* Nuclear Fusion, Vol. 32, No. 12, 2091.

Hinton, F. L., (1983), "*Collisional transport in plasma*," in Handbook of Plasma Physics, Vol. 1, M.N. Rosenbluth and R. Z. Sagdeev, Eds., 147.

Hutchinson, I. H., (1987), *Principles of plasma diagnostics*, Cambridge University Press, pg. 175.

Ivanov, N. V., and A. M. Kakurin, (1979), "*Locking of the kink perturbation frequency in a tokamak,"* Sov. J. Plasma Phy., Vol. 5, No. 5, 541.

Ivers, T. H., E. Eisner, A. Garofalo, *et al*, (1994), *"Passive and active control of MHD instabilities in the HBT-EP tokamak,"* in Plasma Physics and Controlled Nuclear Fusion Research, Barcelona, Spain (IAEA 1995), Vol. 2, 287.

Ivers, T. H., E. Eisner, A. Garofalo, *et al*, (1996), *"Observation of wall stabilization and active control of low-n magnetohydrodynamic instabilities in a tokamak,"* Physics of Plasmas, 3, (5) 1926.

Jaenike, R., *et al*, (1988), "*The effect of tearing modes on temperature and density profiles and on perpendicular transport in the WII-A stellarator*," Nuclear Fusion,Vol. 28, No. 10, 1737.

Jahns, G. L., M. Soler, B. V. Waddell, J. D. Callen, H. R. Hicks, (1978), "*Internal disruptions in tokamaks,"* Nuc Fusion, 18, 5, 609.

Jensen, T. H., and A. W. Leonard, (1991), *"Control of rotation velocity profile of tokamaks by application of slow electromagnetic waves,"* Physics of Fluids B, Vol. 3, No. 12, 3422.

Jensen, T. H., A. W. Leonard, A. W. Hyatt, (1993), *"A simple model for driven islands in tokamaks,"* Physics of Fluids B, Vol. 5, No. 4, 1239.

Kadomtsev, B. B., (1975), *"Disruptive instabiltiy in tokamaks,"* Sov. J. Plasma Phy. 1, 389-91.

Karger, F., H. Wobig, S. Corti, *et al*, (1974), *"Influence of resonant helical fields on tokamak discharges,"* in Plasma Physics and Controlled Nuclear Fusion Research, (IAEA 1995), Vol. 1, 207.

Kim J. S., D. H. Edgell, J. M. Greene, E. J. Strait and M. S. Chance, (1999), *"MHD mode identification of tokamak plasmas from Mirnov signals,"* Plasma Physics and Cont. Fusion, Vol. 41, 1399.

Kobayashi, M., H. Kojima, K. Zhai, et al, (2000), *"Frequency dependence of tokamak plasma response to the externally applied rotating helical fields,"* Physics of Plasmas, Vol. 7, No. 8, 3288.

Kombargi, R., (1997), "*The influence of a conducting wall on disruptions in HBT-EP,"* Ph. D. Thesis, Columbia University Plasma Physics Laboratory Report No. 131.

Kruskal, M. D. and R. M. Kulsrud, (1958), *"Equilibirum of a magnetically confined plasma in a toroid,"* Physics of Fluids, Vol. 1, No. 4, 265.

Kurita, G., T. Tuda, M. Azumi, *et al*, (1992), *"Effect if an external helical field on a rotating magnetic island,"* Nuclear Fusion, Vol. 32, No. 11, 1899.

Landau, L. D. and E. M. Lifshitz, (1987), *Fluid mechanics*, Pergamon, 2nd Ed., pg. 14.

LaHaye, R. J., R. Fitzpatrick, T. C. Hender, *et al*, (1992), *"Critical error fields for locked mode instability in tokamaks,"* Physics of Fluids B, Vol. 4, No. 7, 2098.

LaHaye, R. J., (1997), "*Physics of locked modes in ITER: Error field limits, rotation for obviation, and measurement of field errors,"* General Atomics report, GA-A22468.

LaHaye, R. J., R. J. Buttery, S. Guenter, *et al*, (2000), *"Dimensionless scaling of the critical beta for the onset of a neoclassical tearing mode,"* Physics of Plasmas, Vol. 7, No. 8, 3349.

Lichtenberg, A. J., (1984), *"Stochasticity as the mechanism for the disruptive phase of the m=1 tokamak oscillations,"* Nuclear Fusion, Vol. 24, No. 10, 1277.

Lichtenberg, A. J. and M. A. Lieberman, (1992), Regular and chaotic dynamics, Springer-Verlag New York, Inc., 2nd Ed., pg. 48.

Lima, R., (1992), *"Describing dynamics with a bi-orthogonal decomposition,"* Chaos 2, 315.

Lippmann S., M. Finkenthal, H. W. Moos, *et al*, (1991), *"Effects of an ergodic magnetic limiter on the edge plasma properties of the TEXT tokamak,"* Nuclear Fusion, Vol. 31, No. 11, 2131.

Mauel, M. E., D. Gates, R. Kombargi, et al, (1991), *"Design and fabrication of the HBT-EP tokamak: A large aspect-ratio, high beta, 10msec pulsed tokamak,"* IAEA Technical Committee Meeting: *Research using small tokamaks*, IAEA-TOCDOC-604, 189.

Mauel, M. E., E. Eisner, A. Garofalo, *et al*, (1996), *"Eddy current characterization and plasma rotation control in wall-stabilized tokamak discharges,"* in Plasma Physics and Controlled Nuclear Fusion Research, (IAEA 1997), Vol. 1, 731.

Mauel, M. E., J. Bialek, C. Cates, *et al*, (1998),"*Suppression of magnetic islands through synchronous and asynchronous application of resonant magnetic fields,"* in Plasma Physics and Controlled Nuclear Fusion Research, (IAEA 1999), Vol. 2, 197.

McGuire, K. and D. C. Robinson, (1979), *"Sawtooth oscillations in a small tokamak,"* Nuclear Fusion, Vol. 19, No. 4, 505.

Morris, A. W., T. C. Hender, J. Hugill, *et al*, (1990), *"Feedback stabilization of disruption precursors in a tokamak,"* Phys. Rev. Lett., Vol. 64, No. 11, 1254.

Morozov, A. I. and L. S. Solov'ev, (1966), "*The structure of magnetic fields*," in Reviews of Plasma Physics, Vol. 2, M. A. Leontovich, Ed., 205.

Mikhailovski, A. B., V. D. Pustovitov, A. I. Smolyakov, *et al*, (2000), *"Regularized magnetic islands. I. Hyperviscosity and profile functions,"* Physics of Plasmas, vol. 7, No. 4, 1204.

Mikhailovski, A. B., V. D. Pustovitov, A. I. Smolyakov, *et al*, (2000), *"Regularized magnetic islands. II. The role of polarization current,"* Physics of Plasmas, vol. 7, No. 4, 1214.

Nadle, D. L., (2000), *"Magnetic feedback experiments on the m/n=2/1 tearing mode in the HBT-EP tokamak,"* Ph.D. Thesis, Columbia University Plasma Physics Laboratory Report No. 137.

Nadle, D. L., C. Cates, M. E. Mauel, *et al*, (2000), *"The feedback phase instability in the HBT-EP tokamak,"* Nuclear Fusion, Vol. 28, No. 6, 1085.

Nagayama, Y., G. Taylor, E. D. Fredrickson, *et al.*, (1996), "*Tomography of (2,1) and (3,2) magnetic islands structures on the Tokamak Fusion Test Reactor*," Physics of Plasmas, Vol. 3, No. 7, 2631.

Nardone, C., (1992), "*Multichannel fluctuation data analysis by the singular decomposition method: application to JET MHD modes,"* Plasma Physics and Cont. Fusion, Vol. 34, 1447.

Nave, M. F. F. and J. A. Wesson, (1990), *"Mode locking in tokamaks,"* Nuclear Fusion, Vol. 30, No. 12, (1990).

Nave, M. F. F., *et al.* (1992), "*Observations of MHD structures in JET temperature profiles,"* Nuclear Fusion, Vol. 32, No. 5, 825.

Navratil, G. A., C. Cates, M. E. Mauel, *et al.*, (1998), "*Active control of 2/1 magnetic islands in a tokamak,"* Physics of Plasmas, Vol. 5, No. 5, 1855.

Oasa, K., H. Aikawa, Y. Asahi, *et al*, (1994), *"Plasma response to external rotating magnetic fields in the JFT-2M tokamak,"* in Plasma Physics and Controlled Nuclear Fusion Research, (IAEA 1995), Vol. 2, 279.

Pritchard, D. C., R. F. Gandy, J. D. Hanson, *et al*, (1997), *"Effects of applied rotating magnetic perturbations on ion drift orbits in the Compact Auburn Torsatron,"* Physics of Plasmas, Vol. 4, No. 1, 162.

Rebut, P. H. and M. Hugon,(1984), "*Thermal instability and disruptions in a tokamak*," in Plasma Physics and Controlled Nuclear Fusion Research, London (IAEA 1985), Vol. 2, 197.

Roberts, D. E., J. D. Fletcher, G. Nothnagel, *et al*, (1991), *"Stability of disruption precursors in a tokamak following controlled change of wall boundary conditions,"* Phys. Rev. Lett., Vol. 66, No. 22, 2875.

Roberts, D. E., D. Sherwell, J. D. Fletcher, *et al*, (1991), *"Major disruptions induced by helical coils on the Tokoloshe tokamak,"* Nuclear Fusion, Vol. 31, No. 2, 319.

Rutherford, P. H., (1973), *"Nonlinear growth of the tearing mode,"* Physics of Fluids B, Vol. 16, No. 11, 1903.

Savrukin, P., D. J. Campbell, M. De Beneditti, et al, (1995), "*Numerical simulations of feedback control of coupled tearing modes at JET,"* JET report, JET-R(95)06.

Sankar, M. K. V., E. Eisner, A. Garofalo, *et al*, (1993), "*Initial high beta operation of the HBT-EP tokamak*," Journal of Fusion Energy, Vol. 22, no. 3, 303.

Schissel, D. P., and J. Leuer, (1996), "*Fusion: creating a star on earth,"* http://fusioned.gat.com/Teachers/SlideShow.html.

Scoville, J. T., R. J. LaHaye, A. G. Kellman, *et al*, (1991), *"Locked modes in DIII-D and a method for prevention of the low density mode,"* Nuclear Fusion, Vol. 31, No. 5, 875.

Smolyakov, A. I., (1993), *"Nonlinear evolution of tearing modes in inhomogeneous plasmas,"* Plasma Physics and Cont. Fusion, Vol. 35, 657.

Smolyakov, A. I., A. Hirose, E. Lazzaro, *et al*, (1995), *"Rotating nonlinear magnetic islands in a tokamak plasma,"* Physics of Plasmas, Vol. 2, No. 5, 1581.

Snipes, J. A. and K. W. Gentle, (1986), *"A study of sawtooth phenomena in TEXT,"* Nuclear Fusion, Vol. 26, 1507-1514.

Snipes, J. A., D. J. Campbell, P. S. Haynes, *et al*, (1988), "*Large amplitude quasi-stationary MHD modes in JET*," Nuclear Fusion, Vol. 28, No. 6, 1085.

Snider, R. T., (1990), *"Scaling of the sawtooth inversion radius and the mixing radius on DIII-D,"* Nuclear Fusion, Vol. 30, No.11, 2400.

Strait, E. J., (1995), "*MHD mode analysis in tokamak experiments*," Summer School on MHD Phenomena in Plasmas, University of Wisconsin at Madison, August 14-18, 1995.

Suttrop, W., K. Buchl, J. C. Fuchs, *et al.* , (1997), "*Tearing mode formation and radiative edge cooling prior to density limit disruptions in ASDEX-Upgrade*," Nuclear Fusion, Vol. 37, No. 1, 119.

Sykes, A. and J. A. Wesson, (1976), *"Relaxation instabiltiy in tokamaks,"* Phys. Rev. Lett. 37, 140.

Tabor, M., (1989), Chaos and Integrability in Nonlinear Dynamics, John Wiley and Sons, Inc., pg. 189.

Taylor, E. D., C. Cates, M. E. Mauel, *et al*, (1999), *"Nonstationary signal analysis of magnetic islands in plasmas,"* Rev. Sci. Inst. 70 (12), 4545.

Taylor, E. D., (2000), *"Effect of magnetic islands on local plasma behavior in a tokamak,"* Ph. D. Thesis, Columbia University Plasma Physics Laboratory Report No. 138.

Vallet J. C., L. Poutchy, M. S. Mohamed-Benkadda, *et al*, (1991*) "Stabilization of tokamak ohmic discharges at the density limit by means of the ergodic divertor"* Phys. Rev. Lett., Vol. 67, No. 19, 2662.

Van Milligen, B. P., A. C. A. P. Van Lammeren, N. J. Lopes Cardozo, *et al.*, (1993)., "*Gradients of electron temperature and density across m=2 magnetic islands in RTP*," Nuclear Fusion, Vol. 33, No. 8, 1119.

von Goeler, S., W. Stodiek, N. Sauthoff, (1974), *"Studies of internal disruptions and m=1 oscillations in tokamak discharges with soft X-ray techniques,"* Phys. Rev. Lett. **33**, 1201-3.

Waelbroeck, F. L., and R. Fitzpatrick, (1997), "*Rotation and locking of magnetic islands,"* Phys. Rev. Lett., Vol. 78, No. 9, 1703.

Waidmann, G. and G. Kuang, (1992), "*Density limits and evolution of disruptions in Ohmic TEXTOR plasmas*," Nuclear Fusion, Vol. 32, No. 4.

Wesson, J. A., *et al*., (1989), "*Disruptions in JET*," Nuclear Fusion, Vol. 29, No. 4, 641.

Wesson, J. A., (1986), *"Theory of sawtooth oscillations,"* in Plasma Physics and Controlled Nuclear Fusion Research (IAEA 1987), Vol. 2, 197.

Wesson, J. A., (1997), Tokamaks, Oxford Science Pulications, 2nd Ed., pg 10.

White, R. B., D. A. Monticello, M. N. Rosenbluth, *et al*, (1977), "*Saturation of the tearing mode,"* Physics of Fluids B, Vol. 20, No. 5, 800.

White, R. B., (1983), "*Resistive instabilities and field line reconnection*," in Handbook of Plasma Physics, Vol. 1, M.N. Rosenbluth and R. Z. Sagdeev, Eds., 611.

Wilson, H. R., J. W. Connor, R. J. Hastie, *et al*, (1996), *"Threshold for neoclassical magnetic islands in a low collision frequency tokamak,"* Physics of Plasmas, Vol. 3, No. 1, 248.

Wilson, H. R., M. Alexander, J. W. Connor, *et al*, (1996), *"The collisonality dependence of tokamak β-limits,"* Plasma Physics and Cont. Fusion, Vol. 38, A149.

Xiao, Q. and G. A. Navratil, (1996), "*A photodiode for the measurement of soft x-ray radiation from plasma,"* Rev. Sci. Inst. 67 (9), 3334.

Xiao, Q., (1998), "*Effect of applied resonant magnetic fields on measured MHD mode structure in a tokamak plasma*," Ph.D. Thesis, Columbia University Plasma Physics Laboratory Report No. 135.

Yamazaki, K., K. Kawahata, Y. Abe, *et al*, (1986), *"Disruption control experiments using local modular multiple field coils,"* in Plasma Physics and Controlled Nuclear Fusion Research, (IAEA 1987), Vol. 1, 309.

Yokoyama, M., J. D. Callen, and C. C. Hegna, (1996), "*Effect of Mode locking on toroidal flow evolution*," Nuclear Fusion, Vol. 36, No. 10, 1307.

Yoshida, Z., K. Okana, Y. Seike, *et al*, (1982), *"Suppression of the disruptive instability in the low-q regime by external ergodization of (2,1) island,"* in Plasma Physics and Controlled Nuclear Fusion Research, (IAEA 1983), Vol. 1, 309.

Zohm, H., A Kallenbach, H. Bruhns, *et al*, (1989), *"Plasma angular momentum loss by MHD mode locking,"* IPP report 1/251.